

**WRINKLING BEHAVIOUR OF AUTOMOTIVE DECORATIVE FILMS**

**THERMALLY INDUCED WRINKLING BEHAVIOUR OF  
AUTOMOTIVE DECORATIVE FILMS**

**By**

**MAHDY MAZHARY MALAYERY, B.Sc., M. Eng.**

**A Thesis**

**Submitted to the School of Graduate Studies**

**In Partial Fulfillment of the Requirements**

**For the Degree**

**Master of Applied Science**

**McMaster University**

**© Copyright by Mahdy Mazhary Malayery, September 2010**

**MASTER OF APPLIED SCIENCE (2010)**  
**(Chemical Engineering)**

**McMaster University**  
**Hamilton, Ontario**

**TITLE:**           **Thermally Induced Wrinkling Behaviour of  
Automotive Decorative Films**

**AUTHOR:**       **Mahdy Mazhary Malayery, B.Sc., M. Eng.**

**SUPERVISOR:** **Professor M. R. Thompson**

**NUMBER OF**   **xii - 131**

**PAGES:**

## ABSTRACT

Decorative plastic films are becoming more and more popular in the industry, substituting paint, chrome-plating and hydrographics. Thermal formability of these films is extending the uses of these materials into newer applications within industry, but early observation have shown that certain film constructions will wrinkle upon heating. Despite growing interest and markets to use these films in thermal forming processes, there is insufficient knowledge in the field to explain or compensate for these undesirable surface wrinkles. The purpose of this study is to find out what caused the wrinkles, what the underlying behaviour was and if they could be avoided.

The experiments were performed using a pressure sensitive adhesive coated decorative film, supplied by 3M Canada, which was laminated on one of two different secondary substrates (either steel or polypropylene). Samples were heated in a specially built hot stage with vacuum drawing capability at two different heating rates up to one of two final temperatures (110°C and 150°C) and cooled down at two different rates, afterwards. A CCD camera was used to track the changes in the wrinkle pattern on the surface of sample and relates its wavelength back to the corresponding transient temperature of the hot stage, which allowed on-line monitoring of wrinkle growth. Samples were cooled and then measured for their wavelength and surface roughness (represented by peak-to-valley distance (PV) and a standard roughness value, rms) using a white-light interferometer.

Heating rate was found to be the dominant factor in controlling whether wrinkles occurred or not. Only with high heating rates did this wrinkle phenomenon occur

regardless of the secondary substrate use, though the thermal conductivity of that substrate will impact this heating rate if heated from that side (which is what was being done in this work). For steel laminated samples, a chaotic zigzag wrinkles occurred using fast heating rates (around  $95^{\circ}\text{C}/\text{min}$ ) which had an average equilibrium wavelength of  $450\ \mu\text{m}$ . Plastic laminates, just like their metal counterparts, developed wrinkles but now at high heating rates ( $170^{\circ}\text{C}/\text{min}$ ) which produced a pattern with an average wavelength of  $550\ \mu\text{m}$ . The slow heating rate ( $\approx 2^{\circ}\text{C}/\text{min}$ ) did not produce wrinkles for either substrate. Wrinkles are only the final outcome of thermally induced compression stresses which build within the film sandwich construction as the temperature rises and while slower heating didn't produce wrinkles, initial blister formation still occurred (i.e. nuclei of wrinkles) which increased the surface roughness of samples. Pre-straining a sample up to 20% elongation caused the wrinkle pattern to change from a complex biaxial pattern to longitudinal stripes, which extended the pattern always present along the edges of the sample into the centre of the test specimen.

Of all models for the wrinkling behaviour of a thin film under compressive stresses in the literature, only one single model proposed by Basu *et al.* seemed to predict this behaviour reasonably by taking temperature and secondary substrate effects into account. All other models failed to predict this behaviour because, firstly they did not take the effects of temperature and secondary substrate into account, secondly, they erroneously assume the film always deformed elastically, and thirdly, they are not well suited to the thickness ratio of film to substrate for our case.

## ACKNOWLEDGEMENTS

I would like to extend my most sincere gratitude to my supervisor, Dr. M. R. Thompson, for giving me the opportunity to work on this project and his interminable guidance, flexibility and kind attitude during this research. I would like to express my appreciation to Elizabeth Takacs for her training and Paul Gatt and Dan Wright for their continual help in building new apparatus for the experiments.

I would also like to extend my gratefulness to Kent Nielsen and Frank Brandys from 3M Canada for their technical advice and supplying the materials. My thanks go to Natural Sciences and Engineering Research Council (NSERC), Ontario Centres of Excellence (OCE) and 3M Canada for their financial support of this project. I would also like to thank the Chemical Engineering Department at McMaster University, in particular Nanci Cole, Kathy Goodram and Lynn Falkiner for their constant help during these two years.

Lastly, I would extend my greatest gratitude to my family, specifically my parents who gave me unconditional support, encouragement and confidence in my ability to succeed. And my thanks to my dear friends, Siamak Salari, Emily Nichols, Parsa Tamadonfar, Salman Safari and Mehdi Farazmand who provided me with some help and support.

## **TABLE OF CONTENTS**

|   |             |
|---|-------------|
| <b>ABSTRACT</b> .....                                       | <b>III</b>  |
| <b>ACKNOWLEDGEMENTS</b> .....                               | <b>V</b>    |
| <b>TABLE OF CONTENTS</b> .....                              | <b>VI</b>   |
| <b>LIST OF FIGURES</b> .....                                | <b>VIII</b> |
| <b>LIST OF TABLES</b> .....                                 | <b>XII</b>  |
| <b>CHAPTER I: INTRODUCTION</b> .....                        | <b>1</b>    |
| 1.1.    DECORATIVE FILMS: .....                             | 1           |
| 1.2.    PRODUCTION .....                                    | 2           |
| 1.3.    APPLICATIONS: .....                                 | 3           |
| 1.3.1. <i>Decals and Tapes:</i> .....                       | 3           |
| 1.3.2. <i>Extrusion Lamination:</i> .....                   | 3           |
| 1.3.3. <i>In-Mold Forming:</i> .....                        | 3           |
| 1.3.4. <i>Thermoforming:</i> .....                          | 4           |
| 1.4.    MARKET: .....                                       | 5           |
| 1.5.    BENEFITS:.....                                      | 5           |
| 1.5.1. <i>Economic:</i> .....                               | 5           |
| 1.5.2. <i>Environmental:</i> .....                          | 6           |
| 1.6.    MOTIVATIONS: .....                                  | 7           |
| <b>CHAPTER II: LITERATURE REVIEW</b> .....                  | <b>9</b>    |
| 2.1.    INTRODUCTION .....                                  | 9           |
| 2.2.    ORIGINS OF WRINKLES: RESIDUAL STRESS .....          | 12          |
| 2.2.1. <i>Measurement of residual stresses</i> .....        | 13          |
| 2.3.    WRINKLE FORMATION .....                             | 15          |
| 2.4.    QUANTIFICATION OF WRINKLING .....                   | 20          |
| 2.5.    MODELING .....                                      | 21          |
| 2.5.1. <i>Elastic film/Elastic primary substrate</i> .....  | 23          |
| 2.5.2. <i>Elastic film/Viscous substrate</i> .....          | 27          |
| 2.5.3. <i>Elastic film/Viscoelastic substrate</i> .....     | 31          |
| <b>CHAPTER III: EXPERIMENTAL</b> .....                      | <b>38</b>   |
| 3.1.    MATERIALS.....                                      | 38          |
| 3.1.1. <i>Decorative film</i> .....                         | 38          |
| 3.1.2. <i>Plastic substrate</i> .....                       | 39          |
| 3.1.3. <i>Steel substrate</i> .....                         | 40          |
| 3.2.    LAMINATION .....                                    | 40          |
| 3.3.    ASSESSING DELAMINATION LIMITS.....                  | 41          |
| 3.4.    ANISOTROPIC PROPERTIES TESTING.....                 | 46          |
| 3.5.    THERMAL BEHAVIOUR OF THE FILM.....                  | 48          |
| 3.6.    HOT STAGE APPARATUS.....                            | 49          |
| 3.7.    WRINKLE STUDIES (UNSTRAINED SAMPLES) .....          | 52          |
| 3.7.1. <i>Influence of lamination conditions</i> .....      | 52          |
| 3.7.2. <i>Influence of heating/cooling conditions</i> ..... | 54          |
| 3.8.    WRINKLE STUDIES (STRAINED SAMPLES) .....            | 55          |

|                                      |  |            |
|--------------------------------------|--|------------|
| 3.9.                                 | CHARACTERIZATION .....   | 57         |
| 3.9.1.                               | STRESS RELAXATION.....   | 57         |
| 3.9.2.                               | SURFACE METROLOGY.....   | 58         |
| 3.10.                                | MINITAB:.....  | 59         |
| <b>CHAPTER IV: RESULTS.....</b>      |  | <b>60</b>  |
| 4.1.                                 | STEEL: .....   | 60         |
| 4.1.1.                               | <i>Wrinkles Growth</i> .....   | 60         |
| 4.1.1.                               | <i>Pressure-cure time studies</i> .....                              | 64         |
| 4.1.2.                               | <i>Unstrained:</i> .....   | 69         |
| 4.1.3.                               | <i>Strained Steel:</i> .....   | 73         |
| 4.2.                                 | PLASTIC SUBSTRATE: .....   | 76         |
| 4.2.1.                               | <i>Pressure-Cure Time Studies:</i> .....                             | 76         |
| 4.2.2.                               | <i>Determination of Hot Stage Temperature:</i> .....                 | 78         |
| 4.2.3.                               | <i>Wrinkle growth</i> .....  | 79         |
| 4.2.4.                               | <i>Unstrained</i> .....  | 82         |
| 4.2.5.                               | <i>Strained</i> .....  | 86         |
| 4.2.6.                               | <i>Vacuum-fixed vs. loose Samples</i> .....                          | 89         |
| 4.3.                                 | WRINKLE APPEARANCE THRESHOLD.....                                    | 90         |
| <b>CHAPTER V: DISCUSSION .....</b>   |  | <b>93</b>  |
| 5.1.                                 | EXAMINATION OF WRINKLING IN A FILM STRUCTURE .....                   | 93         |
| 5.2.                                 | DESCRIPTION OF WRINKLING INITIATION AND GROWTH .....                 | 94         |
| 5.3.                                 | COMPARISON OF WRINKLING MODELS .....                                 | 98         |
| 5.3.1.                               | <i>Elastic Models</i> .....  | 102        |
| 5.3.2.                               | <i>Viscous Models</i> .....  | 102        |
| 5.3.3.                               | <i>Viscoelastic Models</i> .....                                     | 103        |
| 5.3.4.                               | <i>Basu's Model – Consideration of the secondary substrate</i> ..... | 104        |
| 5.4.                                 | EFFECTS OF HEATING/COOLING RATE.....                                 | 109        |
| 5.5.                                 | PRE-STRAINING.....   | 111        |
| <b>CHAPTER VI: CONCLUSION .....</b>  |  | <b>113</b> |
| <b>REFERENCES: .....</b>             |  | <b>116</b> |
| <b>APPENDIX A: DMA PLOT.....</b>     |  | <b>128</b> |
| <b>APPENDIX B: BASU'S MODEL.....</b> |  | <b>129</b> |

## LIST OF FIGURES

|   |    |
|---|----|
| <b>Figure 1-1.</b> Conceptual construction of a decorative film   | 1  |
| <b>Figure 2-1.</b> Different modes of interfacial failure in thin films. $\sigma_B$ and $\sigma_w$ are corresponding critical stresses and are given by equations 1 and 2, respectively   | 11 |
| <b>Figure 2-2.</b> Three different patterns due to different compression stresses. (a) uniaxial stress causing stripes, (b) labyrinth structure under isotropic biaxial compression and (c) herringbone structure under anisotropic biaxial compression   | 17 |
| <b>Figure 2-3.</b> Energy level of three different wrinkling patterns   | 18 |
| <b>Figure 2-4.</b> Stabilized patterns under different biaxial compression stresses   | 18 |
| <b>Figure 2-5.</b> Evolution of the wrinkles at different times. $\varepsilon_{11} = \varepsilon_{22} = -0.02$ at all times   | 19 |
| <b>Figure 2-6.</b> Schematic figure representing the film and two different substrates. Thickness ratios are taken into account.  | 22 |
| <b>Figure 2-7.</b> Critical stresses for two different modes of buckling. The hollow signs are numerical values calculated through Eqn. 2-4 for different delamination sizes ( $b/h$ ). The dashed lines are the minimum stress for buckle-delamination and the vertical line is the specific PS/PDMS system under experiment with $\bar{E}_f / \bar{E}_s = 0.0005$ . | 25 |
| <b>Figure 2-8.</b> $R_c$ as a function of delamination size. The curve defines a border below which wrinkling is favored, above which buckle-delamination   | 26 |
| <b>Figure 2-9.</b> Schematic structure of an elastic film on a viscous layer which lies on a rigid substrate. a) Equilibrium state, film is flat and biaxially stressed, b) Wrinkled film   | 28 |
| <b>Figure 2-10.</b> Different patterns of wrinkles from the edges to the center.  | 30 |
| <b>Figure 2-11.</b> Schematic of an elastic film lying on a viscoelastic substrate: a) Equilibrium state; b) Wrinkled film.   | 32 |
| <b>Figure 2-12.</b> Schematic growth of wrinkle amplitude.  | 35 |
| <b>Figure 2-13.</b> Fastest growth rate for a thick substrate for different ratios of rubbery/glassy moduli.  | 36 |

|   |           |
|---|-----------|
| <b>Figure 3-1.</b> DSC result for the plastic substrate.  | <b>39</b> |
| <b>Figure 3-2.</b> Stress-strain curve for the delamination test for laminated 9000J at room temperature with cross-head speed of 100mm/min. Drop in the curve at around 35-45% strain is quite visible.  | <b>43</b> |
| <b>Figure 3-3.</b> Plot of differential strain versus percent strain for determination of the delamination point (seen here at 33% strain). Differential curve corresponds to <i>Sample2</i> in Figure 3-2.   | <b>46</b> |
| <b>Figure 3-4.</b> Image of the Hot Stage device used to heat up the samples.   | <b>50</b> |
| <b>Figure 3-5.</b> Schematic view of the vacuum box used to hold the plastic laminates to the surface.  | <b>52</b> |
| <b>Figure 3-6.</b> The stress relaxation curves versus time for samples strained at 10% strain and sat for 20 minutes. It is clear that after 10 minutes the level of stress does not change significantly.   | <b>57</b> |
| <b>Figure 4-1.</b> Wrinkle growth and their corresponding time and temperatures on steel laminates. This specific sample experienced heating rate of 40°C/min and wrinkles formed into parallel herringbones.   | <b>62</b> |
| <b>Figure 4-2.</b> Wavelength growth on a steel laminate over a period of 8 minutes with fast heating/cooling cycles. The error bars are standard deviation over at least 10 wavelength measurements using image analysis software, SigmaScan Pro5.   | <b>64</b> |
| <b>Figure 4-3.</b> Wavelength values for the pressure-cure time experiments on steel laminates. The error bars represent standard deviation for the center point of experimental condition over four measurements on five samples.  | <b>66</b> |
| <b>Figure 4-4.</b> PV values for the pressure-cure time experiments for steel laminates. The error bars represent standard deviation for the center point of experimental condition over four measurements on five samples.   | <b>66</b> |
| <b>Figure 4-5.</b> Rms values for the pressure-cure time experiments for steel laminates. The error bars represent standard deviation for the center point of experimental condition over four measurements on five samples.  | <b>67</b> |
| <b>Figure 4-6.</b> Trend showing a positive correlation between surface roughness and heating rate for steel laminates heated to 150°C  | <b>70</b> |
| <b>Figure 4-7.</b> Sample surface metrology result window using Zygo NewView interferometer. <i>a)</i> Top 2D view, the bars show the way the wavelengths were measured. They were also used to average the PV values at those four locations. This gave the opportunity to eliminate the erroneous points, <i>b)</i> is the 3D Oblique | <b>71</b> |

Plot of the sample which is just a representation of the surface profile and was not used in measurements, *c*) is the side-view 2D surface profile which was used to manually measure the wavelength and average PV values and finally *d*) is called Solid Plot which is a black and white representation of the top view but at most cases it shows better understanding of the wrinkle patterns.

- Figure 4-8.** Scatter plot of change in surface roughness for the final temperature of 110°C for steel laminates. 72
- Figure 4-9.** Comparison of *a*) wavelength and *b*) surface roughness values of unstrained, 10%- and 20%-strained samples. The error bars are standard deviation over four measurements on four samples. 74
- Figure 4-10.** Solid plots of *a*) unstrained *b*) 10%-strained and *c*) 20%-strained sample 75
- Figure 4-11.** PV values for the pressure-cure time experiments for plastic laminates. Error bars represent standard deviation over four repetitions. 77
- Figure 4-12.** Rms values for the pressure-cure time experiments for plastic laminates. Error bars represent standard deviation over four repetitions. 77
- Figure 4-13.** Positive correlation between the heating rate and surface roughness quantification factors for different hot stage final temperatures. Corresponding heating rate is shown above each temperature. Error bars represent standard deviation over three repetitions. 79
- Figure 4-14.** Wrinkle growth and their corresponding time and temperatures on plastic laminates. 81
- Figure 4-15.** Wavelength growth on a plastic laminate over a period of 3 minutes. Error bars represent standard deviation over at least 10 wavelength measurements for each data point. 82
- Figure 4-16.** Trend showing a positive correlation between surface roughness quantification factors and heating rate for plastic laminates reaching 150°C. 84
- Figure 4-17.** Solid plots of two plastic laminates heated to 150°C on a fast ramp-up/fast ramp-down. Longitudinal direction is horizontal. 84
- Figure 4-18.** Scatter plot of change in surface roughness for the final temperature of 110°C for plastic laminates 86
- Figure 4-19.** Solid plot of strained plastic laminates. *a*) 10% strain *b*) 20% strain 87

|   |            |
|---|------------|
| <b>Figure 4-20.</b> Wavelength changes for unstrained, 10% and 20% strained plastic laminates. Error bars represent standard deviation over four measurements on four samples.  | <b>88</b>  |
| <b>Figure 4-21.</b> Surface roughness changes for unstrained, 10% and 20% strained plastic laminates. Error bars represent standard deviation over four measurements.   | <b>88</b>  |
| <b>Figure 4-22.</b> Solid plot of <i>a)</i> loose sample <i>b)</i> vacuum-fixed sample. Longitudinal direction is horizontal in both cases.   | <b>89</b>  |
| <b>Figure 4-23.</b> 2D top view images obtained from white-light interferometer for three different steel laminates, <i>a)</i> sample heated to 150°C at almost 1°C/min, only small blisters formed on the surface, no wrinkles were formed, <i>b)</i> sample heated to 150°C at around 40°C/min, blisters connected to one another and formed stripes/herringbones, <i>c)</i> sample heated to 150°C at around 146°C/min, not only did the wrinkles form, but also developed into complex labyrinth pattern. | <b>91</b>  |
| <b>Figure 4-24.</b> Graph showing PV values for samples that did and did not experience wrinkling. Hollow and solid markers represent “no wrinkles” and “wrinkled” samples, respectively. Diamonds represent plastic laminates, circles indicate steel laminates. Dashed line shows the threshold of PV values at 7μm above which wrinkles formed.  | <b>92</b>  |
| <b>Figure 5-1.</b> Cross-section view of the detached film sandwich from a steel laminate via quenching in liquid nitrogen.   | <b>94</b>  |
| <b>Figure 5-2.</b> Conceptual description of changes occurring due to increasing temperature to Elastic modulus of the film, stresses and wavelength growth.  | <b>96</b>  |
| <b>Figure A-1.</b> DMA plot for 9000J film  | <b>128</b> |

## *LIST OF TABLES*

|   |            |
|---|------------|
| <b>Table 3-1.</b> Delamination point (%Strain) for the three films at different speeds and temperatures   | <b>44</b>  |
| <b>Table 3-2.</b> Yield stress (MPa) for the three films at different speeds  | <b>44</b>  |
| <b>Table 3-3.</b> Yield stress for the laminated 9000J in three different orientations  | <b>47</b>  |
| <b>Table 3-4.</b> Delamination point for the laminated 9000J in three different orientations  | <b>47</b>  |
| <b>Table 3-5.</b> DMA fixture and other settings used for the tests   | <b>49</b>  |
| <b>Table 4-1.</b> Minitab statistical values regarding the sensitivity of surface roughness on different parameters.  | <b>68</b>  |
| <b>Table 4-2.</b> Surface roughness quantification figures for final temperature of 150°C in $\mu\text{m}$ for steel laminates  | <b>69</b>  |
| <b>Table 4-3.</b> Surface roughness quantification figures for final temperature of 110°C in $\mu\text{m}$ for steel laminates  | <b>73</b>  |
| <b>Table 4-4.</b> Surface roughness quantification figures for final temperature of 150°C in $\mu\text{m}$ for plastic laminates  | <b>83</b>  |
| <b>Table 4-5.</b> Surface roughness quantification figures for final temperature of 110°C in $\mu\text{m}$ for plastic laminates.   | <b>85</b>  |
| <b>Table 4-6.</b> Surface metrology values for the loose and vacuum-fixed plastic laminates in $\mu\text{m}$ .  | <b>90</b>  |
| <b>Table 5-1.</b> Estimated material properties and calculated wavelengths for onset and growth region  | <b>99</b>  |
| <b>Table 5-2:</b> Calculated values based on equations in Appendix B and 5-1 and 5-2 for temperature onset and growth regions for steel and plastic secondary substrates.                 | <b>105</b> |
| <b>Table B-1:</b> Estimated and calculated values based on equations B-1 to B-10 for temperature brackets of 30°C to 130°C and 130°C to 150°C for steel and plastic secondary substrates. | <b>130</b> |

---

**CHAPTER I:*****Introduction***

---

**1.1. Decorative Films:**

Plastic films have various applications such as food packaging, costume masks, medical application and so on. One very important application that has been under development is the use of plastic films for aesthetic purposes. These decorative film laminates, as the title suggests, are composed of multilayer plastic films and can have different appearances from metallic to a glossy blackout finish to a wood grain. The multilayered structures include a clear coat or pre-mask layer, a backing/substrate layer and possibly an adhesive layer (mostly using pressure sensitive adhesives). Figure 1-1 shows a conceptual construction of such films (Poole, 2007).

|                                     |
|-------------------------------------|
| Clear Coat (Film)                   |
| Backing (Primary Substrate)         |
| Adhesive and/or Secondary Substrate |

**Figure 1-1.** Conceptual construction of a decorative film.

## **1.2. Production**

The clear coat in the film itself is either extruded or more commonly, in order to avoid appearance defects and residual stresses, is cast. Although this layer is most often glossy, it can also have textured or matte finishes as well. The materials used in clear coats are mainly polymethyl methacrylate (PMMA), polyvinylidene fluoride (PVDF), polyurethanes (PU) or polyethylene terephthalate (PET). However, each company has their own proprietary mixtures for these polymers which include additives to obtain the desired finish and characteristics. Different pattern can be applied to this layer. Finishes from wood grain to other natural finishes such as marble can be typically achieved by gravure printing. A metallic appearance like coloured clear coats can be achieved with pigments. The decorative layer under this clear coat is protected from weathering.

Depending on the applications of these films the next layer in its construction can vary. The backside of the decorative layer can be either a substrate or an adhesive layer. The substrate is normally much thicker and used to give the whole sandwich support. Commonly used substrates are thermoplastic olefins (TPO), polycarbonate (PC), or acrylonitrile butadiene styrene (ABS). The film and substrate in such a case are molecularly associated to one another to form a permanent construction. Alternatively, depending on the composition of the substrate and/or provide flexibility in end use, an adhesive layer is applied instead to the decorative layer. Some example applications to show the selection of adhesive layer versus permanent substrate are highlighted below (Poole, 2007).

### **1.3. Applications:**

#### **1.3.1. Decals and Tapes:**

One use of decorative film laminates is in the production of pressure sensitive decals. This is the case where a pressure-sensitive adhesive layer on the backing layer is used instead of a permanent substrate. At the time of the application, a backing which protects the adhesive is removed and the decal is placed on the part which now acts as the substrate. Application of pressure activates the adhesive system. These laminated parts can go through forming to mold into various shapes. These structures are widely used in commercial graphic applications, automotive parts, and even have construction purposes.

#### **1.3.2. Extrusion Lamination:**

In this method of application, the decorative film is brought into contact with an extruded substrate immediately after the die. This is very fast-growing method especially for the parts that are hard to paint or mask, such as automotive roof strips and window seal trims.

#### **1.3.3. In-Mold Forming:**

Another popular use of decorative films is referred to as In-Mold Forming (IMF). In the process, the decorative film with a thin substrate is placed into the mold cavity of an injection molding machine and then the mold is closed. Molten polymer is injected into the mold on the backside of the substrate (so the structure and appearance of the film is preserved), to create a thicker walled final part. A melt bond is established with the

laminate and when the cooled part exits the mold the decoration is already attached to it. This method is used for parts that have fairly simple shapes because the film should be stretched by the molten resin, so it cannot experience high amounts of strain. One example for this method is the production of cell phone cases.

#### **1.3.4. Thermoforming:**

For this process the substrate should be thicker than other methods already described because it should provide support for the completed part. In this method the laminate is heated to above the glass transition temperature until it softens but does not melt. Then the softened sheet is pulled on top of a mold to take its form. This is done through either by applied vacuum (vacuum forming) or using high pressure air to push the sheet against the mold walls (pressure forming) or a mixture of the two. This method is mostly used to make different components like casings for exercise equipment and chrome bumpers for heavy truck industry.

Sometimes the In-Mold Forming and Thermoforming methods are combined to make more complicated shapes. Laminates are first thermoformed and then placed into the mold cavity of the injection molding device and then processed as it was described previously. This application has a wide range of uses from computer housings to automotive body parts. This method is called Insert Injection Molding (IIM) (Poole, 2007).

## **1.4. Market:**

The automotive industry is the biggest user of these laminates. With increasing demand for more decorated automobile interior as well as exterior trims, automotive manufacturers feel the urge to fulfill this demand at no extra cost. Being versatile as to patterns and finishes, these decorative films made it possible to have finishes like chrome or wood without actually paying for the real components (or suffering their deficiencies). Another consequence of using these films is that the car company can ask different suppliers for different exterior parts without worrying about color mismatch, since all these suppliers can use the same film product.

Having been used in the automotive industry for a long period, these films are also now securing large markets in various other fields such as furniture, computers and cell phone, and medical devices or basically any industry that uses painting, plating and hydrographics.

## **1.5. Benefits:**

### **1.5.1. Economic:**

For a manufacturer there are mainly three ways to add the capability to make various plastic products with decorative appearance. The first option is to add a production line itself within the company grounds which requires a large area in the plant. Another problem with that is the fact that no matter if we are talking about adding a paint line, chrome plating line or a hydrographic line, they all need a major capital expenditure.

The second option is to send the parts away to another company which specializes in that field. This in turn adds a major shipping cost. Besides, the company is sending good part to another company and the only thing they can do is to hope to get a coated part with the same quality.

The third option is to use pressure-sensitive or hot melt decals/tapes. They only add the cost of product, and for thermoformers it only needs a commitment to cleanliness and some time to familiarize itself with the process. For injection molders adding IMF needs only a small amount of investment and thermoformed inserts can be provided by IIM suppliers. Moreover, these films are all thermoplastics which can be stripped from a defective part, and the part can be then be reground and re-used in most cases, as opposed to coatings that are thermosets and cannot be placed back in the manufacturing line.

### **1.5.2. Environmental:**

With increasing awareness in regards to environmental issues and sustainability, the criteria for a “clean” industry are becoming mandatory. According to a study conducted by an environmental consulting firm on automotive exterior painting options, paint spray produces 95% more volatile organic compounds (VOCs) than paint films do. Chrome plating, on the other hand, is an even larger threat to the environment due to the concern of dispensing heavy metals (mainly hexavalent chromium) while plating. According to Occupational Safety and Health Administration (OSHA) the most recent exposure requirement is less than 5 micrograms per cubic meter in 8 hours. This fact causes the chrome plating lines to mandate a costly volatile and solvent recapturing unit and monitoring systems for their lines. Besides, there is always the risk of apparatus

failure or accidents. Meanwhile, chrome-looking decorative films have the same finish without actually taking the risk of using that compound.

Another issue with paint spray or “dipping” process in chrome-plating and hydrographics is the waste. Extra paint will be a waste if there is no more parts to be painted. So is the issue with “dipping” parts in hydrographics or chrome-plating. This is not a concern when it comes to decorative laminates.

The other fact about decorative laminates is that they weigh much less than their much heavier counterparts. Using these light components in a car results in a lighter car which in turn reduces fuel consumption and in turn the gas emissions (Poole, 2007).

### **1.6. Motivations:**

Considering all the facts that were mentioned earlier there is great driving force to make the best use out of these films. However, nowadays all these methods are progressing with limited knowledge. Previously, the part was made and then these films were applied on top manually. To make the process more automated it would be more prudent to laminate the decals/tape on a plastic substrate and then thermoform or IMF them into the intended parts. During preliminary trials in our research group to look at formability, however, a wrinkling defect was observed in the sections of the molded part that were not highly strained. This observation triggered an incentive to find the cause. The purpose of this work is to find out whether this phenomenon was reproducible and what was causing this surface instability.

In this study we will be focusing on the kinetics of wrinkle growth, what causes them and why. A major part of this thesis will focus on the effects of heating and cooling

rates (as these are important to polymer processing operations) and also the effects of different secondary substrates on the wavelength of the wrinkles, their pattern and surface roughness of the film.

---

---

## ***CHAPTER II:***

### ***Literature Review***

---

---

### ***2.1. Introduction***

Wrinkled materials can have many different applications such as smart adhesion (E. Chan, Smith, Hayward, & Crosby, 2008), stretchable electronics by inorganic semiconductors (Kim & Rogers, 2008), one- and two-dimensional micro/nanochannel networks (Y. Mei, Kiravittaya, Harazim, & Schmidt, 2010), wrinkled surfaces as microfluidic sieves (Efimenko et al., 2005) and also wrinkle-based metrology. However, the application garnering most interest in published literature at this moment is their use in the measurement of mechanical/rheological properties for thin polymeric and metallic films which might not be possible using other methods such as nano-indentation (Espinosa, Prorok, & Fischer, 2003), strip bending test (Oliver & Pharr, 1992), blister test (Xiang, Chen, & Vlassak, 2002) or micro tensile test (Sharpe, Yuan, & Edwards, 1997), when it comes to nano-scale films (H. Choi et al., 2010). The models used to estimate said properties will be discussed later in this chapter.

Several techniques have been used to create ordered structures at micro- or nano-scales within thin films in order to study wrinkling at this scale. Bowden *at al.* (Bowden, Brittain, Evans, Hutchinson, & Whitesides, 1998) thermally expanded a polymer substrate and deposited metal films upon it. Upon cooling, the metal films wrinkled

instantly. They were able to produce complex patterns using this technique. They were also able to produce similar patterns using photochemically modified planar polymer surfaces (Huck et al., 2000), or other people by plasma oxidation of an elastomer (Bowden, Huck, Paul, & Whitesides, 1999; Chua, Ng, & Li, 2000). Wrinkling was also produced in other thin-film structures such as oxide-covered silicon using laser (Lu, Choi, Aoyagi, Kinomura, & Fujii, 1996; Serrano & Cahill, 2002); from relaxation of compression strained SiGe islands on glass (Hobart et al., 2000; Yin et al., 2002); preparing a polypyrrole electrode for electrostrictive polyurethane actuators (Watanabe, Shirai, & Hirai, 2002); making elastic, stretchable metal interconnects to fabricate 3D electronic circuits (Jones, Lacour, Wagner, & Suo, 2003; Lacour, Wagner, Huang, & Suo, 2003); and thermal oxidation of  $\alpha$ -alumina at high temperatures (Tolpygo & Clarke, 1998).

Although these wrinkles can have many different applications, there are so many other situations in which these surface instabilities are not welcome. These instabilities can have two different modes, buckle-delamination and wrinkling, as shown in Figure 2-1. In the former mode, the primary substrate is stiff so it does not deform concurrently with the film, thus buckling results in partial delamination of the thin film from the primary substrate (Gioia & Ortiz, 1997; Hutchinson, Thouless, & Liniger, 1992), while the latter considers no delamination as the primary substrate coherently complies with deformation of the thin film (Groenewold, 2001; Z. Y. Huang, Hong, & Suo, 2005). The difference between these two modes are visually perceptible, while buckle-delamination

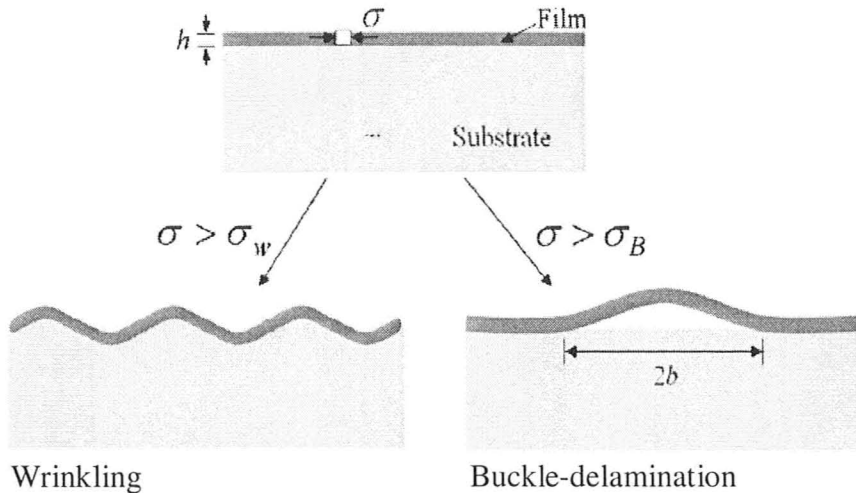


**Figure 2-1.** Different modes of interfacial failure in thin films.  $\sigma_B$  and  $\sigma_w$  are corresponding critical stresses and are given by equations 1 and 2, respectively (H. Mei, Huang, Chung, Stafford, & Yu, 2007).

is normally associated with localised patterning, wrinkling follows a more homogeneous pattern (H. Mei et al., 2007).

The basic mechanism of wrinkling is considered to be a stress-driven instability following the classical Euler buckling of a compressed column, conceptually (R. Huang & Im, 2006). The film buckles in order to minimise the elastic strain energy and the buckling mode depends on the substrate (H. Mei et al., 2007). There have been a considerable number of studies on residual surface stress and their relation to surface instabilities for different composites, which will be discussed in the next section. It should be noted that most of the studies to be discussed are metal films on a soft compliant substrate with few mentions of wrinkling in polymeric thin films.

## **2.2. *Origins of Wrinkles: Residual Stress***

Residual stresses are non-dissipated concentrations of stress retained in the structural ordering of a material after manufacturing and without any external force applied (Cheng, W., Finnie, I., 2007). Such stresses are unavoidable by the normal practices of fabricating engineering components and, depending on the differences in thermal expansion coefficients between the materials, can become quite large (Withers & Bhadeshia, 2001b). Residual stresses can develop in at least four different ways: either by the interaction between misfitting components in an assembly, or through misfits that are induced either chemically, thermally or plastically in different regions of one part (Withers & Bhadeshia, 2001b). Thermally produced residual stresses are either macroscopic or microscopic. Macroscopic thermal residual stress is produced as a result of non-uniform heating or cooling while microscopic thermal stress develops as a result of difference in the thermal expansion coefficient of constituent layers of the material (Fernández, Bruno, & González-Doncel, 2004). The residual stresses at the surface of a material can be either compressive (denoted with a negative sign) or tensile (denoted by a positive sign) depending on the molecular arrangement of the surface (Orowan, 1970). Orowan (Orowan, 1970) expressed that a strong compressive surface stress may result in buckling and cause the outermost layer of the surface to wrinkle in order to relieve the surface pressure. Andreussi and Gurtin (Andreussi & Gurtin, 1977) showed the possibility of wrinkle development in an elastic half-space in the presence of a compressive residual stress. Murdoch (Murdoch, 1978) examined the effects of compressive surface stress on an infinite circular cylinder in regards to surface wrinkling.

It has been understood that the residual stress can have a great influence on the mechanical performance of the material such as static and fatigue strengths, fracture toughness and corrosion/wear resistance. Therefore, the reliability and lifetime of the part directly depends on these stresses which can be detrimental or beneficial (Jang, 2009). As an example, Cheng and Finnie (Cheng, W., Finnie, I., 2007) expressed that tensile residual stresses are destructive to the fatigue life of a part which experiences cyclic loads. On the other hand, a compressive residual stress is quite favourable improving the crack propagation resistance of the part due to stress-corrosion. Chng *et al.* (Chng, Curtin, Tay, & Lim, 2008) through a discrete dislocation (DD) study mentioned that when the residual stress is large enough to cause plastic flow in the film, the DD model predicts the fracture toughness to be far less compared to a zero-stress case. Yang in (Yang, 2004; Yang, 2006) also mentioned that the effective bulk modulus of the composite in his experiments was a function of surface energy.

Due to all these issues, it was of utmost importance for the engineers to quantify this residual stress in order for the designs to be more precise and less prone to failure. There are different ways to measure mechanical stresses. These methods monitor the changes in the components deformation either during the generation of residual stresses or afterwards, by removing the material deliberately to allow the stresses to relax (Clyne & Gill, 1996; Flavenot, 1996).

### **2.2.1. Measurement of residual stresses**

Wrinkling is a special phenomenon for bilayer and multilayered constructions where changes in the residual stress state of different materials across an interface is

rigidly constrained by one of the layers. If the constraining layer is compliant relative to the other then the system will not buckle but rather incur a bending moment instead, which is a more common phenomenon of concern to industry. Curvature measurement is, therefore, one of the most common techniques to estimate the residual stresses of coated and multi-layered constructions (Clyne & Gill, 1996). The bending moment causes the material system to curve. The change in curvature makes it possible to evaluate the variation in stress as a function of the deposited layer thickness (Withers & Bhadeshia, 2001a). Curvature might be measured through contact methods like profilometry or strain gauges, or non-contact methods such as image analysis, laser displacement scanning or double crystal diffraction topology (J. Choi, Kim, & Yoon, 1992). Hole drilling is another method in which a hole is drilled into the sample around which the strain is measured through either a rosette of strain gauges (Sasaki, Kishida, & Itoh, 1997), interferometry based on a rosette of indentations (Keyu, 1997), or holography (Makino & Nelson, 1997; Nelson, Makino, & Fuchs, 1997). Another method for measuring residual stresses is the *compliance method* in which a small section of the sample is cut and monitored for the relaxation of stress near that crack using strain gauge interferometry (Y. Y. Wang & Chiang, 1997). Xu *et al.* (Xu, Zhao, & Yue, 2006) used indentation to measure residual surface stress having assumed that the yield stress of the material was already known, a technique growing in interest within the academic community. Various other methods have also been reported with lesser acceptance including diffraction methods (e.g. electron, laboratory X-Ray or neutrons) or magnetic and electrical techniques (Withers & Bhadeshia, 2001a). When it comes to thin composite films and coatings it can be said that

this residual stress is almost always present due to the fact that the layers consist of different materials with different properties such as their linear thermal expansion coefficient (LTEC) and elastic modulus (Withers & Bhadeshia, 2001b). As for measurement methods, most commonly used ones for these thin films are curvature and X-ray methods (Perry, Sue, & Martin, 1996), however, some other methods including Raman spectroscopy have also been used (Gheeraert, Deneuille, Bonnot, & Abello, 1992). As a comparison between curvature method of evaluating residual stress versus X-ray, Malhotra *et al.* (Malhotra, Yalisove, & Bilello, 1997) found that the curvature methods underestimate the level of stress. It is said to rise from the fact that the curvature methods measure the extrinsic stress while X-ray methods might be influenced by intrinsic or texture effects. Noyan *et al.* (Noyan, Huang, & York, 1995) had similar comments on this issue. Multilayer films are similar to composite films as the layer thickness can be comparable. The curvature method will not be practical in this case because the total stress on different layers may balance and do not cause the whole system to bend. The X-ray method, on the other hand, can measure either the stress on the top layer only or the average of all the layers, depending mainly on the thickness of the layers (Withers & Bhadeshia, 2001b). Additionally, there have been studies on the use of surface wrinkling in order to measure residual stress for thin films that will be discussed later in this Chapter.

### **2.3. Wrinkle Formation**

The necessity to minimize the elastic energy controls the growth and wavelength of the wrinkles. In terms of energy, wrinkles with large wavelengths increase the strain

energy of the substrate therefore pushing the whole system into instability. On the other hand, wrinkles with small wavelengths cause the bending energy of the film to increase which in turn, again, leads to instability of the system. Therefore, film wrinkling is a way to reduce the compressive stress. If this stress is less than the critical value (Eqn. 2-2), regardless of the stage, the elasticity of the substrate prevents further development of the wrinkles. Considering that this substrate elasticity can also prevent wrinkles from forming from the beginning, it can be concluded that substrate elasticity has an impact on the wrinkling in more than one way: preventing the wrinkles from forming for small stress ( $\sigma_0 < \sigma_c$ ) at the early stage, and stabilizing the wrinkle structure at a given stage by preventing the further development of the wrinkles (Shugurov & Panin, 2010).

The structure of the wrinkles depends on the direction and isotropy of the stress. Under uniaxial compression of the film stripes form perpendicular to the direction of the stress. Under biaxial compression various structures might be seen but mainly they would be either labyrinth or zigzag herringbone structure (Shugurov & Panin, 2010). The two latter structures are dependant on whether the compression is isotropic or anisotropic. If the stress is anisotropic, either stripes or ordered herringbone zigzag patterns will form. Herringbones and labyrinth patterns have the same energy level, but because there are far more disordered configurations than ordered ones for isotropic stress, labyrinth pattern will form. In both cases, however, the zigzag pattern selects the width, length and the elbow angles to minimize the compressive stress (Z. Huang, Hong, & Suo, 2004). Figure 2-2 depicts these different structures.

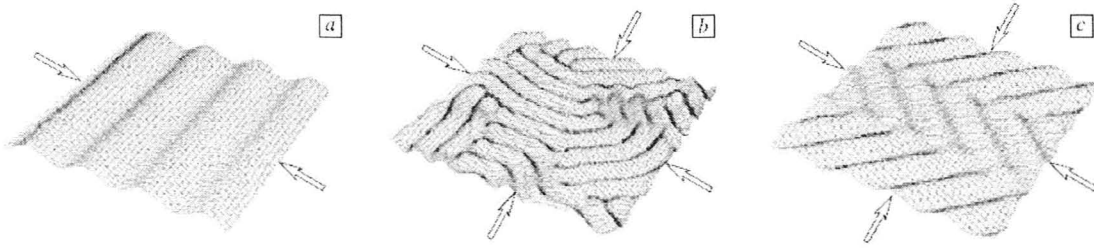


**Figure 2-2.** Three different patterns due to different compression stresses. (a) uniaxial stress causing stripes, (b) labyrinth structure under isotropic biaxial compression and (c) herringbone structure under anisotropic biaxial compression (Shugurov & Panin, 2010).

Herringbone and labyrinth patterns basically result in the same level of system energy. This is lower than that of the striped pattern since the stripe pattern relieves the energy in one direction while the herringbone pattern relieves it in both directions. Figure 2-3 shows the energy level of each of the patterns. The Labyrinth is basically disordered herringbone and they relieve the film compression in all directions. (Z. Huang et al., 2004).

Huang *et al.* (Z. Huang et al., 2004) studied the effects of different compressive strains at one direction ( $\epsilon_{22}$ ) while maintaining that for the other direction ( $\epsilon_{11}$ ). They maintained  $\epsilon_{11}$  at -0.035 and changed  $\epsilon_{22}$ . When  $\epsilon_{22}$  was equal to  $\epsilon_{11}$  the compressive stresses were isotropic therefore a labyrinth pattern formed (not shown in Figure 2-4) when  $\epsilon_{22} = -0.027$ , the symmetry was disturbed, hence a herringbone pattern formed with elbow angles of almost  $90^\circ$ . When the value of  $\epsilon_{22}$  was reduced to -0.02 and -0.018 herringbones still formed but with an obtuse elbow angle. However, when  $\epsilon_{22}$  was further reduced to -0.015, only stripes formed. The trend is shown in Figure 2-4. In the grey scale used, a bright spot represents a crest and dark spots represent troughs.

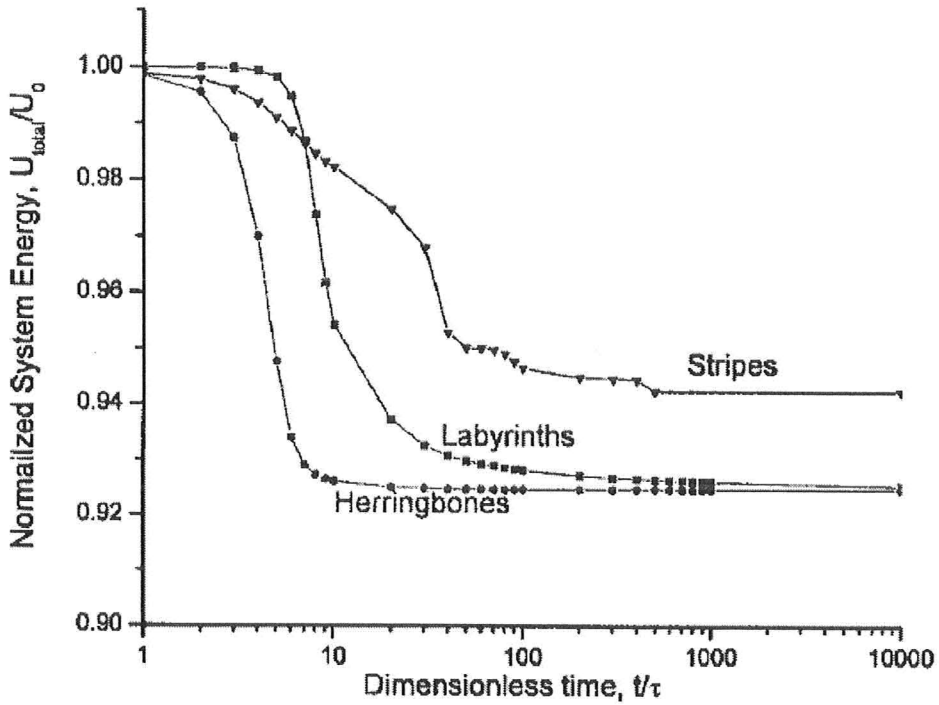


Figure 2-3. Energy level of three different wrinkling patterns (Z. Huang et al., 2004).

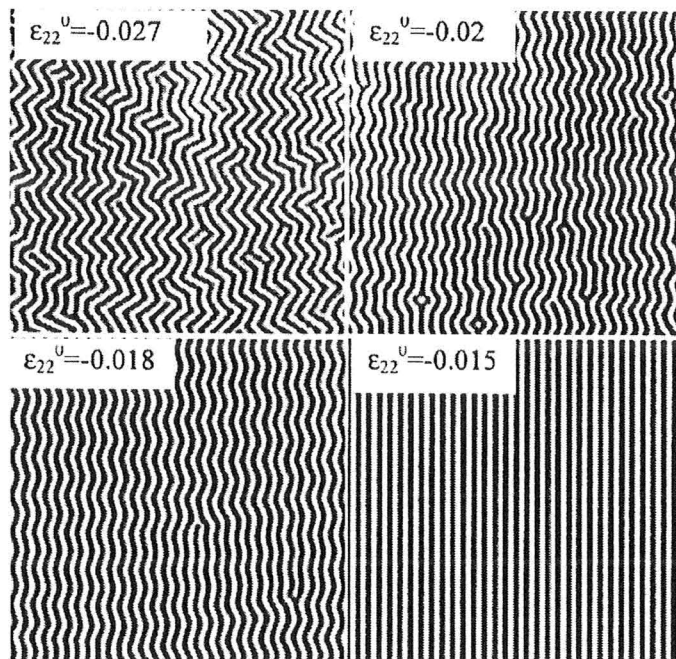
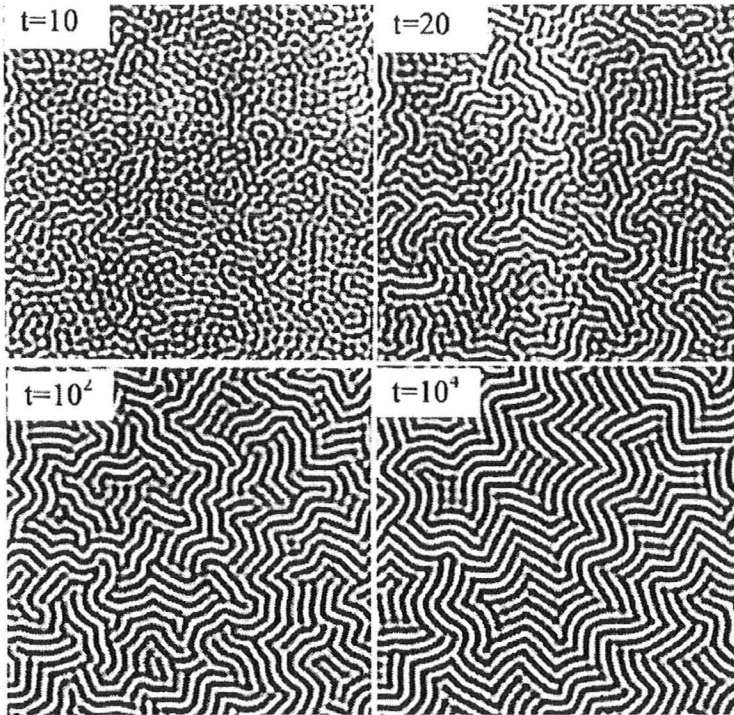


Figure 2-4. Stabilized patterns under different biaxial compression stresses (Z. Huang et al., 2004).



**Figure 2-5.** Evolution of the wrinkles at different times.  $\epsilon_{11} = \epsilon_{22} = -0.02$  at all times (Z. Huang et al., 2004).

Huang *et al.* (Z. Huang et al., 2004) also studied the evolution of wrinkles under equi-biaxial compression stress leading to the labyrinth patterns shown in Figure 2-5. When the strain was small, crests appeared like small blisters. A large deflection disturbed the symmetry and the crest bent in just one direction. The segments evolved to the equilibrium wavelength and pattern and finally formed the labyrinth pattern with lengths quite a few times larger than the equilibrium wavelength.

## **2.4. Quantification of Wrinkling**

The characteristic variables of wrinkling are its amplitude and periodicity (wavelength). The latter is most commonly a required variable of the different models following this section in order to estimate mechanical and/or rheological properties of the films. Therefore, it is necessary to briefly describe the different methods researchers have utilized for its measurement. The early measurements of the surface roughness started a couple of decades ago with the invention of tactile profilometers. This technique has certain shortcomings, for example; the stylus tip could deform the surface and also it only gave a 2D (single line) trace, missing data in the unscanned areas (Yao & Xu, 2007). Nevertheless, some people have used the technique such as Chan *et al.* (E. Chan & Crosby, 2006) to evaluate 2D surface profile of their microlens arrays. In the recent years with the advent of advanced 3D sensors, a variety of non-contact optical methods were developed to quantify surface roughness. The important advantages to these optical methods are their non-contact approach, 3D profile output and high acquisition speeds. Some of the commonly used sensing techniques under this method are laser scattering (S. H. Wang, Quan, Tay, & Shang, 2000) and white-light interferometry (Windecker & Tiziani, 1999). Grove *et al.* (Grove, Grove, & Leyden, 1989) also used digital image processing to quantify the surface topology as well as wavelength of silicon rubber impressions of facial wrinkles. They registered wavelength as well as used commonly employed averaging expressions for peak-to-valley variation, namely Rz and Ra values, for surface roughness. In this study, white-light interferometry was used in order to measure surface roughness and the wavelength.

## 2.5. Modeling

As stated earlier, the formation of wrinkles in compressively stressed films can be used to evaluate its mechanical properties. Different people including but not limited to Stafford (Stafford, Vogt, Harrison, Julthongpiput, & Huang, 2006), Torres (Torres, Stafford, & Vogt, 2009), Tahk (Tahk, Lee, & Khang, 2009) and Nolte (Nolte, Rubner, & Cohen, 2005; Nolte, Cohen, & Rubner, 2006) have used the technique to estimate the modulus of their films. To simplify the analysis they assumed wrinkling in their materials systems (normally not plastics) was an elastic response to intrinsic stresses. In such a case, the following equation is suitable for that purpose:

$$\bar{E}_f = 3\bar{E}_s \left( \frac{\lambda}{2\pi h_f} \right)^3 \quad (2-1)$$

with  $\bar{E}_f$  and  $\bar{E}_s$  ( $\bar{E} = E/(1-\nu^2)$ ) being the plane-strain moduli of the film and the primary substrate, respectively, and  $\nu$  the Poisson's ratio and  $h_f$  the film thickness.

Film

Primary (compliant) Substrate

Secondary (rigid) Substrate

**Figure 2-6.** Schematic figure representing the film and two different substrates. Thickness ratios are taken into account.

There have been different studies (mostly modeling) of a thin film with elastic, viscous and viscoelastic primary substrates. Here we spend some time briefly discussing each case. Since there have been different terminologies, it is necessary to establish a universal terminology to avoid confusion in this thesis. In all cases there is a film lying on top of a compliant substrate which in turn sits on a rigid substrate. Here we call the compliant substrates as the primary substrate and the “rigid” substrate as the secondary substrate, and wherever we mention substrate it denotes the primary substrate. This terminology will be employed for both experimental and modeling sections in the reporting of data in this thesis. Figure 2-6 shows a schematic of this sandwich.

### 2.5.1. Elastic film/Elastic primary substrate

For an elastic film/substrate combination interfacial instability is limited by the substrate; therefore, in order for the wrinkling to happen, the substrate needs to be relatively compliant (H. Mei et al., 2007). Huang *et al.* (Z. Y. Huang et al., 2005) studied the case of a thin elastic film on a compliant substrate to derive an equation for the critical wrinkling stress. Based on energetics analysis they suggested the following equation for wrinkling critical stress ( $\sigma_c$ ) (Z. Y. Huang et al., 2005) and stated that when the compressive stress is greater than this value, wrinkles form and establish a particular wavelength in order to minimise the elastic energy in the film and the substrate.

$$\sigma_c = \frac{\bar{E}_f}{4} \left( \frac{3\bar{E}_s}{\bar{E}_f} \right)^{2/3} \quad (2-2)$$

However, this will not be the case for less compliant substrates. In that situation, buckling deformation is extremely restricted which causes areas with greater stress concentration to form. This stress may be relieved by a localized partial delamination, hence buckling of the film, which in turn causes development of interfacial fracture (Gioia & Ortiz, 1997; Hutchinson et al., 1992). Hutchinson *et al.* (Hutchinson et al., 1992) studied the case of a rigid substrate and suggested the following equation for the critical stress for the onset of buckling ( $\sigma_{B0}$ ) based on certain assumptions:

$$\sigma_{B0} = \frac{\pi^2}{12} \left( \frac{h}{b} \right)^2 \bar{E}_f \quad (2-3)$$

where  $h$  and  $b$  were previously defined in Figure 2-1. However, Yu *et al.* by taking the elastic deformation of the substrate into account derived an implicit equation which

showed that the critical stress for buckling can be considerably lower than that predicted by Hutchinson *et al* (Hutchinson et al., 1992):

$$\sqrt{\frac{\sigma_{B0}}{\sigma_B} \tan\left(\pi \sqrt{\frac{\sigma_B}{\sigma_{B0}}}\right)} = \frac{\pi h}{12b} \left( \frac{a_{12}^2}{b/h + a_{11}} - a_{22} \right) \quad (2-4)$$

with  $a_{11}$ ,  $a_{12}$  and  $a_{22}$  being calculated numerically. Mei *et al.* (H. Mei et al., 2007) presented a graph to compare the critical stresses for two types of buckling. The graph shows the trend by which each of these stresses behave based on the delamination size ( $b/h$ ) and also the relative stiffness. They also defined a critical stiffness ratio ( $R_c$ ) as the intersection of the lines indicating the critical stresses. This value is used to predict whether buckle-delamination or wrinkling would occur. For compliant substrates  $\bar{E}_f / \bar{E}_s$  is smaller than  $R_c$  and according to the graph the wrinkling stress is lower than the buckling stress, therefore, the film wrinkles. Otherwise holds true, as well. Figure 2-7 illustrates this graph.

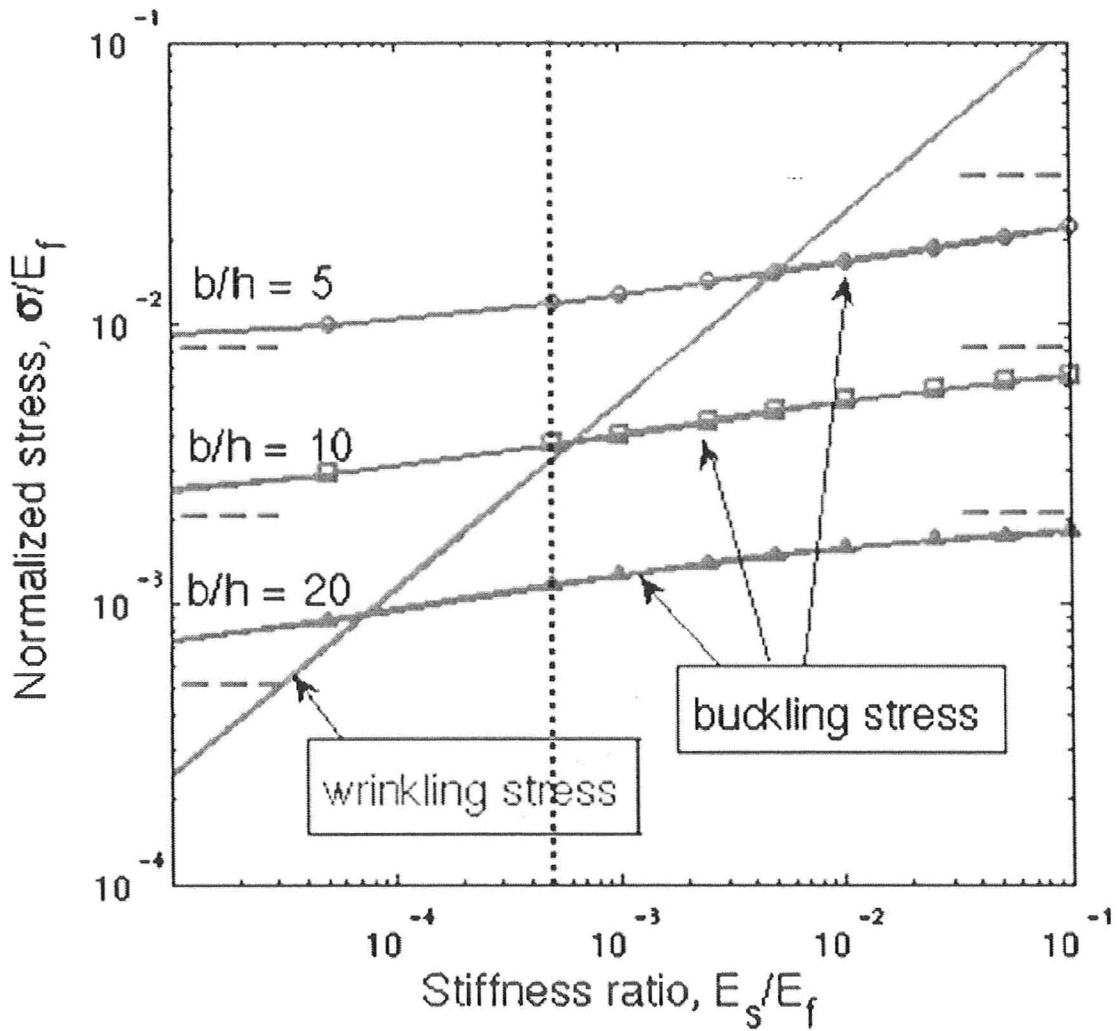


**Figure 2-7.** Critical stresses for two different modes of buckling. The hollow signs are numerical values calculated through Eqn. 2-4 for different delamination sizes ( $b/h$ ). The dashed lines are the minimum stress for buckle-delamination and the vertical line is the specific PS/PDMS system under experiment with  $\bar{E}_f / \bar{E}_s = 0.0005$ . (H. Mei et al., 2007)

Since the critical stiffness ratio is a function of delamination size, Mei *et al.* (H. Mei et al., 2007) also came up with a graph depicting this trend. The plot shows a “*buckling mode selection map*”. So if the intersection of the stiffness ratio and the delamination size end up above the curve for  $R_c$ , buckle-delamination occurs. Otherwise, wrinkling is

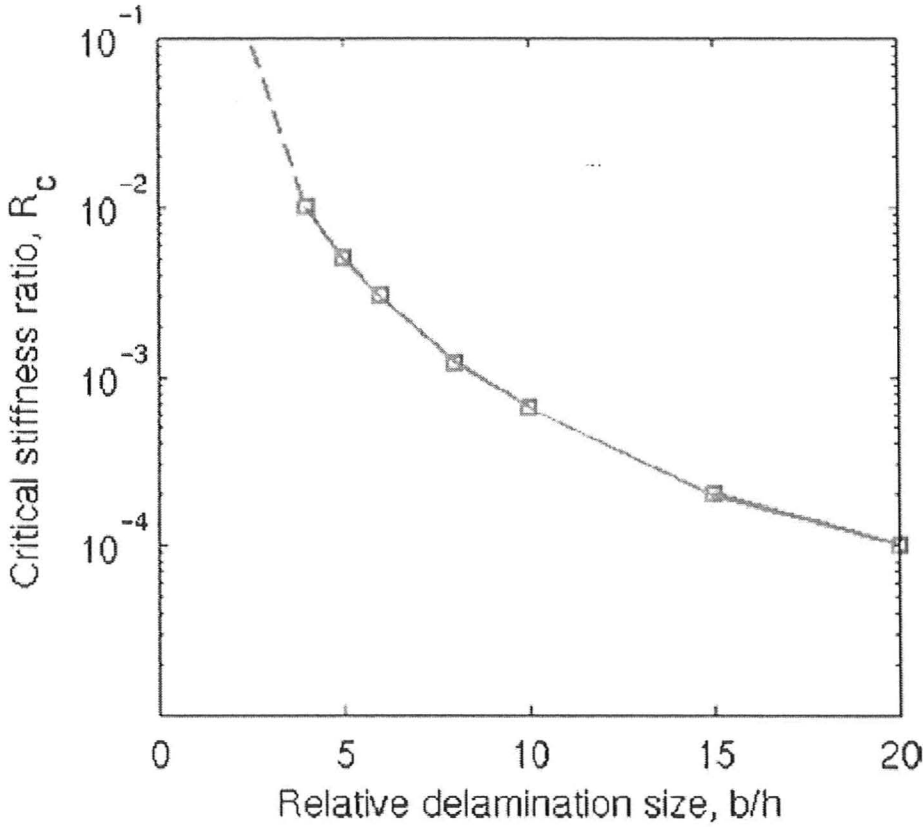


**Figure 2-8.**  $R_c$  as a function of delamination size. The curve defines a border below which wrinkling is favored, above which buckle-delamination (H. Mei et al., 2007).

favoured. This plot is shown in Figure 2-8. Since buckle-delamination is not part of this study, we do not go for more details in that and from now on we focus on wrinkling.

Huang *et al.* (R. Huang, 2005) also came up with equilibrium amplitude for the wrinkles based on an approximation made in using the average membrane force.

$$A_{eq} = \frac{2\sqrt{1-\nu_f^2}}{k} \left[ -\frac{\sigma_0}{E_f} - \frac{(kh_f)^2}{12(1-\nu_f^2)} - \frac{2}{\gamma_{22}} \frac{E_s}{E_f} \frac{1}{kh_f} \right] \tag{2.5}$$

$\nu_f$ ,  $h_f$  and  $E_f$  are Poisson’s ratio, thickness and elastic modulus of the film respectively.

$k=2\pi/\lambda$  is the wavenumber and  $E_s$  is the elastic modulus of the substrate.  $\gamma_{22}$  is a

dimensionless coefficient related to Laplace transform of the Poisson's ratio of the substrate (R. Huang, 2005). The stability of the film depends on the three terms in the bracket of Eqn. 2-5. For a compressed film ( $\sigma_0 < 0$ ) the first term is positive and promotes the wrinkling to relax the in-plane compression. The second and third terms are always negative and deprecate small wavelengths due to flexural rigidity of the film and long wavelengths because of elastic constraint of the substrate, respectively.

### 2.5.2. Elastic film/Viscous substrate

Other studies were carried out by Huang *et al.* (R. Huang & Suo, 2002a; R. Huang & Suo, 2002b) for an elastic thin film on a compliant viscous substrate which in turn lies on a secondary "rigid" substrate. The schematic of this sandwich is shown in Figure 2-9. Through linear perturbation analysis they determined a critical wavenumber and the growth rate for unstable modes of wrinkling. They considered both effects of deflection and in-plane extension in the kinetics of wrinkling since they were inherently coupled. As they stated in (R. Huang & Suo, 2002b): "*...the flow conserves the volume of the viscous layer and the deflection relaxes the compressive stress in the elastic film.*"

They first used nonlinear theory of thin plate subject to in-plane and out-of-plane loads to model the elastic film and the theory of lubrication (Reynolds, 1886) to model the viscous layer and because of the latter they had the limiting assumption that the thickness of the viscous layer,  $H$ , is small compared to the wavelength of the wrinkles (R. Huang & Suo, 2002b). Based on that they derived the following equations for Critical wave number,  $k_c$ :

$$k_c h_f = \sqrt{-12\varepsilon_0(1 + \nu_f)} \quad (2-6)$$

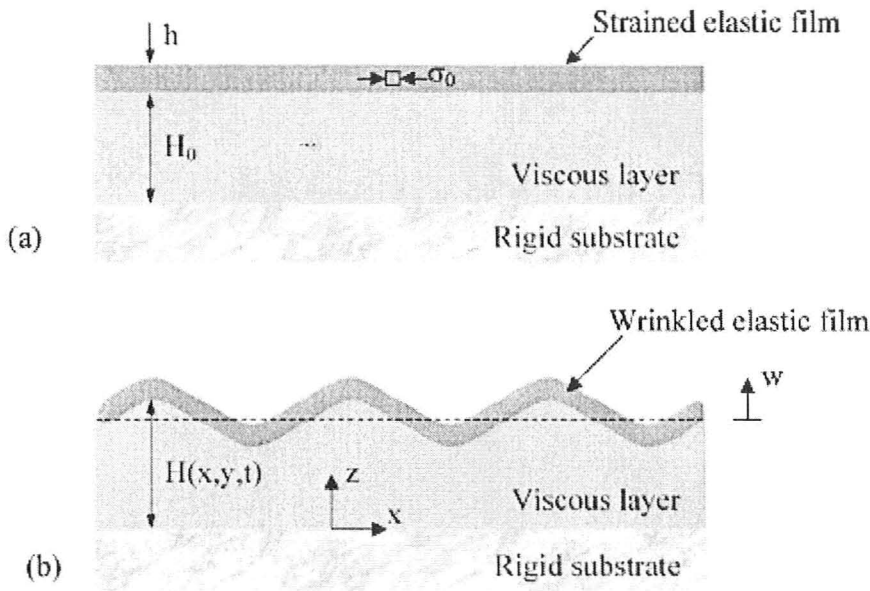


**Figure 2-9.** Schematic structure of an elastic film on a viscous layer which lies on a rigid substrate. a) Equilibrium state, film is flat and biaxially stressed, b) Wrinkled film (R. Huang & Suo, 2002b)

In a more recent paper, Huang *et al.* (R. Huang & Suo, 2002a) presented a more rigorous analysis that was no longer limited by the range of thickness and with the new analysis they came up with the same equation for the critical wavelength. However, Im *et al.* (Im & HUANG, 2005) noted that this critical wavelength should be equal to:

$$\lambda_c = \pi h_f \sqrt{\frac{E_f}{3(1 - \nu_f^2)\sigma_0}} \tag{2-7}$$

Huang *et al.* (R. Huang, 2005) mentioned that the wavelength is independent of whether the substrate is viscous or viscoelastic and came up with the fastest growing wavelength as:

$$\lambda_m = \pi h_f \sqrt{\frac{E_f}{(1-\nu_f^2)\sigma_0}} \quad (2-8)$$

For a completely viscous substrate (i.e. viscous layer that does not store any elastic energy) the film wrinkles at any given compressive stress and the wrinkling is determined by kinetics (Shugurov & Panin, 2010). The driving force of the relaxation phenomenon is provided by the elastic strain energy which in turn has two components: bending and in-plane deformation. In order to reduce the elastic energy the film wrinkles, however, upon wrinkling the film gains some bending energy. When the wrinkles develop, the strain energy as a result of in-plane deformation decreases, while the strain energy due to bending increases. However, the total strain energy decreases and reaches an equilibrium value (R. Huang & Suo, 2002b). When a film is under compression, the resultant of the energy relieved due to in-plane deformation of the film and gained through bending, defines the critical wave number. When the wave number value matches that of the critical wave number (i.e.  $k=k_c$ ) both energies are in balance and the growth rate is zero. When there is a large wave number (short wavelength,  $k>k_c$ ) the bending energy is stronger and causes the wrinkles to decrease therefore giving a negative growth rate. For deformations with small wave numbers, however, the decrease in the compression energy dominates the bending energy and causes a positive growth rate (R. Huang & Suo, 2002a).

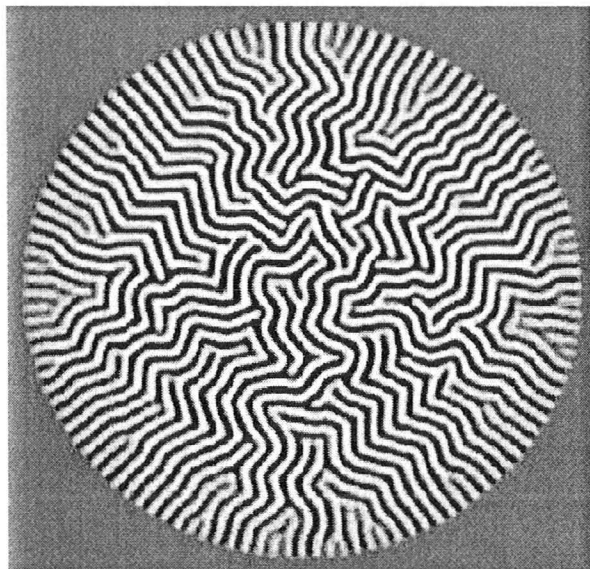


**Figure 2-10.** Different patterns of wrinkles from the edges to the center. (Z. Y. Huang et al., 2005)

Huang *et al.* (R. Huang & Suo, 2002a) also proved that the thickness ratio between the viscous layer and the elastic film does not affect the critical wave number. However, the flow of the viscous layer does affect the time scale of the appearance of the wrinkles as the growth rate is inversely proportional to the viscosity. Yin *et al.* (Yin et al., 2002) discovered that when an elastic film is laid on a viscous substrate no wrinkles are observed at the corners. However, straight stripes perpendicular to the edge appear around the edge due to edge stresses. At some distance away from the edges almost periodic zigzag pattern forms. And finally at the center of the sample where stresses are more isotropic, labyrinth wrinkles forms. Figure 2-10 is an example of a circular labyrinth wrinkled film.

### 2.5.3. Elastic film/Viscoelastic substrate

Having talked about elastic and viscous substrates, in practical experiments in which film wrinkling is observed, the substrate is usually viscoelastic. This means that the substrate first deforms in its elastic regime and then after further stress (strain) it passes this regime and enters into plastic flow. Therefore, as described earlier, in the elastic region the wrinkles are governed through energetics and in the viscous region by the kinetics of the process (Shugurov & Panin, 2010). But unlike the elastic and viscous substrate, viscoelastic substrate has a significant influence on both energetics and kinetics of wrinkling (R. Huang, 2005).

Huang *et al.* (R. Huang, 2005) studied the case of an elastic film on a viscolastic substrate which sits on top of a secondary rigid substrate. The film was under a compressive biaxial stress. Under the stress, the film deformed elastically to relax the stress and the substrate followed accordingly to keep the bond with the film at the interface. Figure 2-11 shows the schematic of this sandwich. They employed von Karman plate theory to model the elastic film. The plane-strain deformation was described by a deflection and in-plane displacement. The top surface of the film was free from any tractions while the surface bonded to the substrate experienced both normal and shear tractions.

For a viscoelastic material, the elastic modulus,  $E_s(t)$ , is a function of time where  $E_s(0) = E_{s0}$  and  $E_s(\infty) = E_{s\infty}$  are the glassy and rubbery limits for the moduli, respectively. For a typical polymer these moduli can be up to 4 orders of magnitude different. Poisson's ratio is also a function of time but due to its weak dependence it was assumed

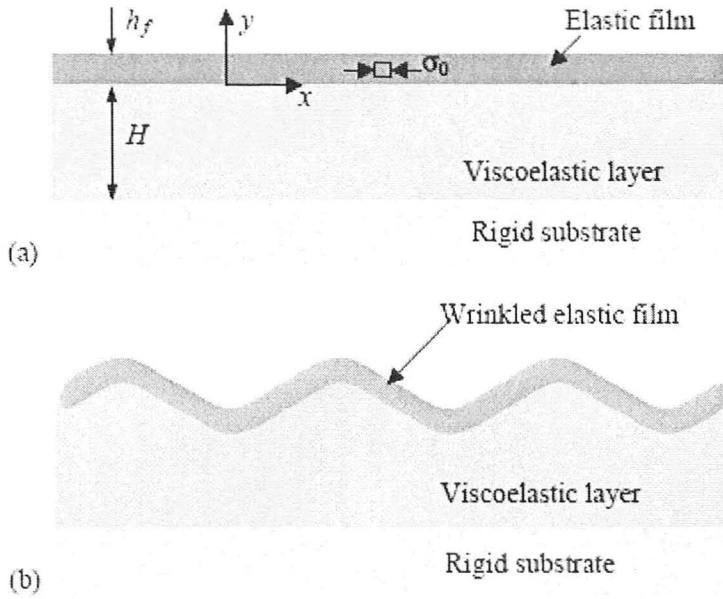


**Figure 2-11.** Schematic of an elastic film lying on a viscoelastic substrate: a) Equilibrium state; b) Wrinkled film. (R. Huang, 2005)

that it was constant. Therefore, wrinkling of an elastic film on a viscoelastic layer with these specifications becomes a kinetic process (R. Huang, 2005).

The critical stresses at these two extremes for thick substrates are as follows (R. Huang, 2005):

$$\sigma_{c0} = -E_f \left( \frac{9}{16(1 - \nu_f^2)(1 - \nu_s^2)} \right)^{1/3} \left( \frac{E_{s0}}{E_f} \right)^{2/3} \tag{2-9}$$

$$\sigma_{c\infty} = -E_f \left( \frac{9}{16(1 - \nu_f^2)(1 - \nu_s^2)} \right)^{1/3} \left( \frac{E_{s\infty}}{E_f} \right)^{2/3} \tag{2-10}$$

The difference in two critical stresses for a typical polymer is about 2 orders of magnitude. There are three different cases to study these critical stresses, first when the stress is small ( $\sigma_0 < \sigma_{c\infty}$ ), second when the stress is big ( $\sigma_0 > \sigma_{c0}$ ) and finally, the third

case when the stress has an intermediate level ( $\sigma_{c\infty} < \sigma_0 < \sigma_{c0}$ ). When the stress is smaller than the rubbery critical stress, it is obvious that the film is stable at both rubbery and glassy states. Therefore, no wrinkles will form. For the second case when the stress is larger than the glassy critical stress, wrinkles form immediately at the glassy state. As the substrate softens, the wavelength grows from the selected glassy state to the rubbery state wavelength based on the following equations (R. Huang, 2005):

$$\lambda_0 = 2\pi h_f \left[ \frac{1 - \nu_s}{6(1 - \nu_f^2)} \frac{E_f}{E_{s0}} \right]^{1/3} \quad (2.11)$$

$$\lambda_\infty = 2\pi h_f \left[ \frac{1 - \nu_s}{6(1 - \nu_f^2)} \frac{E_f}{E_{s\infty}} \right]^{1/3} \quad (2.12)$$

The wavelength normally increases by more than one order of magnitude for normal cross-linked polymers ( $\lambda_\infty/\lambda_0 \approx 20$ ). In the third case when the stress has an intermediate level, the film is quite stable in its glassy state; however, unstable in the rubbery state. They also came up with a time-dependant equation for amplitude that showed that the wrinkles developed even at the glassy state and the rate of the evolution of the wrinkles depends on the viscoelastic behaviour of the substrate:

$$A(t) = A_0 \exp \left[ \frac{\alpha E_f - E_{s\infty}}{E_{s0} - \alpha E_f} p_1 t \right] \quad (2.13)$$

where  $p_1 = E_{s0} / \eta$  and according to Im *et al.* (Im & HUANG, 2005):

$$\alpha = \frac{(1 - 2\nu_s) k^2 H h_f}{24(1 - \nu_s)(1 - \nu_f^2) k h_f} \left[ -k^2 h_f^2 - \frac{12(1 - \nu_f^2) \sigma_0}{E_f} \right] \quad (2.14)$$

They defined  $s = a - \mu_\infty / E_f$  ( $\mu_\infty$  is the elastic shear modulus of the rubbery state) and concluded that if  $s < 0$  for all wavenumbers,  $k$ , the film was stable. However,  $s > 0$  makes the bilayer unstable and perturbations start to grow to develop wrinkles. For a limiting case of a viscous substrate with a viscosity of  $\eta$  the equation reduces to:

$$A(t) = A_0 \exp\left[\frac{\alpha E_f}{\eta} t\right] \quad (2-15)$$

Im *et al.* (Im & HUANG, 2005), through numerical simulations identified three different stages in wrinkle growth; the first stage is the initial growth with the fastest growth rate, then the intermediate stage with mode transition and finally the equilibrium wrinkle state. This behaviour is not only discernible in Figure 2-12, but also is in accord with experimental observations (Yoo & Lee, 2003). As mentioned before, energetics control the wavelength in an elastic substrate while kinetics defines it for viscoelastic substrates. The important note that was mentioned by Huang *et al.* (R. Huang, 2005) is that the fastest growing wavelength does not depend on the substrate, i.e. kinetic modeling approaches the same wavelength no matter whether the substrate is viscous or viscoelastic. However, this wavelength, unlike the energetically selected wavelength, depends on the compressive stress and for a thin substrate does not depend either on the substrate's thickness or Poisson's ratio, significantly.

$$\lambda_m = \pi h_f \sqrt{-\frac{E_f}{(1 - \nu_f^2)\sigma_0}} \quad (2-16)$$

It should be noted that in a more recent paper (Im & HUANG, 2005) this equation was derived for thin substrates ( $H/h_f > 10$ ) as follows.

$$\lambda_m = \pi h_f \sqrt{\frac{2E_f}{3(1-\nu_f^2)\sigma_0}} \quad (2-17)$$

Huang *et al.* (R. Huang, 2005) mentioned the evolution of the wavelength as being dominated by the fastest growing wavelength exponentially at the early stages and then slowed down as the amplitude/film thickness ratio increased, and eventually reached an equilibrium plateau. Figure 2-12 depicts the behaviour of amplitude growth. Eventually the wavelength reaches the energetically selected value of  $\lambda_\infty$  and its corresponding equilibrium amplitude that was mentioned before.

Huang *et al.* (R. Huang, 2005) pointed out that for a thick substrate ( $H/h_f > 40$ ) when the compressive stress of the film is higher than the critical stress,  $\sigma_{c0}$ , the growth rate approaches infinity as the glassy modulus of the substrate decreases. The trend is shown in Figure 2-13.

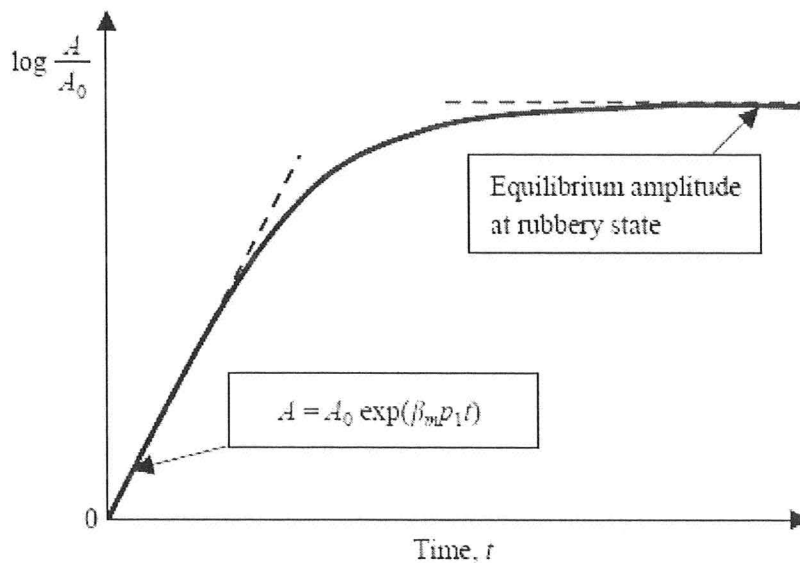


**Figure 2-12.** Schematic growth of wrinkle amplitude. (R. Huang, 2005)

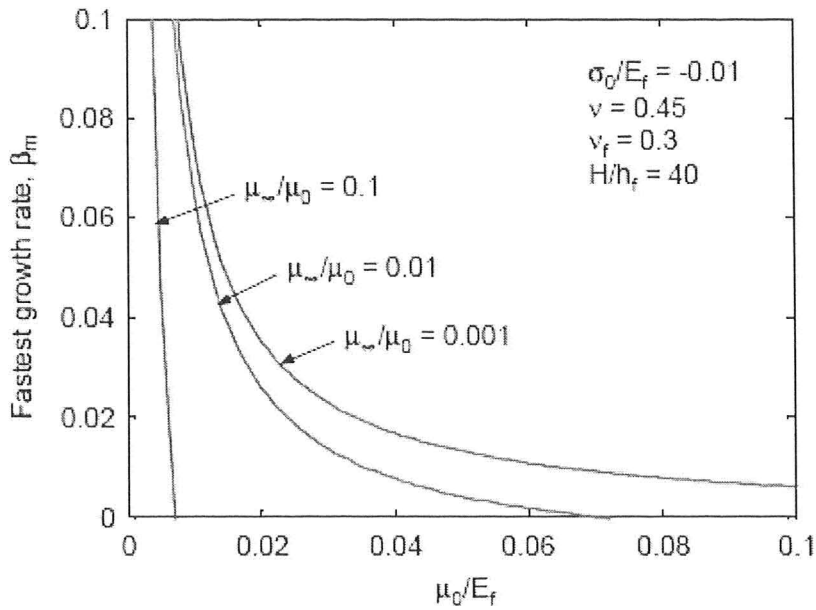


**Figure 2-13.** Fastest growth rate for a thick substrate for different ratios of rubbery/glassy moduli. (R. Huang, 2005)

Im *et al.* (Im & HUANG, 2005) derived the following equations for equilibrium amplitude and wavelength for the case of a thin substrate:

$$A_{eq} = \frac{2\sqrt{1-\nu_f^2}}{k} \left[ -\frac{\sigma_0}{E_f} - \frac{(kh_f)^2}{12(1-\nu_f^2)} - \frac{2(1-\nu_s)}{1-2\nu_s} \frac{E_{s\infty}}{E_f} \frac{1}{k^2 H h_f} \right]^{1/2} \quad (2.18)$$

$$\lambda_{eq} = \pi h_f \left[ \frac{2(1-2\nu_s)E_f H}{3(1-\nu_s)(1-\nu_f^2)E_{s\infty} h_f} \right] \quad (2.19)$$

They pointed out that this equilibrium wavelength and the fastest growing wavelength (Eqn. 2-17) can be completely independent of each other. The fastest growing wavelength, dominating the initial growth, is kinetically determined and is independent of the viscoelastic behaviour of the substrate and totally depends on the compressive stress of the film. The equilibrium wavelength, however, is energetically determined and

depends on the thickness and rubbery modulus of the substrate and is independent of the stress on the film. This independence is actually helpful in determining the residual stress and rubbery modulus from the initial and final wrinkle wavelengths.

---

---

## *CHAPTER III:*

### *Experimental*

---

---

### **3.1. Materials**

The principle materials involved in the tests were a selected commercial automotive grade decorative blackout film, and a suitable plastic and steel substrate.

#### **3.1.1. Decorative film**

A commercial decorative blackout film with pressure sensitive adhesive, designated as 9000J, was provided by 3M Canada in a 100-m roll. All samples for the wrinkling experiments were taken from the same roll; therefore, there was no need to take batch-to-batch variability into account when it came to analysing the data. The film itself is a multi-layered construction comprised of a pressure sensitive adhesive layer of 35- $\mu\text{m}$  thickness, an 85- $\mu\text{m}$  polypropylene/polyethylene copolymer base layer, and a 20- $\mu\text{m}$  layer of polyethylene terephthalate (PET) clear glossy as a pre-mask. The thickness of the whole sandwich was around 140- $\mu\text{m}$ . The average modulus of the film came out to be  $160 \pm 48$  MPa during the experiments using DMA tensile fixture at room temperature (25°C). Other properties regarding the composition of the film layers were proprietary and are not relevant to this study.

### 3.1.2. Plastic substrate

The plastic substrate was a 550- $\mu\text{m}$  thick polypropylene (PP) sheet treated with maleated polyethylene on one side to improve adhesion with the film(s). The tensile modulus of this substrate was around 485 MPa. The linear thermal expansion coefficient for the PP was  $8.6 \times 10^{-5}/^{\circ}\text{C}$ , measured using DMA. Figure 3-1 shows the DSC result on this sheet. In the figure the two melting peaks of PE and PP are quite visible at around 118 and 165 $^{\circ}\text{C}$ , respectively. The PP sheet was supplied as a roll by 3M Canada with a width of 59cm.

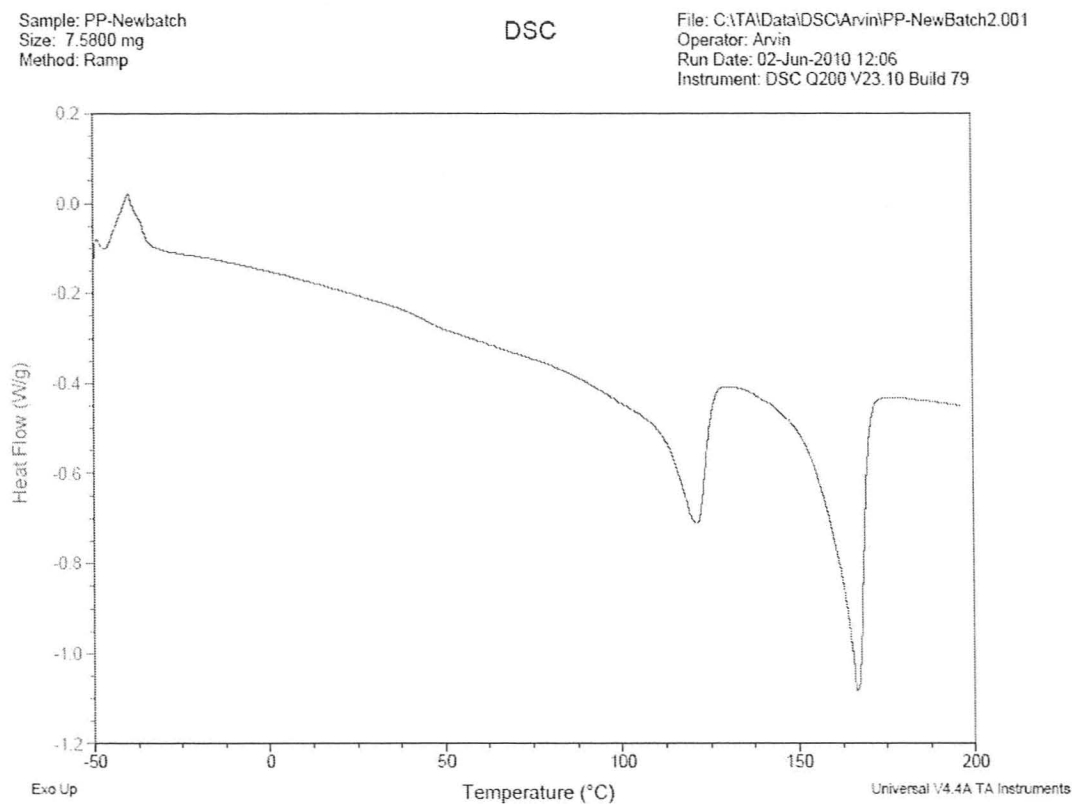


**Figure 3-1.** DSC result for the plastic substrate.

### **3.1.3. Steel substrate**

To observe the effect that substrates with different thermal expansion had on wrinkling behaviour, a metal substrate was selected for comparison with the polymer. Due to the huge difference in physical properties of steel (such as modulus and the coefficient of thermal expansion) and the film, it was believed that the intensity of the wrinkles was not compromised by the steel substrate. The carbon steel substrate used in the experiments was AISI 1018 steel with a thickness of 1.5mm, hardness of Rb 73, and modulus of 200 GPa. The linear thermal expansion coefficient of the metal was  $11.5 \times 10^{-6}$  /°C, all according to ASTM A29. The steel substrate was pre-cut into coupons with dimensions of 2.5 by 7.5cm before lamination.

## **3.2. Lamination**

Both metal and polymer laminates were prepared using a ChemInstruments hot roll laminator (Model No.: HL-101, Cincinnati Ohio). The plastic substrate as well as the steel was first cleaned with acetone (reagent grade), at least two times to make sure there is no grease or other residues left before lamination. The protective layer on the adhesive side of the film was partially removed and mounted on the plastic substrate and removed continuously when the sandwich was going through the laminator. However, the top protective layer on the film was left in place and was not removed until the actual experimental runs. The film then was placed on the substrate and ran through the laminator's rollers. The gap between the rollers of the laminator was set to 80% of the total thickness of the film and the substrate (i.e. 0.56mm for the case of plastic substrate and 1.34mm for the steel substrate). Lamination was performed at room temperature and

345kPa for the case of steel and 620kPa in the case of plastic substrate and the speed of the rollers was set at 1 which is an equivalent of 60cm per minute. Both types of samples were left to experience a cure time of 72 hours. The reason behind choosing the mentioned lamination conditions will be described later in section 3.7.1 of this chapter. For the cases of materials with an apparent longitudinal (machine) direction (i.e. the film and PP sheet which were supplied in rolls), this orientation was maintained through the laminator rollers. *Note: early mechanical testing on the film (Section 3.4) showed different properties depending on its orientation in the grips indicating anisotropic residual stresses in the supplied material, making orientation important when the samples were prepared in the wrinkling experiments.*

In case of the plastic substrate, the prepared laminate sheets were cut into rectangular shapes of 2.5 by 7.5cm afterwards. For the steel substrate which had already been cut prior to lamination, the coupons were placed on the adhesive side of the film in groups of 12 and were laminated all at the same time. Direction of the steel was not taken into consideration here because it was believed that it did not affect the results due to the huge difference in physical properties of steel as opposed to the polymers used in the film.

### **3.3. Assessing Delamination Limits**

Prior to the wrinkling study in this thesis where some sets of samples would be strained uniaxially before heating, it was necessary to determine the limits of longitudinal deformation corresponding to the onset of film delamination. These delamination tests were done using an Instron 3366 universal mechanical tester fitted with either a 5 KN or a

500 N load cell. Temperature of the sample was controlled using an environmental oven set to either 23°C or 100°C. The cross-head speed was varied between 100-500 mm/min.

The testing was done only for the laminated sheets of 9000J film on PP substrate as the adhesive strength on the plastic was weaker than on the metal (based on 180° peel tests at both temperatures). The plastic laminate was cut into rectangular samples of 2.5 by 7.5cm. Before running each test, the sample's dimensions were measured precisely using a 150-mm digital calliper. The test was run once the sample had thermally equilibrated in the chamber (normally 10 minutes based on thermocouple measurements) and the point where the film failed (delaminated) was determined both visually as well as by stress measurement. The delamination point produced a small drop in the strain-stress curve, most notable for the room temperature condition as shown in Figure 3-2. To accurately detect the point, the stress-strain measurements were converted to differential data ( $d\sigma/d\varepsilon$ ). At 100°C the drop in the load was below the sensitivity of the device so no drop was observed in the curve; therefore, all the data for that temperature was estimated visually. The onset of delamination for the two temperature conditions and different cross-head speeds is summarized in Table 3-1.

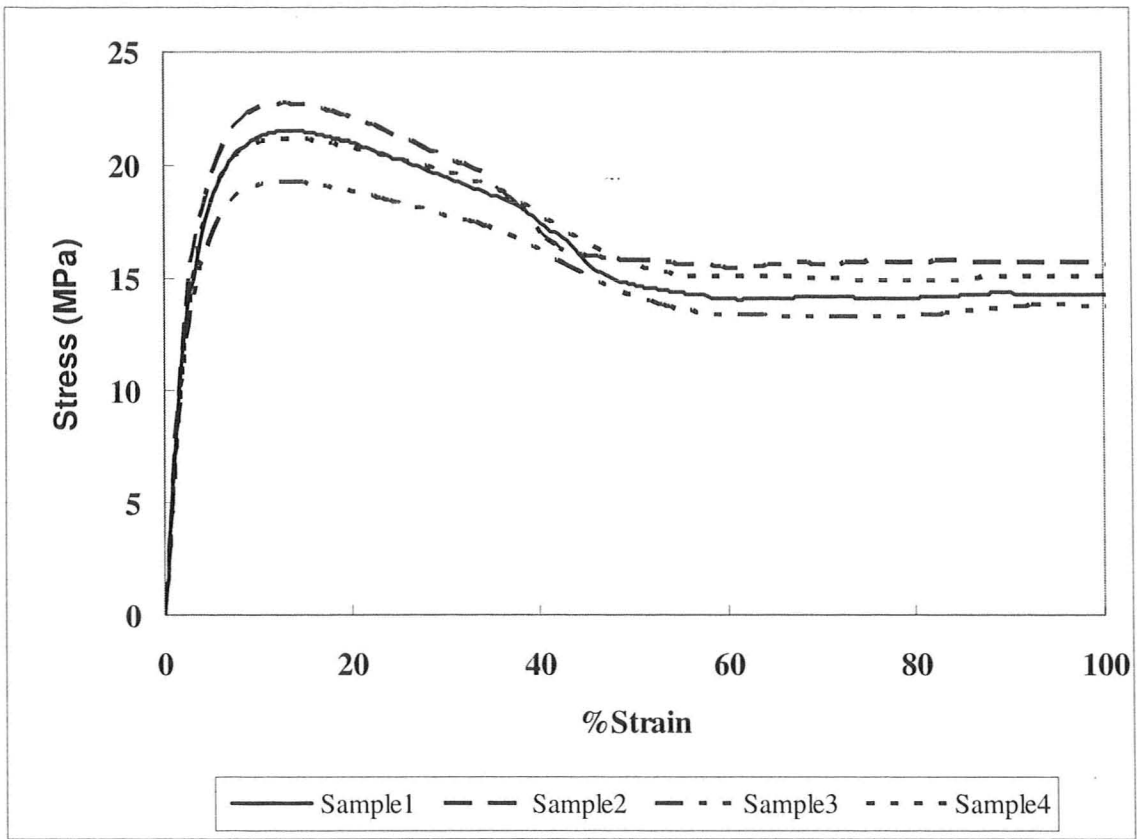


**Figure 3-2.** Stress-strain curve for the delamination test for laminated 9000J at room temperature with cross-head speed of 100mm/min. Drop in the curve at around 35-45% strain is quite visible.

The data for room temperature showed a clear trend showing higher tolerance to deformation prior to delamination as the cross-head speed increased. This is due to the rate of entanglement by the polymer chains. Unentanglement is a function of strain rate. When the strain rate is high, chains do not have enough time to unentangle therefore the entangled chains increase the yield strain of the material making it more resistant to failure.

**Table 3-1.** Delamination point (%Strain) for the three films at different speeds and temperatures

| Film   | Temperature      | Speed (mm/min)   |      |       |
|--|------------------|--|------|-------|
|  |                  | 100  | 300  | 500   |
| 9000J  | Room Temperature | 40*  | 53** | 61*** |
| 9000J  | 100°C            | 49^  | 55^^ | 57^^^ |
| * Standard Deviation: 6.7<br>** Standard Deviation: 8.6<br>*** Standard Deviation: 6.8 |                  | ^ Standard Deviation: 5.5<br>^^ Standard Deviation: 3.3<br>^^^ Standard Deviation: 3.7 |      |       |

As for the yield stress, it was expected based on the same entanglement theory that the values go up as the strain rate increased, however the values showed only a little increase in the yield stress for each temperature. Obviously increasing the temperature had a negative correlation with the yield stress values due to the mobility of the chains at high temperatures. Table 3-2 depicts the trend.

**Table 3-2.** Yield stress (MPa) for the three films at different speeds

| Film   | Temperature      | Speed (mm/min)  |         |          |
|--|------------------|---|---------|----------|
|  |                  | 100   | 300     | 500      |
| 9000J  | Room Temperature | 21.41*  | 21.48** | 22.59*** |
| 9000J  | 100°C            | 4.56^   | 4.79^^  | 4.68^^^  |
| * Standard Deviation: 1.23<br>** Standard Deviation: 1.57<br>*** Standard Deviation: 0.8 |                  | ^ Standard Deviation: 0.42<br>^^ Standard Deviation: 1.03<br>^^^ Standard Deviation: 0.66 |         |          |

For the tests done at 100°C, where chain mobility was already high, it was understandable that this behavior of delamination was more difficult to observe. Besides, the adhesive tends to flow above 70°C (based on lap shear testing conducted by E. Takacs) making delamination less likely compared to film failure. The visually registered data, yet, showed an increase in strain at which delamination occurred for the 100mm/min, a slightly increased value for 300mm/min and a small decrease for the case of 500mm/min compared to the tests at room temperature. It is possible to conclude that

for the case of 300 and 500 mm/min cross-head speeds, temperature did not play a significant role in changing the materials behaviour. The obtained results might be compromised by the sensitivity of the device and the load cell at high temperature. However, for each temperature there was an increase in the delamination point strain as the strain rate increased.

Based on these experiments it was possible to determine the critical strain at which the film would fail for different strain rates at two different temperatures. Therefore, in order to do the experiments later on with the strained samples, it was necessary to stay clear of these critical strains. It was decided that the strain levels for those tests be 10 and 20%, respectively. Figure 3-3 shows the drop in the differential curve due to film failure.

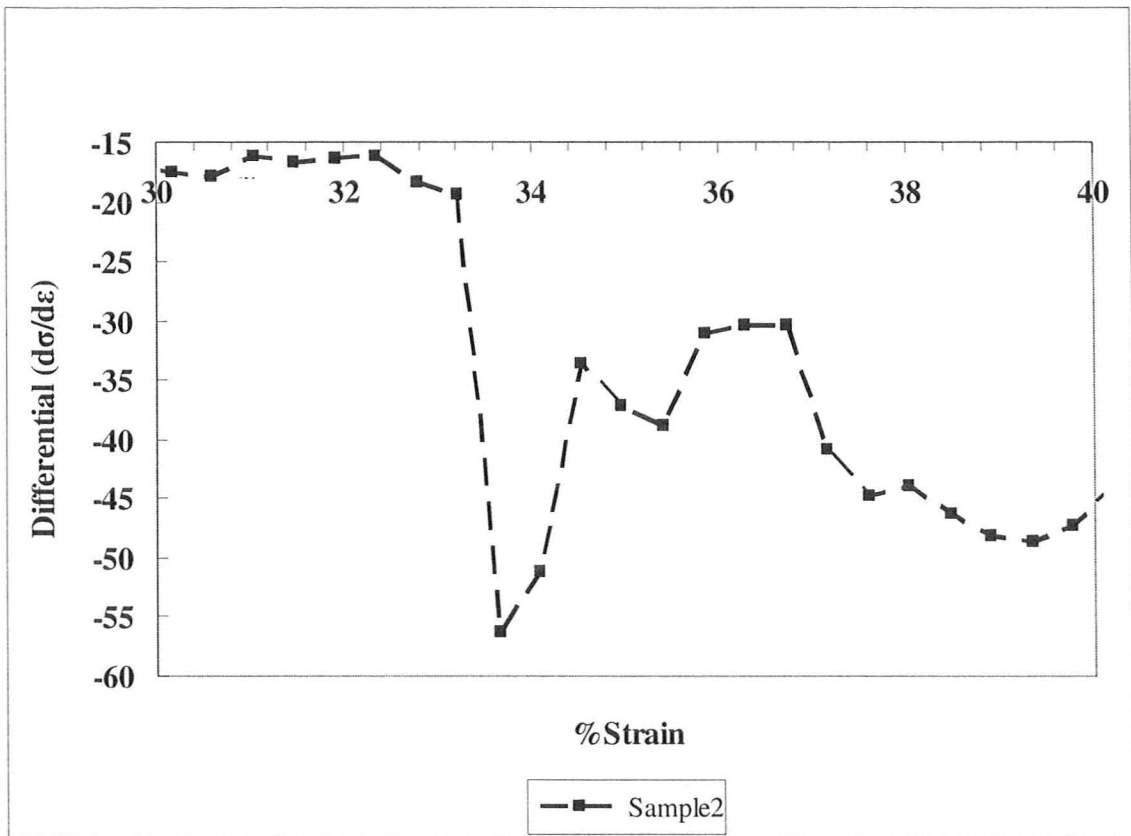


**Figure 3-3.** Plot of differential strain versus percent strain for determination of the delamination point (seen here at 33% strain). Differential curve corresponds to *Sample2* in Figure 3-2.

### 3.4. Anisotropic Properties Testing

In order to study the anisotropy of the materials some tensile tests were initially conducted in different orientations for only the film/plastic substrate combination. The reason this test was not performed for the steel substrate was that the large modulus of the steel would make it impossible to study anisotropy of the film.

To perform this set of experiments the plastic laminates were cut in three different directions: longitudinal, transverse in-plane and 45-degree diagonal. The tests were done using the tensile testing device mentioned previously with either a 5KN or a 500N load

cell. The strain rates varied a bit due to different initial gauge lengths, however every attempt was made to keep the gage lengths as constant as possible. The cross-head speed of the unit was set to 100mm/min at room temperature. Based on the approximate initial gauge length of the grips the strain rate was around  $4.25\text{min}^{-1}$ . Delamination was evaluated in the same manner as in the previous section.

The outcome of the tests is shown in Tables 3-3 and 3-4 for maximum yield stress and delamination point, respectively. Although the results show no difference in the maximum yield stress in different orientations, there is a clear trend which shows higher resistance to delamination from longitudinal to transversal orientation. Due to this difference in tolerance to delamination, it was decided that the orientation of the film be considered in the experiments. Having had the lowest threshold to delamination, longitudinal direction was chosen as a basis for all the experiments.

**Table 3-3.** Yield stress for the laminated 9000J in three different orientations

| Film  | Yield Stress (MPa) |         |             |
|---|--------------------|---------|-------------|
|   | Longitudinal       | 45 Deg. | Transversal |
| 9000J   | 0.58*              | 0.58**  | 0.58***     |
| * Standard Deviation: 0.06<br>** Standard Deviation: 0.01<br>*** Standard Deviation: 0.04 |                    |         |             |

**Table 3-4.** Delamination point for the laminated 9000J in three different orientations

| Films  | Delamination Point (%Strain) |         |             |
|--|------------------------------|---------|-------------|
|  | Longitudinal                 | 45 Deg. | Transversal |
|  | 52*                          | 58**    | 62***       |
| * Standard Deviation: 4.1<br>** Standard Deviation: 3<br>*** Standard Deviation: 4.7 |                              |         |             |

### **3.5. Thermal Behaviour Of The Film**

It was important to recognize thermal transitions in the film to understand the wrinkling phenomenon, ascertaining how certain temperatures were relevant to structural changes. Owing to the multilayered structure of the film, this was not easily accomplished and two different techniques, DSC and DMA were used.

DSC tests were conducted on the 9000J film, the PET clear pre-mask and the plastic substrate by a TA Instruments Q200 DSC. The samples were studied over a temperature range of  $-50^{\circ}\text{C}$  to  $200^{\circ}\text{C}$  to make sure that the samples' behaviour is studied for a safe range of temperature as for observing glass transitions and melting points or other probable transitions. Very small pieces of samples were cut using a razor so they could fit into the DSC pans. Aluminium hermetic DSC pans were used for this set of experiments. The weight of the prepared samples was between 5 to 10 mg. Only one heating ramp was performed to study the behaviour of the material with the thermal history that they carried, because that was how the material would behave during thermoforming. The ramp up heating rate was set to a normal value of 10 degrees per minute. In the case of the PET layer, the transition was not detected even when testing using the more sophisticated Modulating option on the DSC (MDSC). Modulated DSC works basically like a normal DSC run; however, it increases the temperature in a sinusoidal manner, making it possible to distinguish the reversing from the non-reversing phenomena. Test conditions for MDSC were exactly as it was for DSC with a 1Hz frequency and  $\pm 1^{\circ}\text{C}$  for the sinusoidal increase.

DMA tests were conducted using a TA Instruments DMA 2980 at École Polytechnique, Université de Montréal (Dr. B. Favis) for both the 9000J film as well as a

sample of the PET film separately. Good results were found for 9000J, however, the experiments were not successful with the PET film. The reason to the unsuccessful experiments was assumed to be the thickness of the PET film. The DMA runs covered a temperature range from  $-100^{\circ}\text{C}$  to  $160^{\circ}\text{C}$  to ensure it covers the behaviour of the film for a wide range of temperature. Since it was important for us to study the tensile modulus of the film, the tensile fixtures of the DMA device were utilized. Table 3-5 shows other settings with which the tests were conducted. All samples were around 7mm in width and less than 10mm in length. Long thin samples became so soft during the test and if the sample stiffness dropped below 100N/m the device stopped registering data. Therefore, one solution to avoid that problem was to keep the width/length ratio of the sample as high as possible. DMA graph is included in Appendix A.

**Table 3-5.** DMA fixture and other settings used for the tests

| Setting      | Value           |
|--------------|-----------------|
| Grip fixture | Tensile         |
| amplitude    | 5 $\mu\text{m}$ |
| Static force | 0.025N          |
| Frequency    | 1Hz             |

### 3.6. Hot Stage Apparatus

Wrinkling behavior of the 9000J film was understood to happen during cooling process; however, during some random experiments it was realized that it occurred during the heating cycle. Therefore, it was necessary to build a heating device that could accommodate the samples to be heated. A picture of the apparatus is shown in Figure 3-4.

The *hot stage device* consisted of an aluminum block with dimensions of 13 by 13 by 16cm (L, W, H) enclosed in two 4-cm thick layers of glass wool around its sides. This

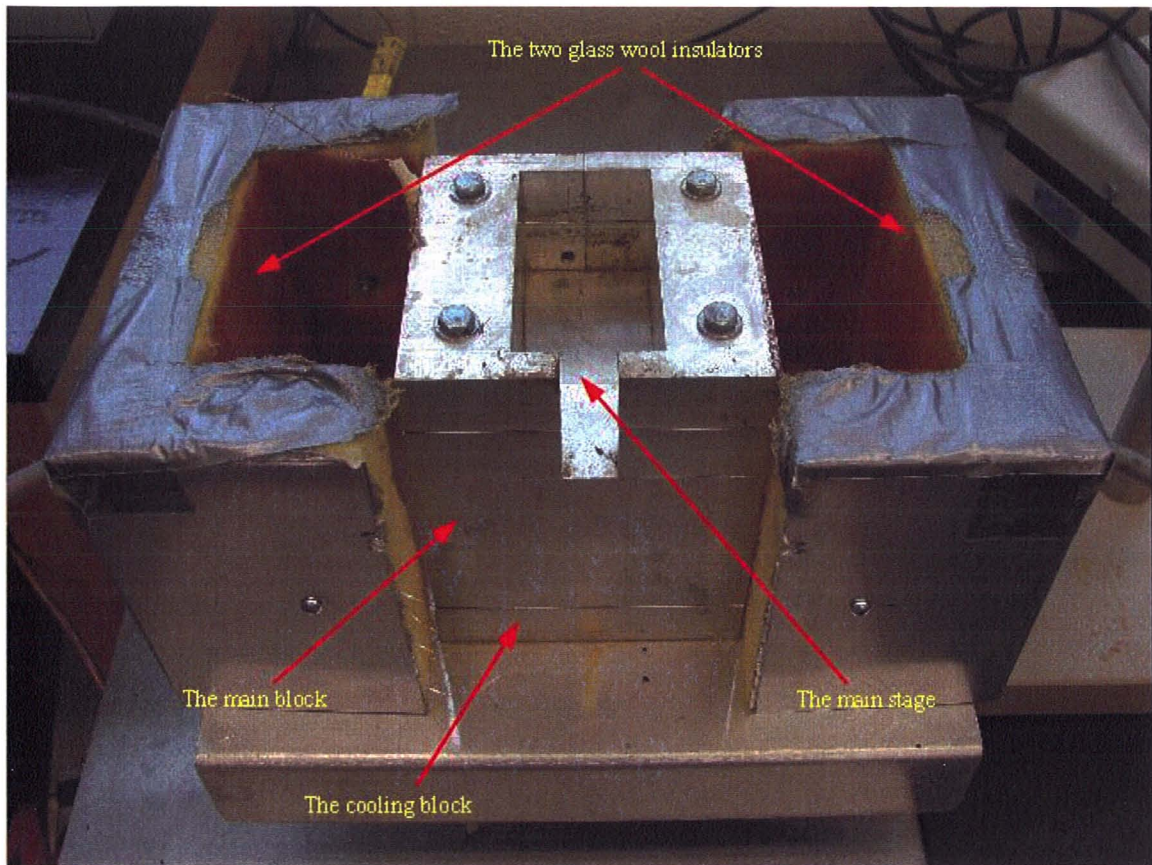


**Figure 3-4.** Image of the Hot Stage device used to heat up the samples.

insulation layer not only made temperature control easier by the controller (due to less heat loss) but also provided lower cooling rates for the experiments. The *main stage* in which the samples were placed was dug 5cm deep into the aluminum box to avoid the effects of air draft. The bottom side of the aluminum box was drilled in a grid pattern for cooling purposes. Both water and oil could flow through the channels to provide faster cooling rates in case it was necessary. This hot stage has three 1000-kW cartridge heaters mounted at 4cm below the main stage. There was a k-type thermocouple attached to the wall of the aluminum box and was connected to an over-temperature switch in the control

box that would shut off the system should it get too hot. The shut-down temperature could be manually set inside the controller box. There was also a computer GUI (Graphical User Interface) to control the set points and other parameters such as heating power and so on.

The device made it possible to control the heating rate, log the temperature versus time, and accurately control the set point temperature ( $\pm 1^{\circ}\text{C}$ ) without overshoot (through a PID controller and a data logger). It should be mentioned that the controller monitored its set point versus the wall temperature of the hot stage and not the sample itself. The reason to do this was that controlling the set point based on the wall temperature of the device was more efficient and the controller was more responsive and therefore the response was quicker. Therefore, in order for the sample to reach a certain temperature, some calibrating runs were performed to determine the required box temperature needed for the sample to reach the desired temperature.

For the metal substrate, no special apparatus was necessary but for the plastic substrate a special device was necessarily fashioned similar to a thermoforming vacuum box so it could hold the warped sample onto the hot stage. This vacuum box was a 1-cm- thick aluminum block that fit into the hot stage, sat on the main stage and was connected to an Edwards RV3 vacuum pump. The vacuum was applied through six holes drilled into the surface of the box so that it kept the edges of the sample to the surface. Figure 3-5 is a schematic view of the vacuum box.

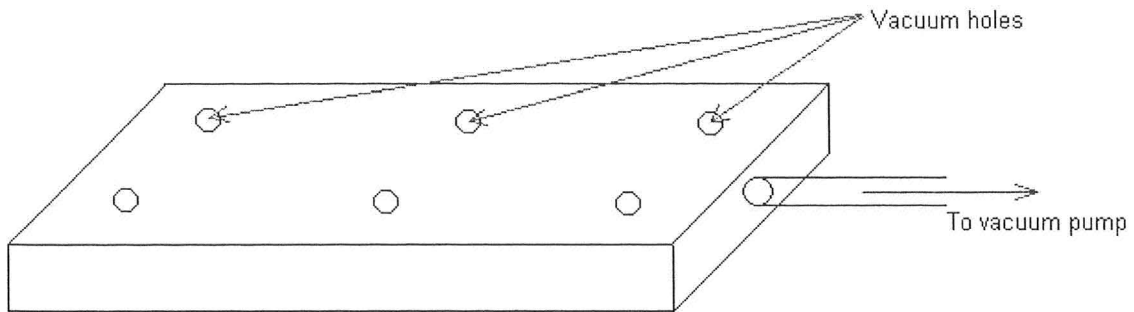


**Figure 3-5.** Schematic view of the vacuum box used to hold the plastic laminates to the surface.

### **3.7. Wrinkle Studies (Unstrained samples)**

These sets of experiments constituted the main body of the project. The purpose of these experiments was first to determine the effect of lamination pressure and cure-time and second to study the effects of heating and cooling rates, as well as final temperature on the appearance and pattern of the wrinkles. For this section the films and substrates were used as supplied without any pre-strain. Experiments were done on laminates of plastic as well as steel substrate.

#### **3.7.1. Influence of lamination conditions**

The force of lamination was varied by varying the laminator roll pressure from 345-620kPa. The prepared laminates were then left to cure for both zero hour (instantly) and 72 hours. The reasoning for this was that an industrial user of these laminates would not readily accept long cure times before forming the material into a desired shape and so it was determined necessary to see if cure time was important. The hot stage device was heated (155°C for the metal substrate and 180°C for the plastic substrate) and was allowed

to stabilize at that temperature. This temperature was determined to correspond to a sample temperature of  $150^{\circ}\text{C}$  ( $\pm 3^{\circ}\text{C}$ ). A stereoscope (CCD camera with low magnification optics) was placed above the hot stage and connected to a computer through an image capture device (Pinnacle Systems, 710-USB Rev. 1). The software used for processing the images was Pinnacle Studio, Ultimate Version 12. As it was mentioned earlier the controller GUI provided an option of logging the temperatures of both the stage and the sample versus time on the same computer logging images so that the temperature of the sample viewed in each image was known. The sample temperature was monitored using a self-adhesive, precision fine wire K-type thermocouple provided by Omega Engineering Inc. which was attached to the film surface. As soon as the sample was placed in the hot stage, filming and data logging were started simultaneously. This was the most aggressive heating rate used in the subsequent heating/cooling trials, corresponding to an average heating rate of  $95^{\circ}\text{C}/\text{min}$  for steel and  $230^{\circ}\text{C}/\text{min}$  for plastic laminates. After the steel samples reached their final temperature, it was allowed to stay in the hot stage at that temperature for about 8 minutes to stabilize. Plastic laminates however, were removed as soon as they hit the final temperature because otherwise the wrinkles lost their intensity. It should be mentioned again that this temperature was prone to fluctuations of  $\pm 3^{\circ}\text{C}$ .

In order to freeze the wrinkle structure after being heated to  $150^{\circ}\text{C}$ , fast quenching was performed using iced water. This method gave an average cooling rate of  $8^{\circ}\text{C}/\text{s}$  and was the most aggressive cooling rate used in the subsequent heating/cooling study.

The image data were studied for the onset temperature of the wrinkle appearance. Surface roughness was measured using a Zygo NewView 5000 (ZYGO CORPORATION) providing peak-to-valley (PV) and average roughness values (Ra and rms values). Wrinkle wavelength was also studied using the 2D surface profile of the same device. The Zygo device and the analysis of roughness will be described in a following section.

### **3.7.2. Influence of heating/cooling conditions**

Based on the results of the previous experiments for the steel substrate a single lamination condition was used in this set of runs (i.e. 345 kPa and a 72-hr cure time for the metal substrate and 620 kPa and 72-hr cure time for the plastic substrate). The purpose of these experiments was to study the effects of heating and cooling rates and different final temperature on the wavelength of the wrinkles and also surface roughness of the samples. Two different heating and cooling rates were examined as well as two different final temperatures. It was suspected that heating and cooling rates would have some effects on the wrinkles in general.

The final temperatures were chosen based on the lowest and highest limits of a forming process, namely 110°C and 150°C, respectively. The fast heating rate for the sample to reach 150°C corresponded to an average rate of 95°C/min for the steel and around 230°C/min for plastic laminates, while the slow heating rate for the same temperature was about 1°C/min and 2°C/min for steel and plastic laminates, respectively. On the other hand, the aggressive cooling rate (sample removal and immersion in iced water) was about 8°C/s and the slow cooling rate (stagnant air in the hot stage) was

~1°C/min for both types of samples. However, these rates were different for two different final temperatures. To reach 110°C the fast heating rate for the steel substrate was 84°C/min and around 215°C/min for the plastic laminates. The slow heating rate was 1.8°C/min and 2°C/min for steel and plastic laminates, respectively. Slow cooling rate from this temperature was about 0.6°C/min for steel and 0.9°C/min for the plastic. Fast quenching rates are relatively the same as the case with 150°C. The procedure for running the experiments was the same as stated in Section 3.7.1.

### **3.8. *Wrinkle Studies (Strained samples)***

In order to study the effects of pre-strain of the sample on the wrinkling behaviour, the samples were first uniaxially stretched to two different degrees of strain. The greatest challenge in this set of experiments was maximizing the area subject to strain while allowing some of the specimen to be held in grips during stretch, all the while maintaining a shape that would fit in the hot stage afterwards. For the tests, the cross-head speed was decided to be 50mm/min for metal laminates and 500mm/min for plastic laminates. Based on the delamination tests noted in Section 3.3 the limiting strain there was considered in selection of the two strain conditions used in these tests. For the cross-head speed chosen it was observed that a strain up to 30% was possible before the test specimen would start to slip within the grips for the metal laminates. Therefore, in order to stay clear of that point, 10% and 20% apparent strain were the selected conditions considered in these experiments; the strain was apparent only since it considered only longitudinal displacement and not any transverse contraction. It should be noted that since the samples were not dog-bone shape but rather rectangular (recalling that the specimen

must fit in the hot stage afterwards), so the stress that was achieved was not uniform. In order to avoid slippage it was decided that 29mm (1.15 inches) of the sample be placed in the grips. That left an 18mm gage length of the specimen considered to have been strained for study in the subsequent wrinkling experiment. Based on the gage length, the strain rate that the samples experienced was almost  $2.8 \text{ min}^{-1}$ .

After straining the sample, it was placed in the hot stage device and heating at  $90^\circ\text{C}/\text{min}$ . Just like the other hot stage experiments with fast heating and fast cooling cycles, the sample remained in the hot stage for about 8 minutes and then was quenched in iced water to preserve the pattern and intensity of the wrinkles. The rest of the experiment was run similar to other tests, including measuring the surface roughness and collecting images of the developing wrinkle pattern.

For the plastic laminates, however, the straining process was a bit different. Samples were cut in 12.5 by 2.5 cm and the 2.5 cm of each end was placed in the grips. Therefore we ended up with a 7.5-cm long sample that was strained to either 10 or 20%. As it was mentioned earlier, the cross-head speed for plastic substrate was 500 mm/min as it was a closer simulation of what happens during thermoforming. After straining the samples they remained under strain for 10 minutes so they chains could change orientation and relax the stress. This time was determined after some stress relaxation tests. These tests showed that after 10 minutes stress decreased insignificantly. This is further described in section 3.9.1 of this chapter. For the fast heating rate the built device was heated to  $185^\circ\text{C}$  and after the temperature was stabilized the sample was put on the

vacuum box. Due to the temperature difference of the sample and the oven, the necessary heating rate for the film to wrinkle was provided.

### 3.9. Characterization

#### 3.9.1. Stress Relaxation

When a plastic is strained, the chains need some time to re-orient in the new direction, or in other words relieve the stress. This time is measured through stress relaxation tests. It was necessary to have this time in order for the samples to experience the same stress relaxation level.

The strain relaxation tests were conducted using the tensile testing device mentioned previously with either a 500N load cell at room temperature. The tests showed

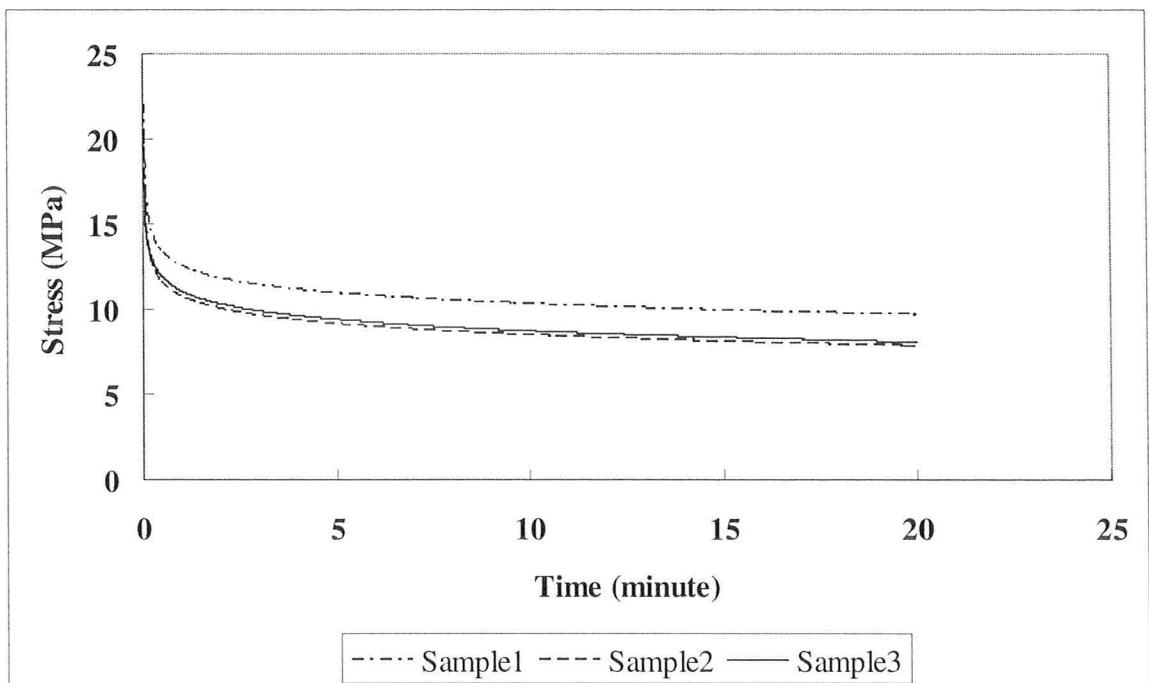


**Figure 3-6.** The stress relaxation curves versus time for samples strained at 10% strain and sat for 20 minutes. It is clear that after 10 minutes the level of stress does not change significantly.

that after almost ten minutes the level of stress barely changed, therefore it was decided that the time for the samples to relieve the stress be 10 minutes. Figure 3-6 shows the Stress vs. Time graphs of the test.

### **3.9.2. Surface Metrology**

Zygo NewView 5000 (Zygo Corporations) is a white light interferometer non-contact surface roughness profilometer. It provides the user with a 2D and 3D surface profile. The 2D surface profile was used to manually measure the wavelength of the wrinkles at 4 different places on the surface. A 100-times magnification setting with a resolution of  $2.27\mu\text{m}$  was set for the device. The scan area covered by the device was 1.45 by 1.09mm, but the total area of analysis was 5 by 5mm, done using the Stitch feature of the software. The area analyzed was chosen to be at the center of the test specimen so the wrinkle pattern was least influenced by edge stresses. In order to save time, and after being sure it was not a necessary step, the auto-focus feature of the device was turned off. This meant that after a manual focus for the first stitch, the device took that focal point as universal and measured the surface based on that focal point. A 150- $\mu\text{m}$  scan depth was set to measure the roughness of the surface. This means that after the manual focus is performed, the device scans a depth of  $\pm 75\mu\text{m}$  with respect to that point. All the data was taken to MS Excel worksheets and then inserted into MiniTab Ver. 15 statistical software (Minitab Inc.) to analyse the trends and sensitivity of the results on different factors. The MiniTab process will be discussed later.

### **3.10. MiniTab:**

Design of experiments for the pressure-cure time studies and also the unstrained samples was done through MiniTab. For the pressure-cure time studies a full factorial design with four repetitions were designed, lamination pressure and cure-time being the factors. There were three levels for the lamination pressure (i.e 345, 480 and 620 kPa) and 3 levels for the cure-time (i.e. 0-hour, 72 hours and 1 week). Then after inputting all the data into MiniTab different graphs were studied, such as Normal probability plot, residual plot and so on. R-squared values were also taken into account as for a measure of how well the data has been fitted into the model.

As for the unstrained samples, a full 2-level factorial design was performed with three factors, final temperature, heating rate and cooling rate being the factors. The rest of the process was done the same as the previous part.

---

---

## *CHAPTER IV:*

### *Results*

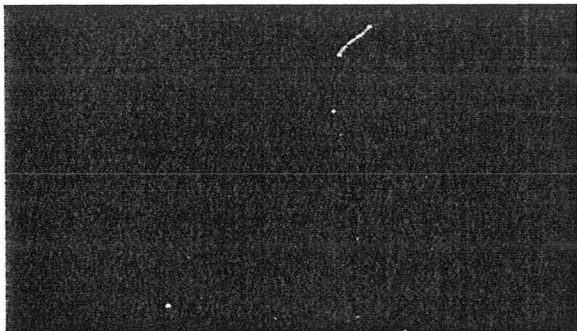
---

---

#### **4.1. Steel:**

##### **4.1.1. Wrinkles Growth**

The process of wrinkle growth was captured using a CCD camera as stated in the Experimental Chapter. The following sequence of images highlights this phenomenon over time with the corresponding temperature at each time step. The sequence is arbitrary and presented to familiarize the reader with the growth of wrinkles in 9000J film without being intended at this moment to be an examination of the parameters/variables involved.



Time = 0, 25°C



60 seconds, 132°C



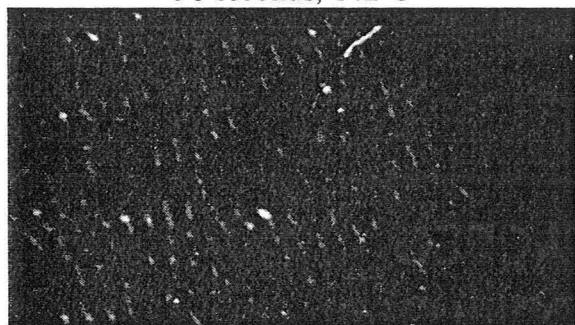
70 seconds, 137°C



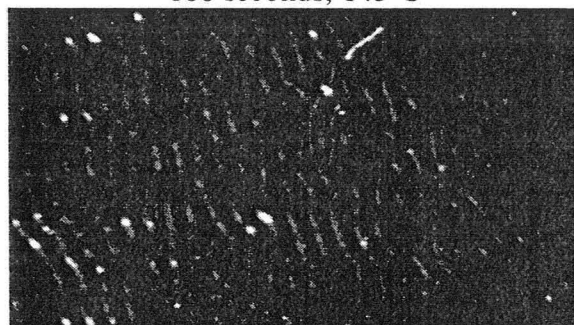
80 seconds, 140°C



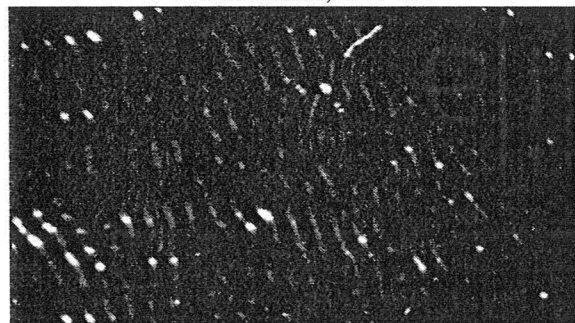
90 seconds, 142°C



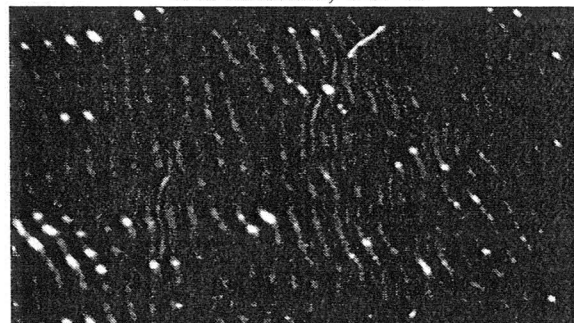
100 seconds, 143°C



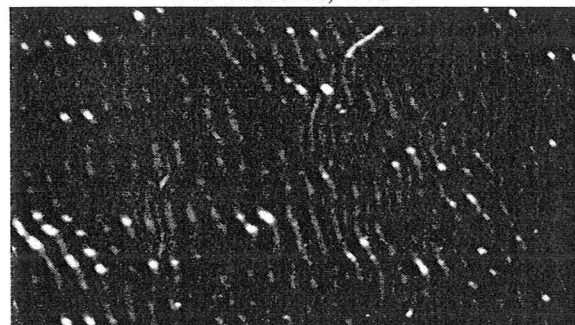
110 seconds, 144°C



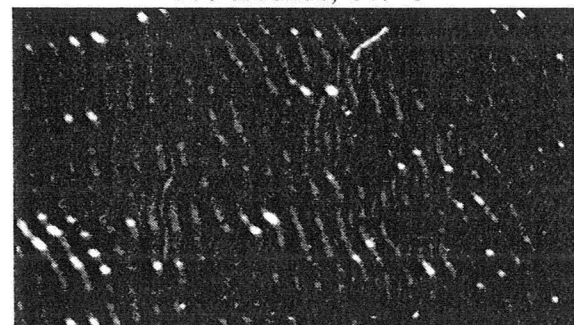
120 seconds, 145°C



140 seconds, 146°C



160 seconds, 147°C



180 seconds, 147°C



240 seconds, 148°C



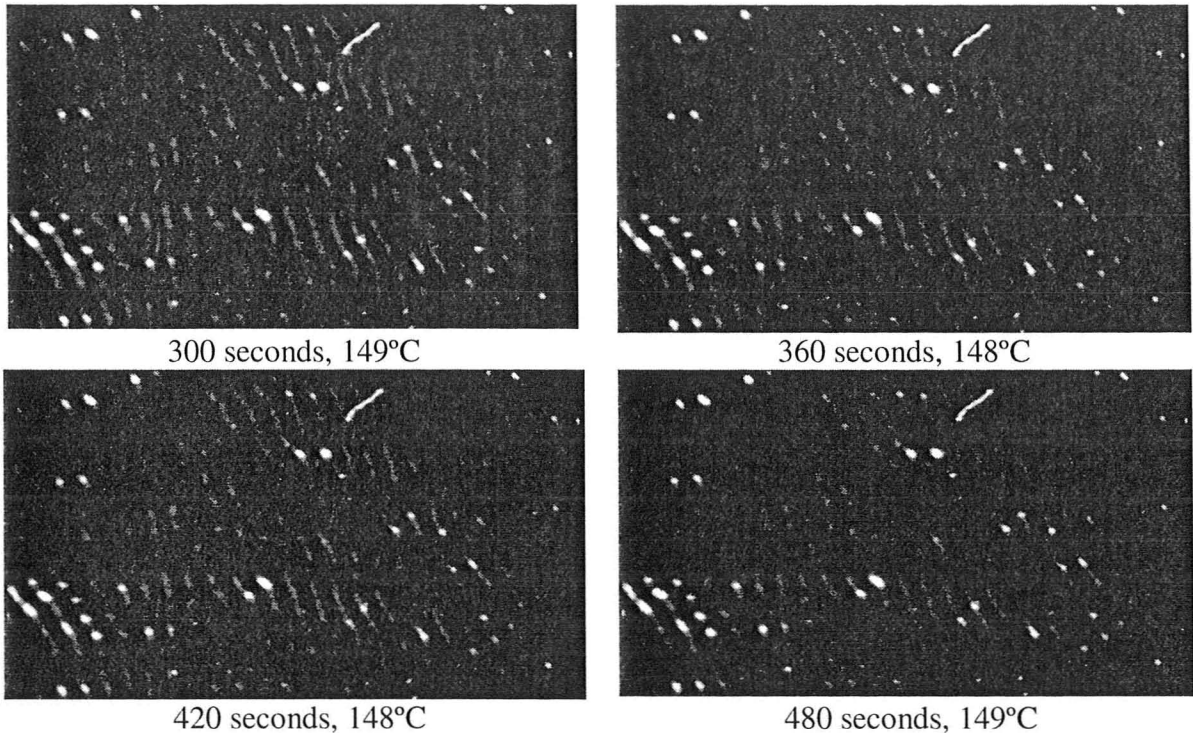


**Figure 4-1.** Wrinkle growth and their corresponding time and temperatures on steel laminates. This specific sample experienced heating rate of 40°C/min and wrinkles formed into parallel herringbones.

Each photo represents an area of almost 6mm by 10mm. The wrinkles appeared primarily oriented lengthwise across the film though impinging wrinkles in a few locations created more complex patterns though at no time was the labyrinth patterning reported by Shugurov (Shugurov & Panin, 2010) observed. The reason for that is that this specific sample did not experience a very fast heating rate (40°C/min). When the heating rate was not high enough wrinkles did not form into complex patterns. This will be discussed more in-depth in the following chapter. Gross scale wrinkling of 9000J on the metal substrate was not visible for this sample until 90s (>140°C) by the images but even at one minute the compressive stresses were evidently building up in the film. This highlights a point

which will be quantified later in the chapter, that a threshold in surface roughness must be reached before the wavelength of the wrinkle can be quantified. Using image analysis, the wavelength of the wrinkles was quantified from these images. Figure 4-2 graphs development of wrinkles' wavelength over the period of 8 minutes. The plot shows the kinetics of this phenomenon, which indicates a rapid increase in wavelength and then equilibration close to 400  $\mu\text{m}$ . The wavelength of the same sample measured by the white-light interferometer was  $400 \pm 30 \mu\text{m}$  (standard deviation from four repeated measurements over different sections of the sample). This equilibrium wavelength is almost five times larger than the thickness of the primary substrate. Huang *et al.* (R. Huang & Suo, 2002b) based on the theory of lubrication (Reynolds, 1886) had the limiting case in which thickness of the primary substrate was small compared to the wavelength. In their studies this ratio was around 0.4. Since the primary substrate-to-wavelength ratio in our studies was smaller  $\sim 0.2$ , we can be sure that we are within the limiting range. It is unfortunate that this image analysis technique, while best suited to providing in-situ data of the wrinkling phenomenon, does not give sufficient resolution to capture its initiation which is considered as an induction period while heat transfer was the rate-limiting step.

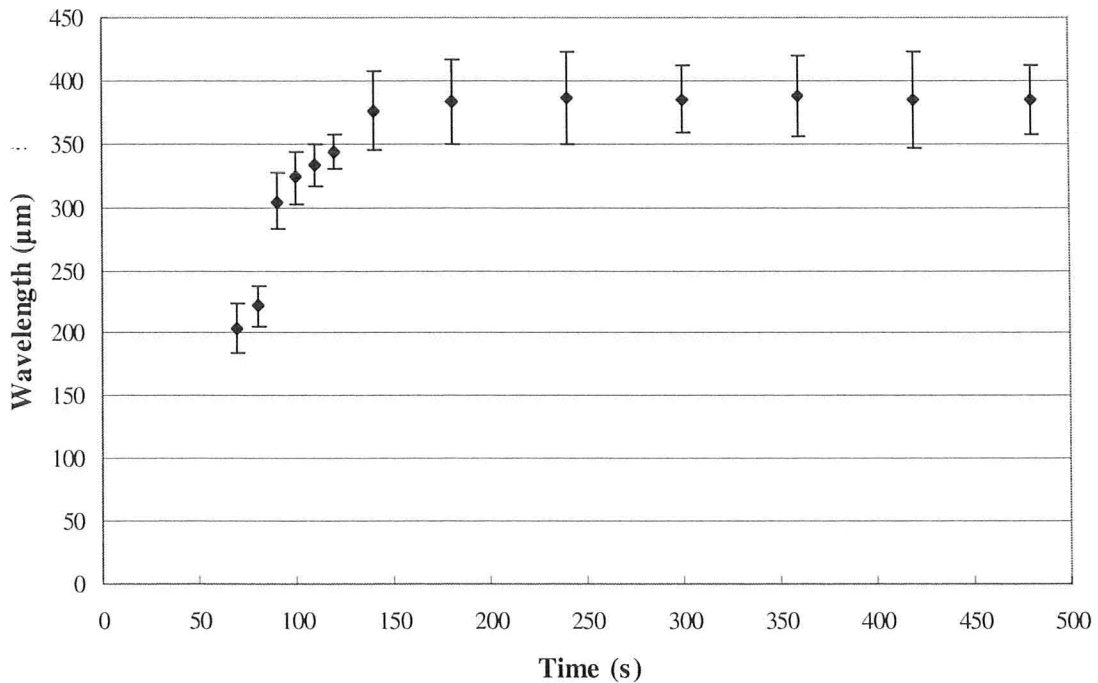


**Figure 4-2.** Wavelength growth on a steel laminate over a period of 8 minutes with fast heating/cooling cycles. The error bars are standard deviation over at least 10 wavelength measurements using image analysis software, SigmaScan Pro5.

#### 4.1.1. Pressure-cure time studies

The lamination procedure was examined first in this study for each substrate to see which conditions were most sensitive to subsequent wrinkling. Realizing that thermal forming of a laminate structure similar to ours by an industrial user would unlikely consider cure times longer than a few minutes for a Just-In-Time operation, a zero cure time condition was included though it is far from desirable for allowing the specimen to reach an equilibrium state before testing. The other cure time selected in this study was three days (72 h); one week (168 h) was also tested originally but not considered in this analysis since it offered no new information from the three day cure time. All samples

experienced fast heating/cooling rates. The following graphs show the response variables of peak-to-valley distance (PV), root mean square roughness (rms) and wavelength for the wrinkle pattern produced in a sample heated to 150°C after lamination at one of three different lamination pressures (i.e. 345, 480 and 620 kPa) and with one of two different cure times (i.e. 0 h and 72 h). The surface roughness measures of PV and rms were important to include as qualifiers of wrinkling in this work since, as already mentioned and as will be discussed in depth later, not all samples developed wrinkles to the extent that their wavelength could be quantified, especially at slow heating rates or at lower equilibrium temperatures. Therefore, wavelength could not be used to compare the effects of our tested variables at all conditions. Wavelength, if developed, was important for our later discussions related to modeling the wrinkling behaviour. Figures 4-3, 4-4 and 4-5 depict the trend in wrinkling as determined by wavelength, PV and rms values from these lamination experiments, respectively. Laminated steel samples before being heated were measured for surface metrology to be used as a control. The measured values were  $3.7 \pm 0.2 \mu\text{m}$  and  $0.3 \pm 0.1 \mu\text{m}$  for PV and rms, respectively.

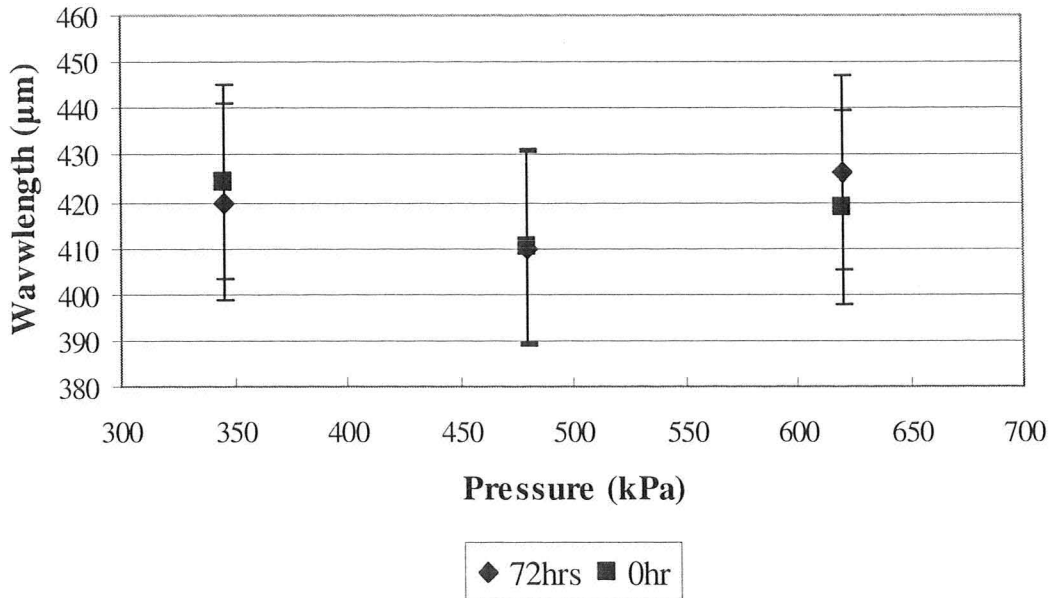


**Figure 4-3.** Wavelength values for the pressure-cure time experiments on steel laminates. The error bars represent standard deviation for the center point of experimental condition over four measurements on five samples.

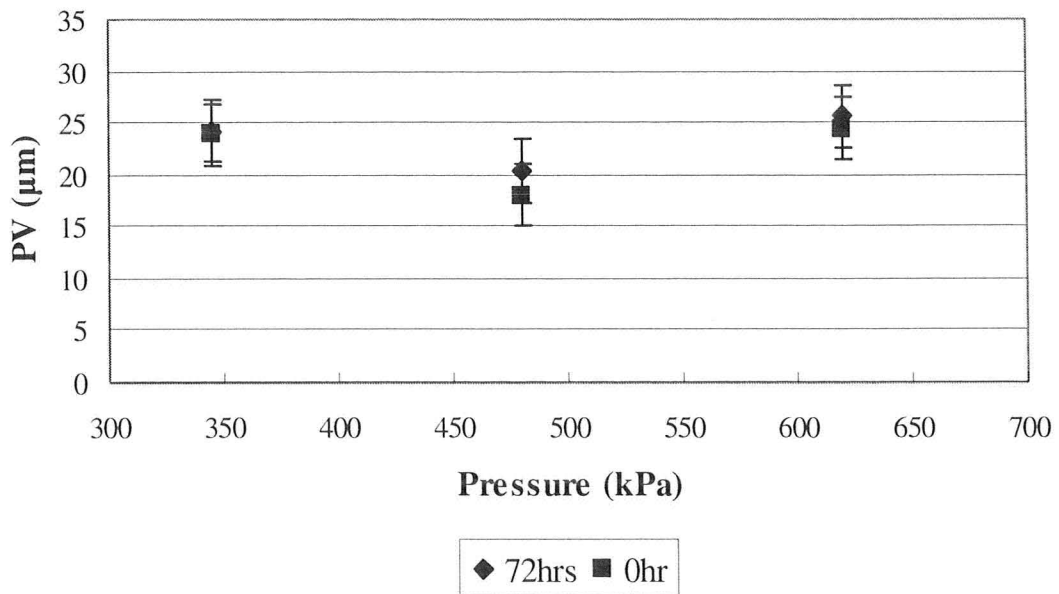


**Figure 4-4.** PV values for the pressure-cure time experiments for steel laminates. The error bars represent standard deviation for the center point of experimental condition over four measurements on five samples.

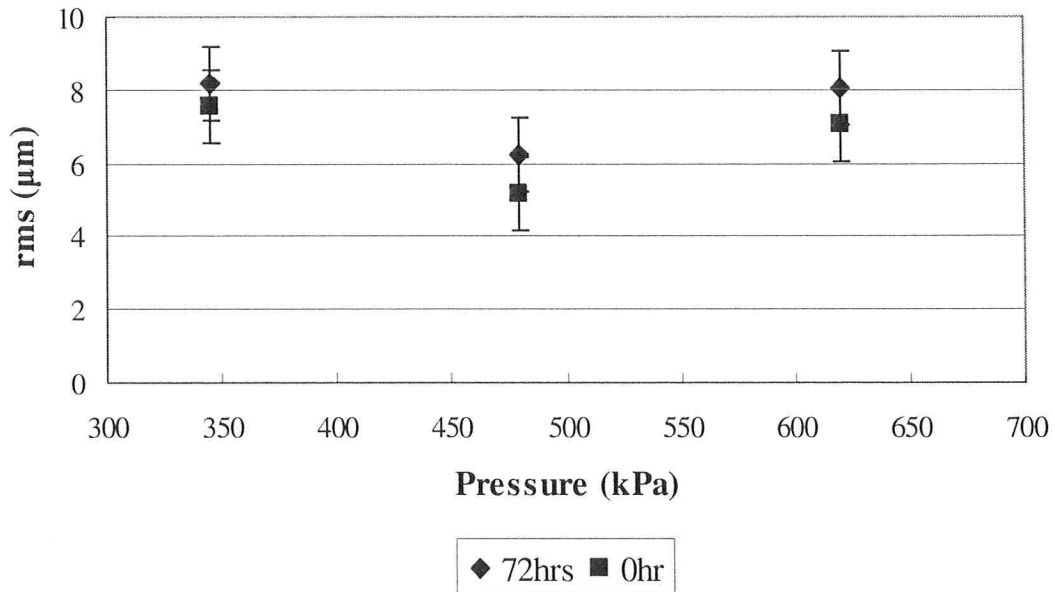


**Figure 4-5.** Rms values for the pressure-cure time experiments for steel laminates. The error bars represent standard deviation for the center point of experimental condition over four measurements on five samples.

The standard deviation was determined by five repeats for the center point experimental condition (i.e. 480 kPa and 72 h of cure time) and it was assumed to be a reasonable representation of uncertainty over other cases. According to the error bars the values are not statistically different in wrinkling response to the different lamination conditions for the metal laminates. More detailed calculations were done to compare the population means using the unpaired t-test method. For that purpose, it was assumed that we have normal distribution; therefore the z value was taken as 2 for a 95% confidence interval to see if the two data points can be taken as statistically insignificant from one another. The results confirmed the previously stated fact that there was no difference. Data analysis using Minitab showed no sensitivity for PV, rms or wavelength to either of

the two factors, cure time or lamination pressure, with P-values higher than 0.05. It also gave very low correlation coefficient for the fitted data. Sensitivity values of 0.05 and less show higher sensitivity of that parameter to the corresponding factor.

The correlation coefficient of the analysis was greatly improved by considering the subsequent heating rate for testing the wrinkling behaviour as a covariate. Sensitivity to heating rate for PV, rms and wavelength is highlighted in Table 4-1.

**Table 4-1.** Minitab statistical values regarding the sensitivity of surface roughness on different parameters.

| Covariant            | R <sup>2</sup> . (%) |     |           | Sensitivity of PV to: |        |     | Sensitivity of rms to: |       |     | Sensitivity of $\lambda$ to: |       |     |
|----------------------|----------------------|-----|-----------|-----------------------|--------|-----|------------------------|-------|-----|------------------------------|-------|-----|
|                      | PV                   | rms | $\lambda$ | CT*                   | Pres.* | HR* | CT                     | Pres. | HR  | CT                           | Pres. | HR  |
| Without Heating Rate | 34                   | 40  | 4         | 0.23                  | 0.09   | -   | 0.14                   | 0.05  | -   | 0.95                         | 0.78  | -   |
| With Heating Rate    | 74                   | 80  | 74        | 0.26                  | 0.05   | 0.0 | 0.1                    | 0.01  | 0.0 | 0.3                          | 0.5   | 0.0 |

\* CT: Cure Time  
 Pres.: Pressure  
 HR: Heating Rate

For this part of the study, since surface roughness quantification values (i.e. PV and rms) seemed to be statistically similar, there is no indication that the lamination condition has a significant effect on the tendency to wrinkle under subsequent heating. This is at least a positive outcome for an industrial user of these films in their forming operations. Yet, it was decided to avoid excessive pressure which might have caused extra residual stress and proceed with the lowest lamination pressure. As for the cure time, 72 h was chosen in order to be consistent with plastic laminates and other researchers in the group.

#### 4.1.2. Unstrained:

Unstrained steel samples were heated to either 110°C or 150°C, as described in the Experimental chapter. What follows are the results for the 150°C case first. The samples were tested at both fast and slow heating rates as well as fast and slow cooling rates. Based on the results of final surface roughness for each heating rate (i.e. fast and slow) with the two cooling rates, it was understood that the cooling rate did not play a significant role in the determination of final surface roughness. Table 4-2 shows the quantifying values for roughness produced by wrinkling, along with their corresponding standard deviations.

**Table 4-2.** Surface roughness quantification figures for final temperature of 150°C in  $\mu\text{m}$  for steel laminates

| <b>Fast Ramp up (95°C/min)</b> | <b>Wavelength</b> | <b>PV</b>   | <b>Rms</b> |
|--------------------------------|-------------------|-------------|------------|
| Ramp Down 1°C/min              | 407 $\pm$ 30      | 24 $\pm$ 6  | 7 $\pm$ 2  |
| Ramp Down 480°C/min            | 476 $\pm$ 86      | 28 $\pm$ 7  | 8 $\pm$ 2  |
| <b>Slow Ramp up (1°C/min)</b>  |                   |             |            |
| Ramp Down 0.6°C /min           | -                 | 9 $\pm$ 6   | 2 $\pm$ 1  |
| Ramp Down 480°C/min            | -                 | 15 $\pm$ 13 | 4 $\pm$ 3  |

In this part of the study due to the different heating rates covering almost from 0.8°C/min to 190°C/min, not all samples experienced wrinkling, especially those going through slow heating rates. Therefore, it was decided that the PV and rms values be taken as determining roughness quantification factors for the effects of heating/cooling rates and leave the wrinkle wavelength for a later section of this thesis.

Plotting these surface roughness quantification values versus rate (Figure 4-6) shows a positive correlation between surface roughness values and the heating rate. The data showed greater sensitivity of PV measurements to the heating rate compared to the

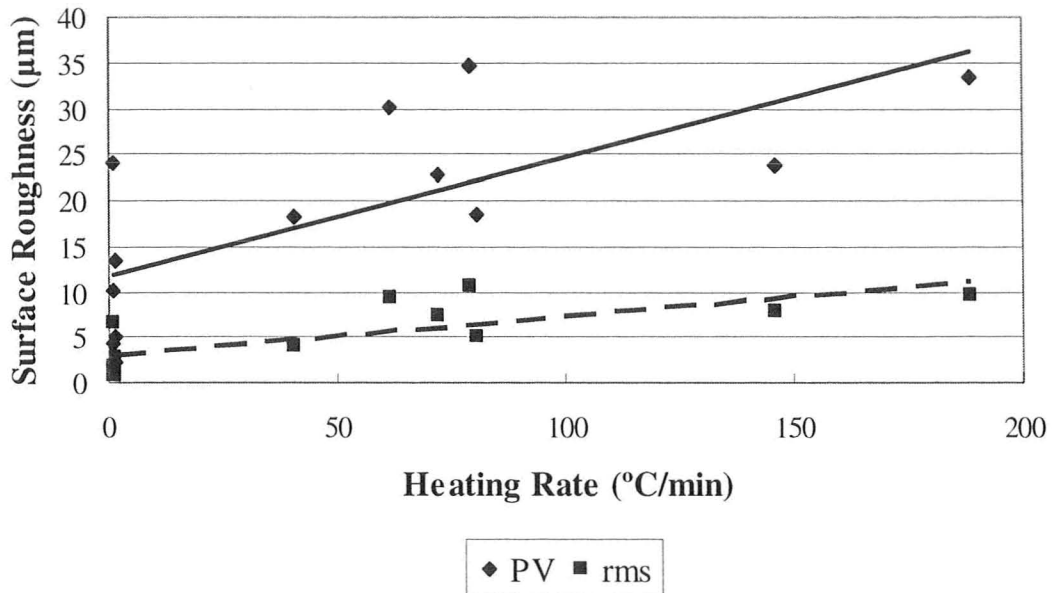
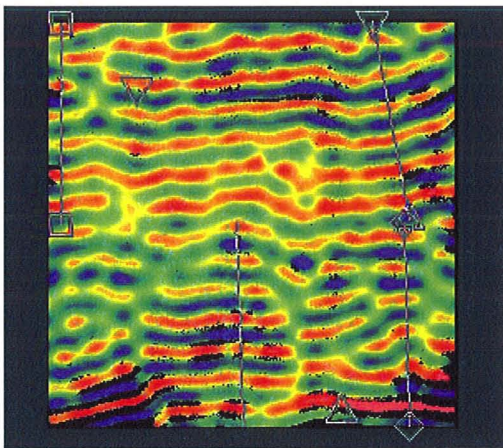


**Figure 4-6.** Trend showing a positive correlation between surface roughness and heating rate for steel laminates heated to 150°C

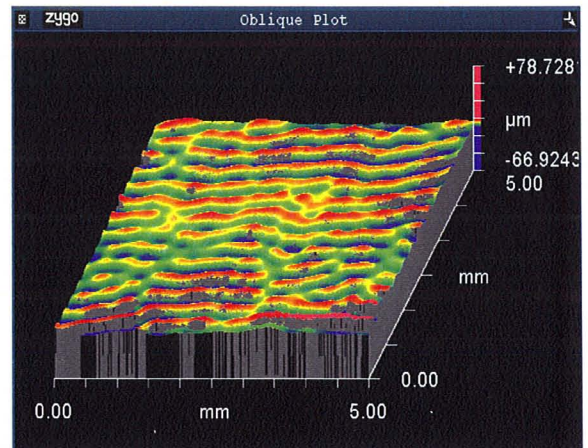
rms values since it is not an averaged quantity but rather states the largest variance in material thickness found within the scanned area of the sample. Since PV measurements are essentially outliers in surface features rather than a nominal representation, it was expected its data showed more variance than the rms data. The lines are linear regression fitted to the data and are just to help the reader to figure out the trend.

In order to get familiarized with the images and data which was obtained through the white-light interferometer a series of images are presented below. Figure 4-7 presents 2D and 3D surface profiles of an example sample measured on the instrument. The top (2D) and the oblique (3D) views show the surface pattern of the sample. The “surface profile” window which is a side-view 2D profile was used to manually measure the wavelength on the sample at four different places. PV value is the difference between the

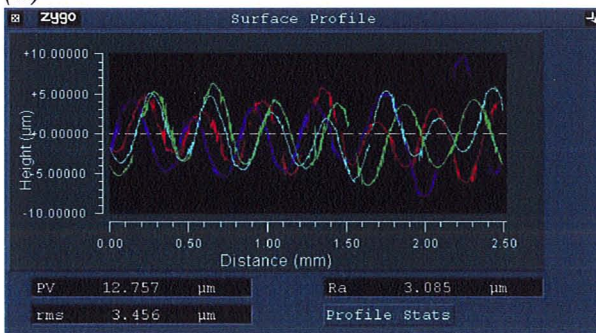
highest and lowest points on the surface, seen from the side-view surface profile. However, it is prone to large errors because it can be sensitive to defects. In order to dampen the influence of defects on the measurement, the quoted PV value in each case is an average based on the four scanned surface areas of the film.



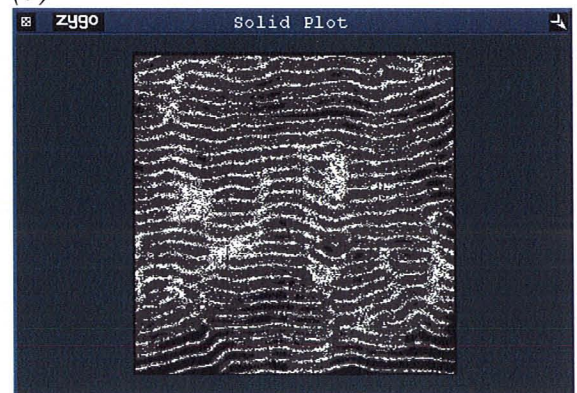
(a)



(b)



(c)



(d)

**Figure 4-7.** Sample surface metrology result window using Zygo NewView interferometer. *a)* Top 2D view, the bars show the way the wavelengths were measured. They were also used to average the PV values at those four locations. This gave the opportunity to eliminate the erroneous points, *b)* is the 3D Oblique Plot of the sample which is just a representation of the surface profile and was not used in measurements, *c)* is the side-view 2D surface profile which was used to manually measure the wavelength and average PV values and finally *d)* is called Solid Plot which is a black and white representation of the top view but at most cases it shows better understanding of the wrinkle patterns.

For the samples heated to the lower temperature of 110°C the observations were different. Even those with a fast heating rate did not wrinkle and basically surface roughness did not change with the heating rate (Figure 4-8). It should be noted that the surface roughness for the 110°C case was much lower than for 150°C (from  $18 \pm 10 \mu\text{m}$  to  $2.6 \pm 0.6 \mu\text{m}$  for PV and from  $5.2 \pm 3 \mu\text{m}$  to  $0.5 \pm 0.04 \mu\text{m}$  for rms, respectively). Therefore it was concluded that not only is heating rate important, but also final temperature plays a role too in establishing wrinkles.

Table 4-3 shows the surface roughness values and their standard deviation for this set of experiments. It should be noted that no wrinkles formed in these experiments therefore there is no wavelength value available.

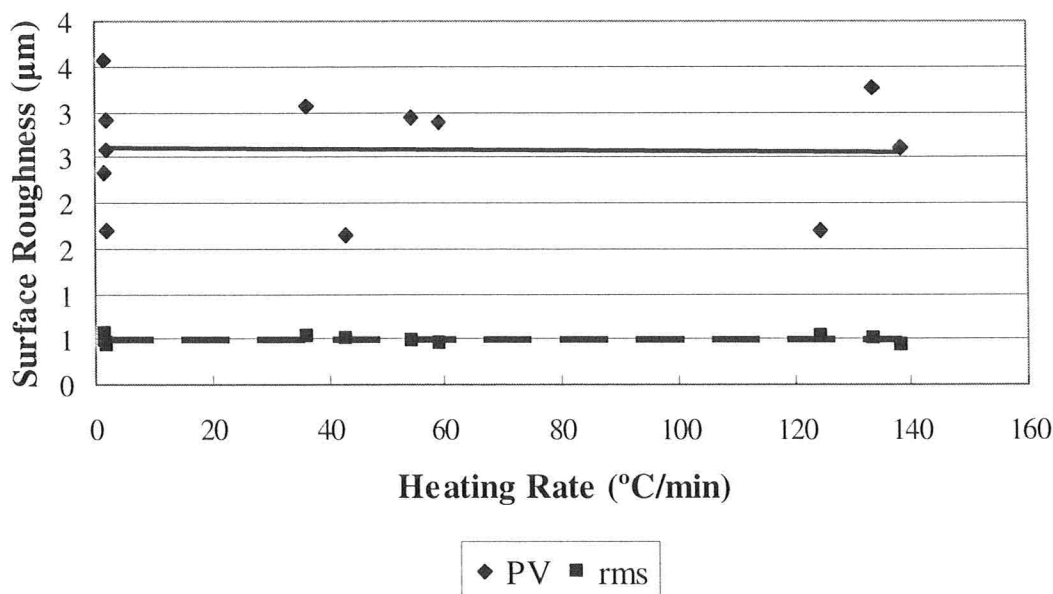


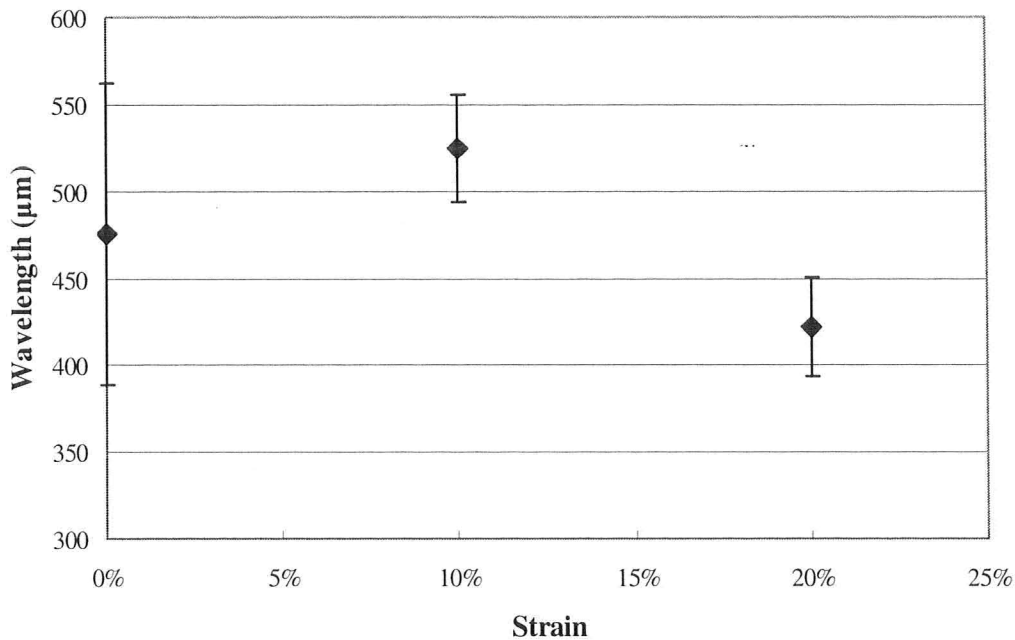
**Figure 4-8.** Scatter plot of change in surface roughness for the final temperature of 110°C for steel laminates.

**Table 4-3.** Surface roughness quantification figures for final temperature of 110°C in  $\mu\text{m}$  for steel laminates

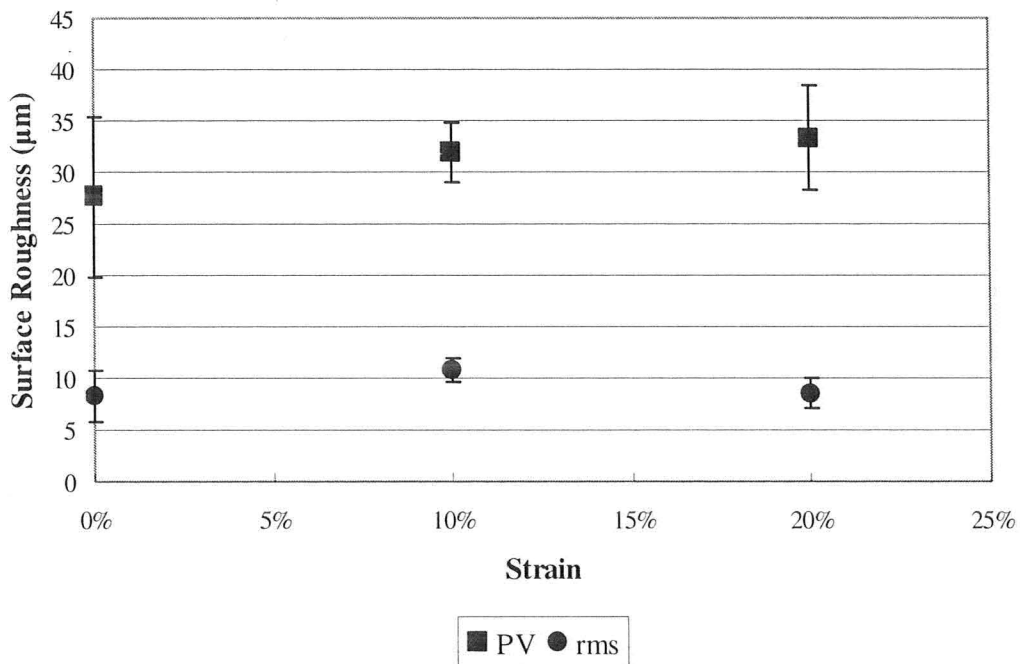
| <b>Fast Ramp up (84°C/min)</b>  | Wavelength | PV             | rms            |
|---------------------------------|------------|----------------|----------------|
| Slow Down (0.6°C/min)           | -          | 2.4 $\pm$ 0.63 | 0.5 $\pm$ 0.05 |
| Fast Down (400°C/min)           | -          | 2.7 $\pm$ 0.73 | 0.5 $\pm$ 0.03 |
| <b>Slow Ramp up (1.8°C/min)</b> |            |                |                |
| Slow Down (0.6°C/min)           | -          | 2.5 $\pm$ 0.17 | 0.5 $\pm$ 0.05 |
| Fast down (400°C/min)           | -          | 2.7 $\pm$ 0.96 | 0.5 $\pm$ 0.07 |

#### 4.1.3. Strained Steel:

Steel laminates were strained to 10% and 20% strain, as was described in the Experimental Chapter, before being heated in the hot stage. From the surface roughness measurements it was clear that a transition in the wrinkle pattern occurred for levels of strain greater than 10%. The 10% strained samples presented wrinkle patterns consistent with the previously discussed unstrained specimens, both holding a disordered zigzag structure (labyrinth). It is believed that the only difference caused by straining the sample to 10% of its original dimensions was the wavelength, now being 525  $\mu\text{m}$  rather than 476  $\mu\text{m}$  for unstrained. The surface roughness qualifiers increased by 14% and 33% for PV and rms, respectively between these two cases. However, due to the large standard deviation of the unstrained samples, the increase for wavelength and PV cannot be statistically proven. Figures 4-9 depicts the trend for wavelength ( $\lambda$ ) and surface roughness values. Figure 4-10 shows solid plots (which were defined in Figure 4-7) of these samples for an area of 5 mm by 5 mm from the center. The pattern changed from a disordered zigzag (labyrinth) to ordered stripes parallel to the direction of strain.



(a)



(b)

**Figure 4-9.** Comparison of *a)* wavelength and *b)* surface roughness values of unstrained, 10%- and 20%-strained samples. The error bars are standard deviation over four measurements on four samples.

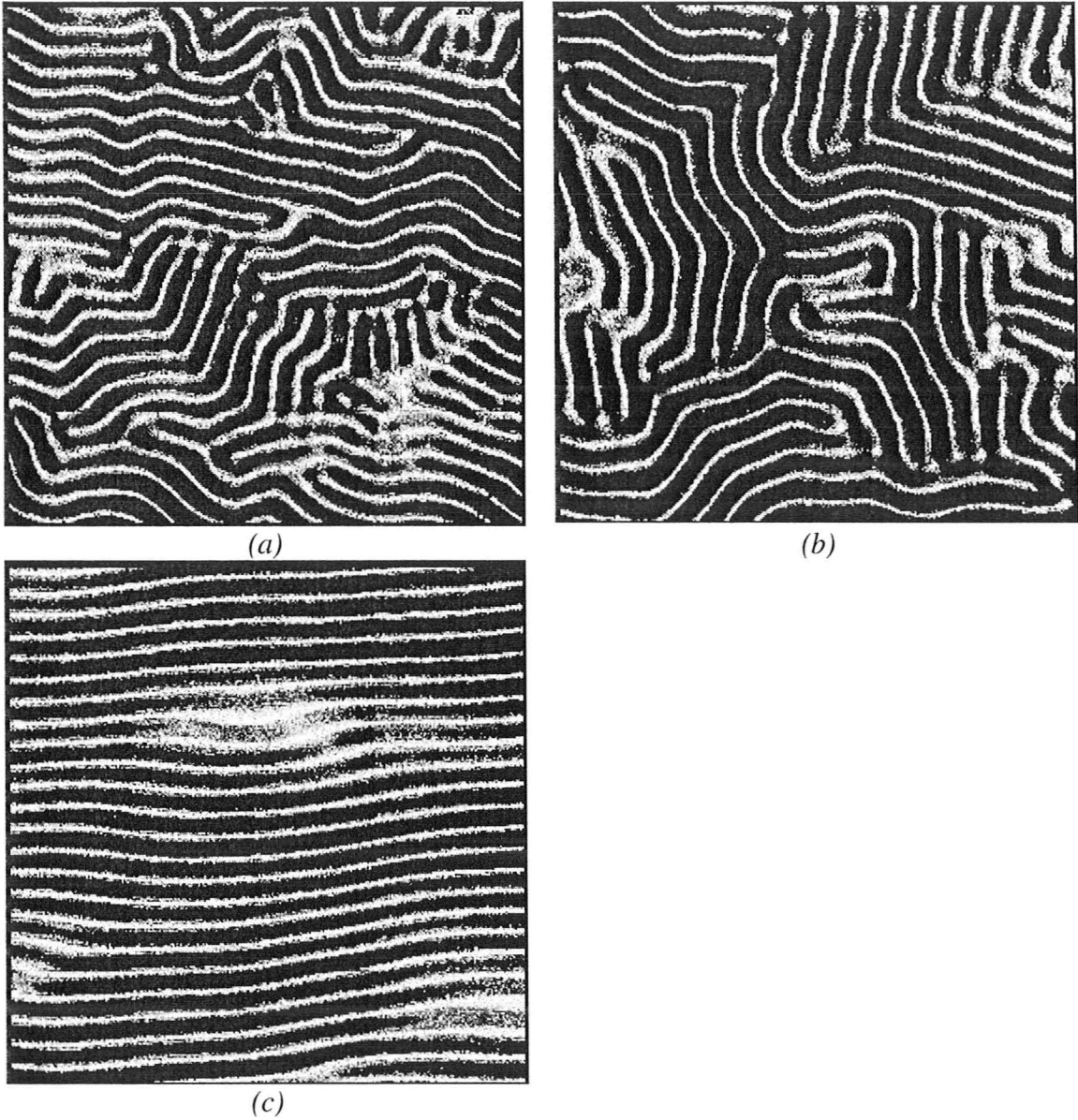


**Figure 4-10.** Solid plots of *a)* unstrained *b)* 10%-strained and *c)* 20%-strained sample

## **4.2. Plastic Substrate:**

### **4.2.1. Pressure-Cure Time Studies:**

The same sets of experiments as completed for the steel laminates were conducted to decide what lamination conditions would be used for the plastic laminates. As a control sample, laminated plastic samples before being heated were measured for their surface metrology. PV and rms values for the control sample were determined to be  $2.4 \pm 0.2 \mu\text{m}$  and  $0.2 \pm 0.1 \mu\text{m}$ , respectively. Like the case for the steel laminates, surface roughness did not show significant differences in PV and rms values for the different lamination conditions. However, the data received for the conditions of 620 kPa roller pressure and 72 h cure time showed less variance than the other sets. Thus, it was decided that these conditions would be applied for lamination. Having used 175°C for the hot stage temperature during these lamination trials, it should be mentioned that no wrinkles were observable in the laminates. The relevance of this issue will be discussed in the next section. Figures 4-11 and 4-12 graph the values of PV and rms, respectively from the lamination tests.

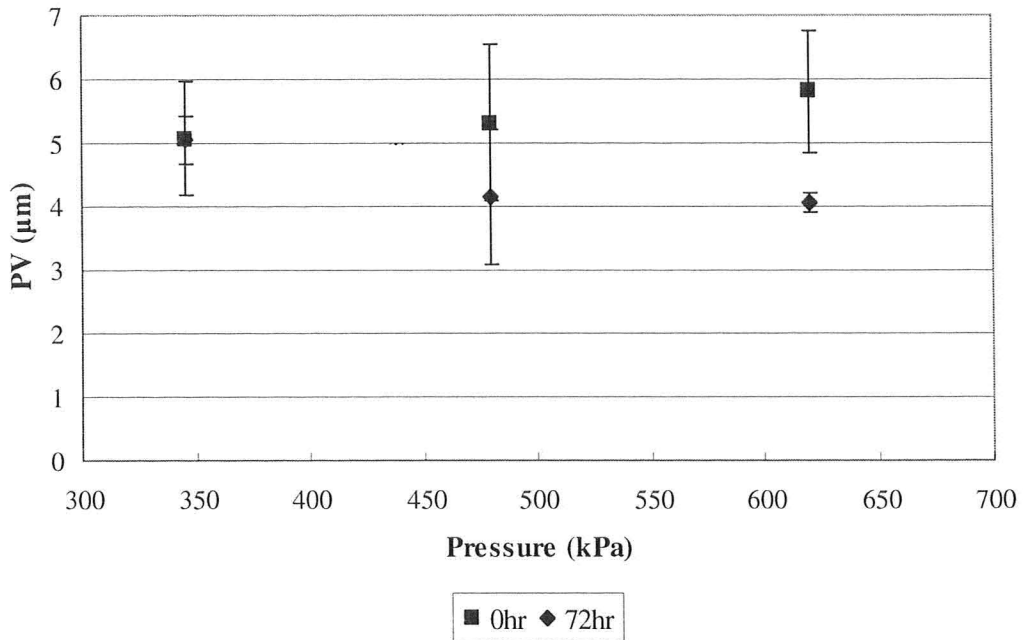


**Figure 4-11.** PV values for the pressure-cure time experiments for plastic laminates. Error bars represent standard deviation over four repetitions.

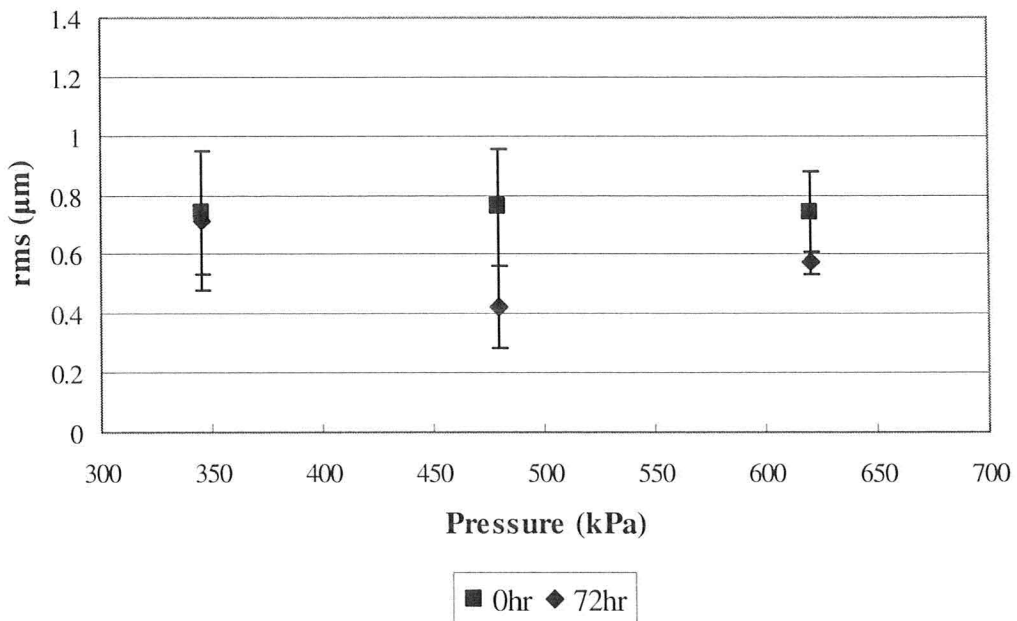


**Figure 4-12.** Rms values for the pressure-cure time experiments for plastic laminates. Error bars represent standard deviation over four repetitions.

#### 4.2.2. Determination of Hot Stage Temperature:

With consideration for the lower thermal conductivity of plastics relative to metal, it was necessary that the hot stage be heated up to 175°C in order for the plastic laminates to reach 150°C. As these trials began it was observed that the fast heating rate did not produce any wrinkles. Having discovered the importance of heating rate with the metal laminates, it was hypothesized that the actual heating rate at the film was not enough to produce wrinkling. To increase the rate further meant increasing the temperature of the hot stage which conversely meant the sample had to be removed as soon as they reached 150°C lest they overshoot in temperature and begin to melt. Since the final temperature did not represent an equilibrium value for the sample any longer (as it did for the metals), the sample's final temperature was prone to  $\pm 3^\circ\text{C}$  variation. To seek a heating rate condition which did produce wrinkles in the plastics substrate three other hot stage temperatures (180°C, 185°C and 190°C) were studied. These hot stage temperatures (including 175°C which was originally used) corresponded to 120°C/min, 170°C/min, 200°C/min and 250°C/min heating rates, respectively. The PV and rms values, as it was expected, increased with heating rate. It should be noted again that a higher hot stage temperature corresponds to a faster heating rate.

Graphing the average PV values and rms values based on the final temperature of the hot stage shows a clear positive correlation with increasing temperature (i.e. increasing heating rate). Figure 4-13 shows the trend.

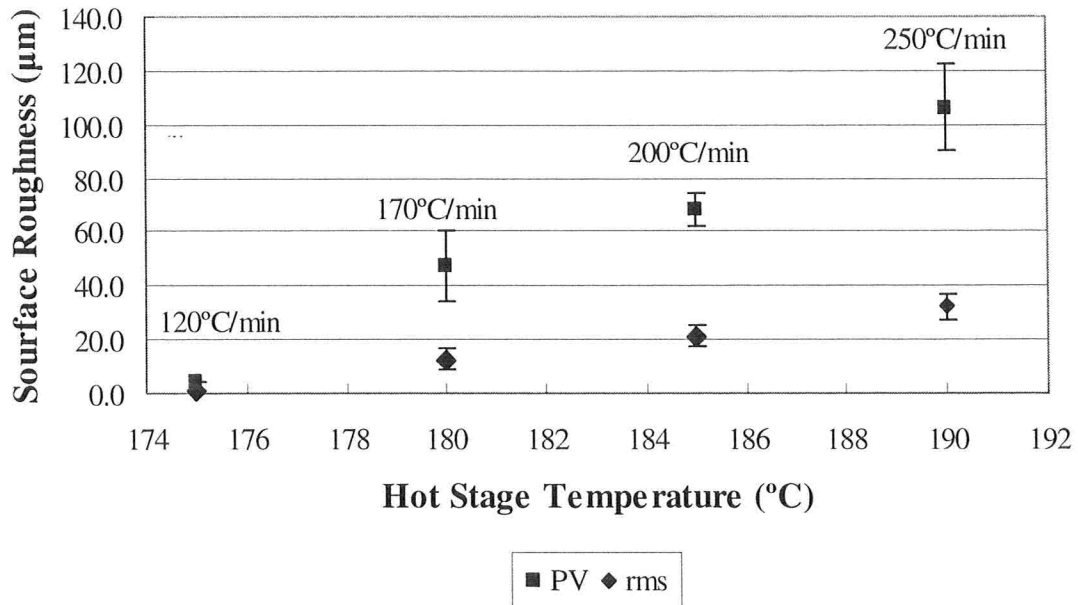
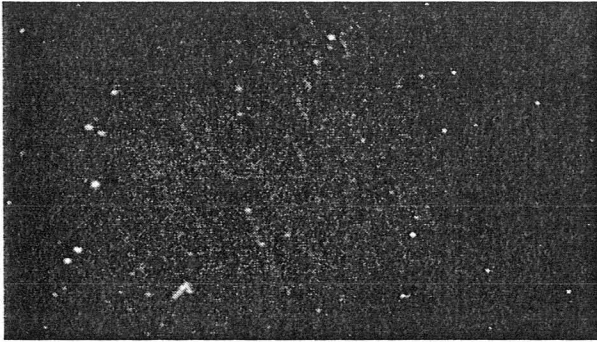


**Figure 4-13.** Positive correlation between the heating rate and surface roughness quantification factors for different hot stage final temperatures. Corresponding heating rate is shown above each temperature. Error bars represent standard deviation over three repetitions.

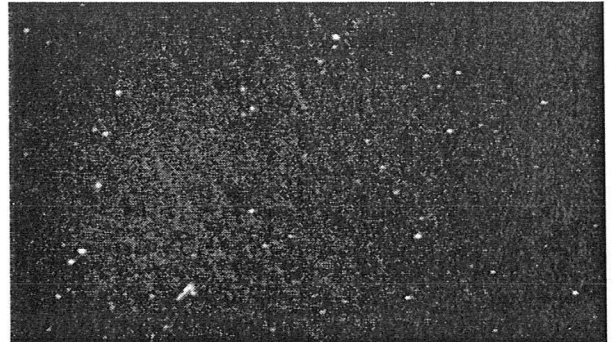
After these experiments it was decided to have the hot stage temperature set at 180°C because it did not heat the samples to higher than 150°C, therefore, quick removal of the samples was not necessary.

### 4.2.3. Wrinkle growth

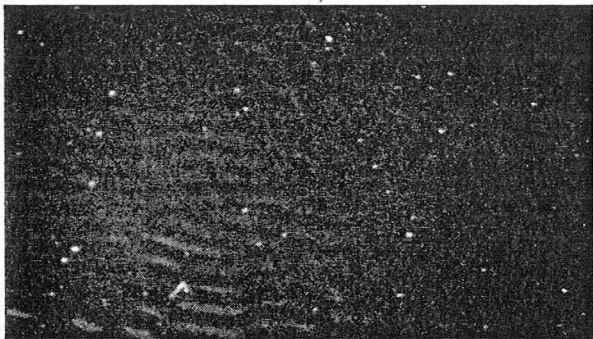
Development of wrinkles in plastic laminates was quantified in the same manner as it was done for the steel laminates. Figure 4-14 shows the chronological development of wrinkles in a plastic laminate being heated under the fast heating rate (170°C/min) condition with respect to time, along with the corresponding temperature at each time step.



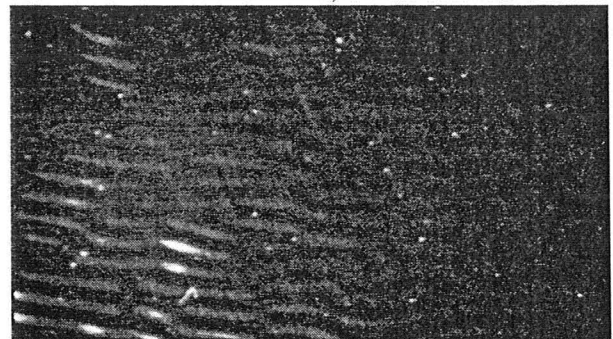
Time = 0, 25°C



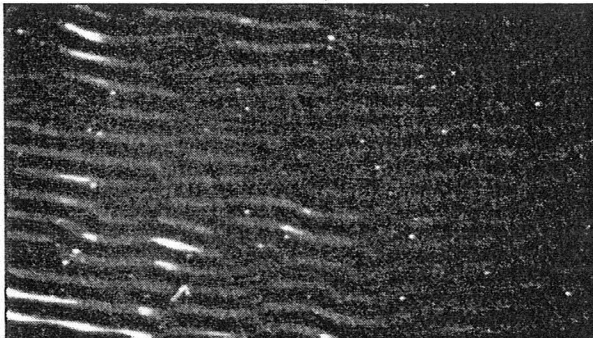
10 seconds, 131°C



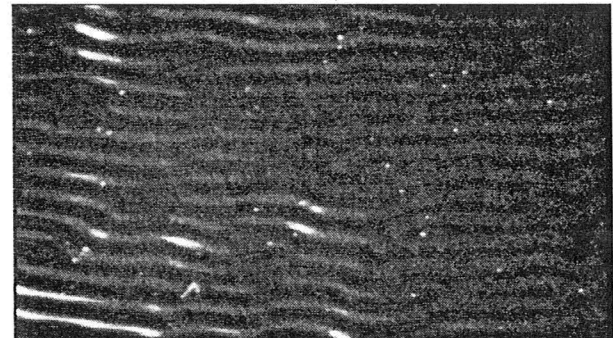
12 seconds, 136°C



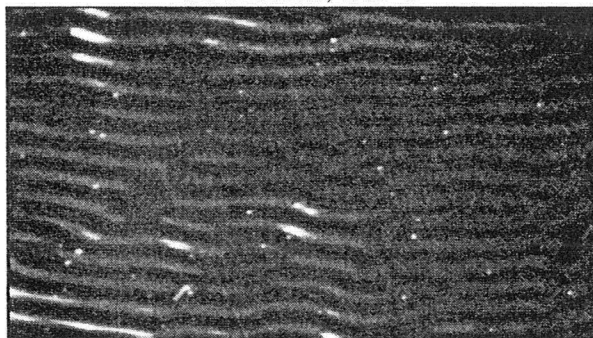
14 seconds, 139°C



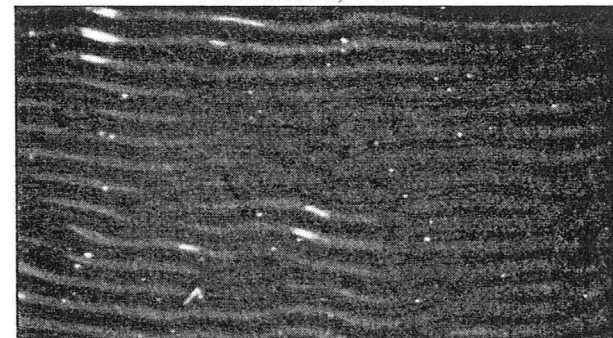
16 seconds, 141°C



18 seconds, 142°C



20 seconds, 142°C



25 seconds, 145°C

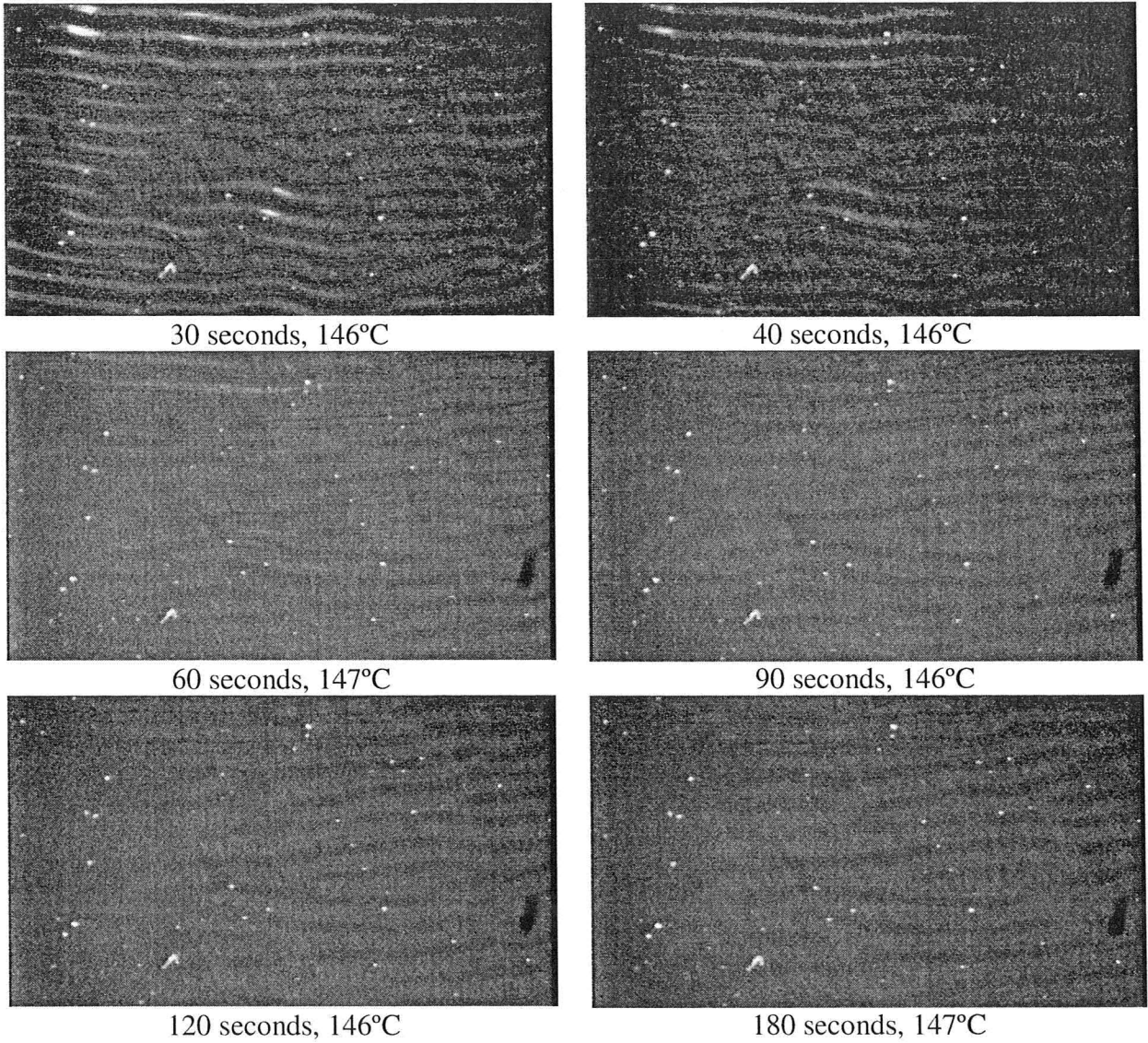


**Figure 4-14.** Wrinkle growth and their corresponding time and temperatures on plastic laminates.

Plastic laminates, in general, required faster heating rates compared to their steel counterparts to produce wrinkles. The sample in Figure 4-14 experienced a heating rate of 170°C/min as opposed to 40°C/min for the corresponding steel laminate sample in Figure 4-1; therefore, for the sample in Figure 4-14, wrinkles started to develop earlier and the wavelength growth was faster, as well. Moreover, based on visual observations, after 3

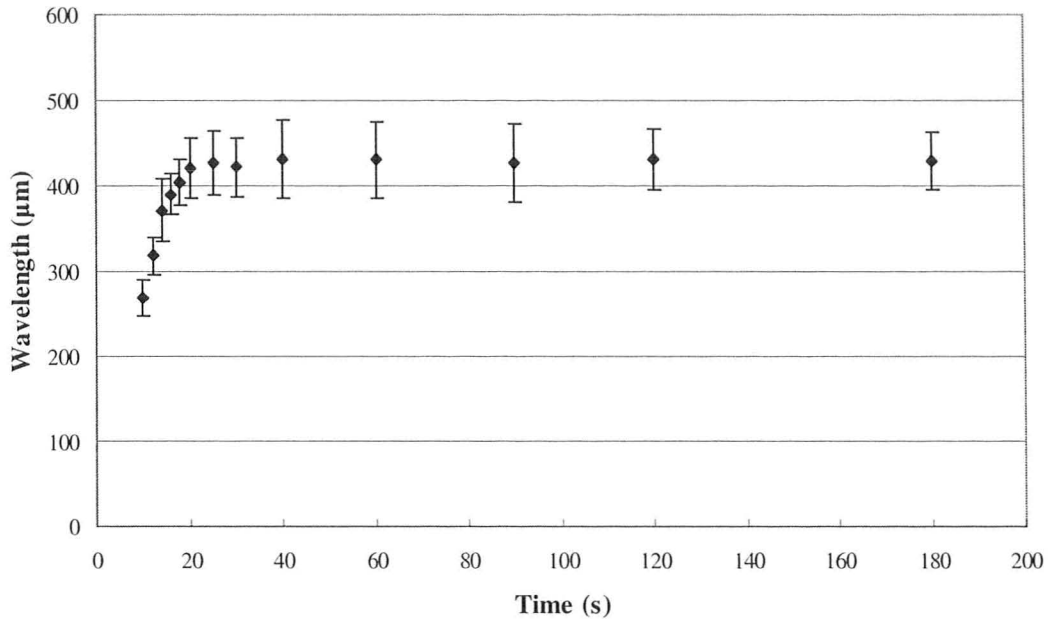


**Figure 4-15.** Wavelength growth on a plastic laminate over a period of 3 minutes. Error bars represent standard deviation over at least 10 wavelength measurements for each data point.

minutes the wrinkles seemed to have reached their equilibrium value although their amplitude decreased over the last 150 seconds of this 3-minute period. In general, the same trend for the steel laminates was observed here; a sharp increase in the wavelength at the beginning and then reaching equilibrium at around 430 µm.

#### 4.2.4. Unstrained

The plastic laminates were subjected to the same sets of experiments as the steel laminates. They were heated up to 110°C and 150°C with a fast (170°C/min) and slow (2°C/min) heating rate, and went through either a fast (water quenching at around 450°C/min) or slow (free air convection at around 1°C/min) cooling process. The slow heating rate did not yield any wrinkles, and therefore there are no measurements of

wrinkle wavelength in Table 4-4. For the fast heating rate, the results demonstrated no difference in the final wavelength between the two different cooling rates although they suggest a decrease in the surface roughness for the samples that were air cooled as they took longer to decrease in temperature (48% for PV and 50% for rms values); compliance of the softened film was occurring as the compressive thermal stresses were allowed to relax under the slow cooling condition. For the samples heated slowly there seemed to be no difference in the surface metrology.

**Table 4-4** Surface roughness quantification figures for final temperature of 150°C in  $\mu\text{m}$  for plastic laminates

|                                 |               |               |               |
|---------------------------------|---------------|---------------|---------------|
| <b>Fast Ramp up (170°C/min)</b> | Wavelength    | PV            | rms           |
| Slow Down (1°C/min)             | 551 $\pm$ 105 | 16 $\pm$ 7    | 5.5 $\pm$ 2.3 |
| Fast Down 450(°C/min)           | 551 $\pm$ 44  | 33 $\pm$ 20   | 11 $\pm$ 7    |
| <b>Slow Ramp up (2°C/min)</b>   |               |               |               |
| Slow Down (1°C/min)             | -             | 4.1 $\pm$ 1.4 | 1.3 $\pm$ 0.2 |
| Fast Down 450(°C/min)           | -             | 3.7 $\pm$ 1.4 | 1.0 $\pm$ 0.2 |

As expected there was a positive correlation between heating rate and surface roughness quantification factors as shown in Figure 4-16.

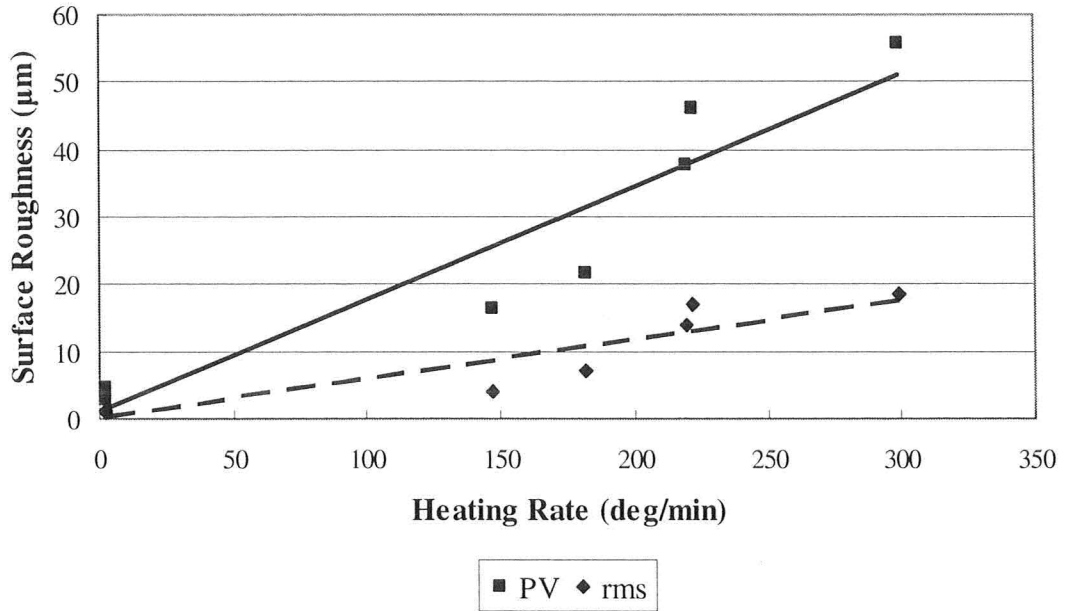


Figure 4-16. Trend showing a positive correlation between surface roughness quantification factors and heating rate for plastic laminates reaching 150°C.

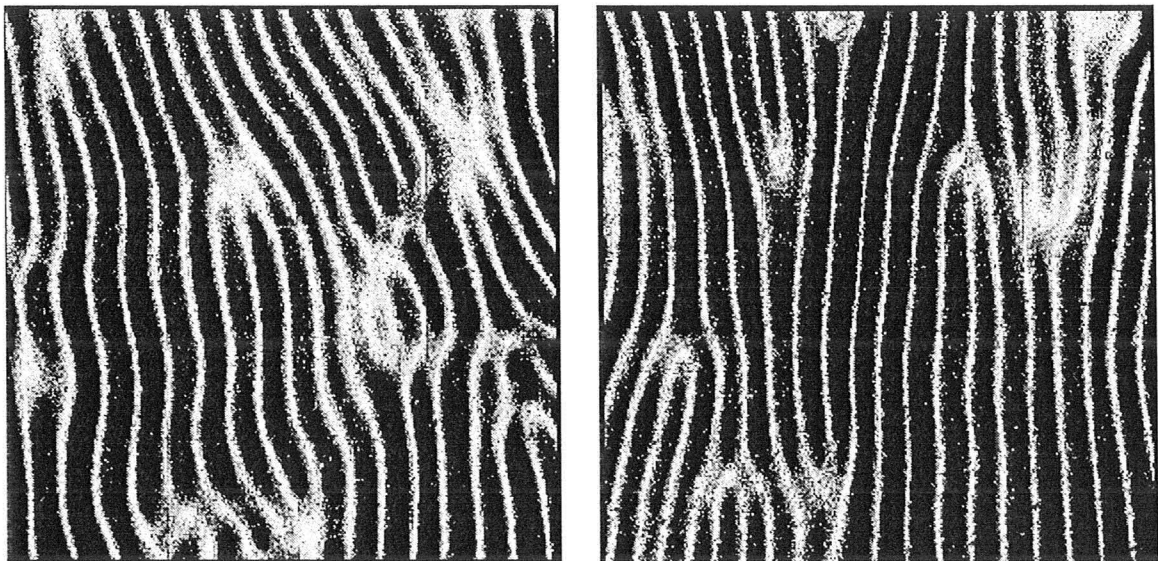


Figure 4-17. Solid plots of two plastic laminates heated to 150°C on a fast ramp-up/fast ramp-down. Longitudinal direction is horizontal.

The wrinkles formed in these experiments were mostly in the transversal direction in the form of stripes/herringbones rather than a chaotic zigzag pattern which was observed in steel laminates. Figure 4-17 shows solid plot of two samples.

For the samples heated to 110°C, again, no wrinkles were observed and the changes in the surface metrology were minimal. Table 4-5 shows the values regarding surface metrology. Figure 4-18 demonstrates that there was no change in surface roughness for samples heated up to 110°C regardless of heating rate. Each data point represents one experiment. The lines are linear regression fitted to the data and are just to guide the viewer figure out the trend.

**Table 4-5.** Surface roughness quantification figures for final temperature of 110°C in  $\mu\text{m}$  for plastic laminates.

| <b>Fast Ramp up (170°C/min)</b> | Wavelength | PV            | rms           |
|---------------------------------|------------|---------------|---------------|
| Slow Down (0.9°C/min)           | -          | 2.1 $\pm$ 0.8 | 0.5 $\pm$ 0.2 |
| Fast down (400°C/min)           | -          | 2.5 $\pm$ 0.8 | 0.7 $\pm$ 0.2 |
| <b>Slow Ramp up (2°C/min)</b>   |            |               |               |
| Slow Down (0.9°C/min)           | -          | 2.3 $\pm$ 0.8 | 0.5 $\pm$ 0.2 |
| Fast down (400°C/min)           | -          | 2.4 $\pm$ 0.8 | 0.7 $\pm$ 0.2 |

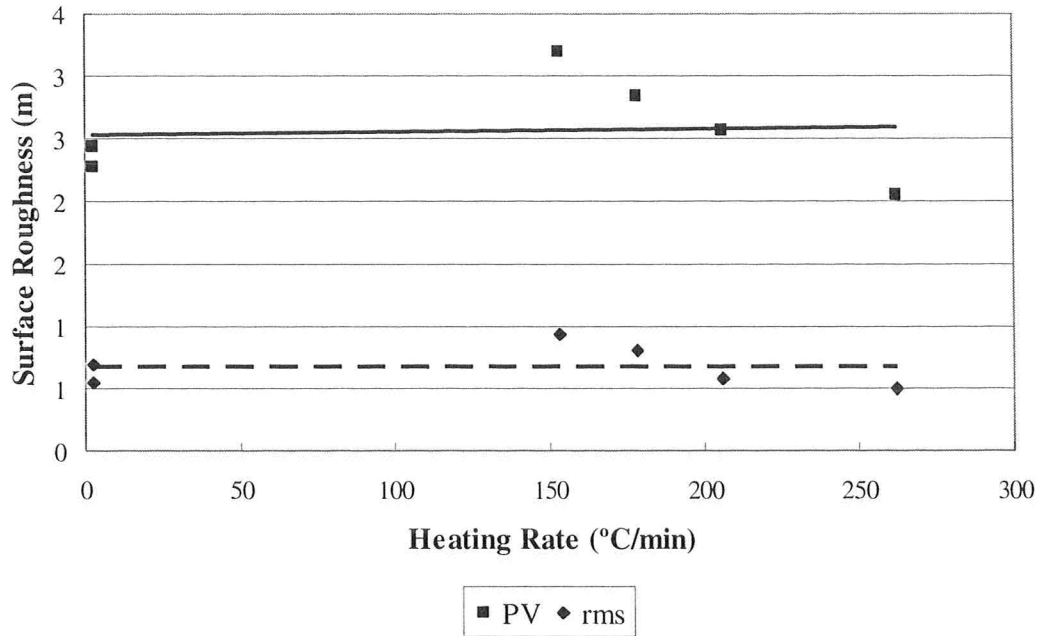


**Figure 4-18.** Scatter plot of change in surface roughness for the final temperature of 110°C for plastic laminates

#### 4.2.5. Strained

For strained plastic laminates the wrinkle pattern changed from the transversal to longitudinal orientation at both 10 and 20% strain conditions. Figure 4-19 shows the solid plot of the strained samples.

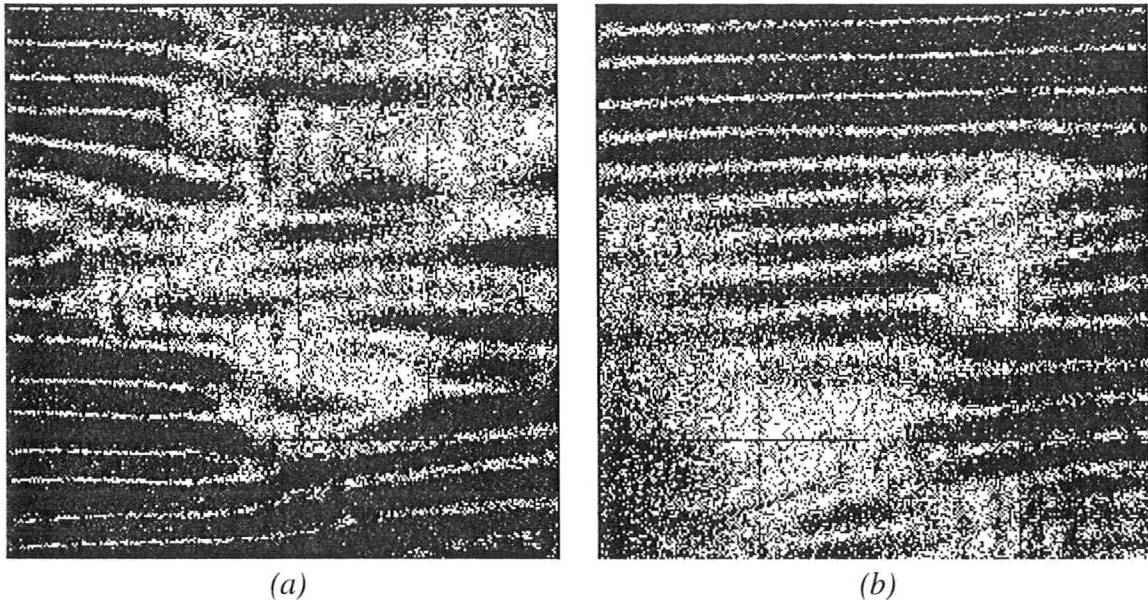


**Figure 4-19.** Solid plot of strained plastic laminates. *a)* 10% strain *b)* 20% strain

A comparison of unstrained samples with strained ones did not show statically different wavelengths ( $537 \pm 3 \mu\text{m}$  for unstrained,  $562 \pm 105 \mu\text{m}$  for 10% and  $469 \pm 30 \mu\text{m}$  for 20% strained samples); however, it showed a decrease in PV and rms values for 10% strained samples compared to the unstrained ones (from  $47 \pm 9 \mu\text{m}$  for to  $14 \pm 4 \mu\text{m}$  for PV and from  $16 \pm 2 \mu\text{m}$  to  $9 \pm 1.5 \mu\text{m}$  for rms). Between the 10% and 20% strained samples only PV values seemed to increase slightly from  $14 \pm 4 \mu\text{m}$  to  $20 \pm 4 \mu\text{m}$ . Figures 4-20 and 4-21 depict these trends.

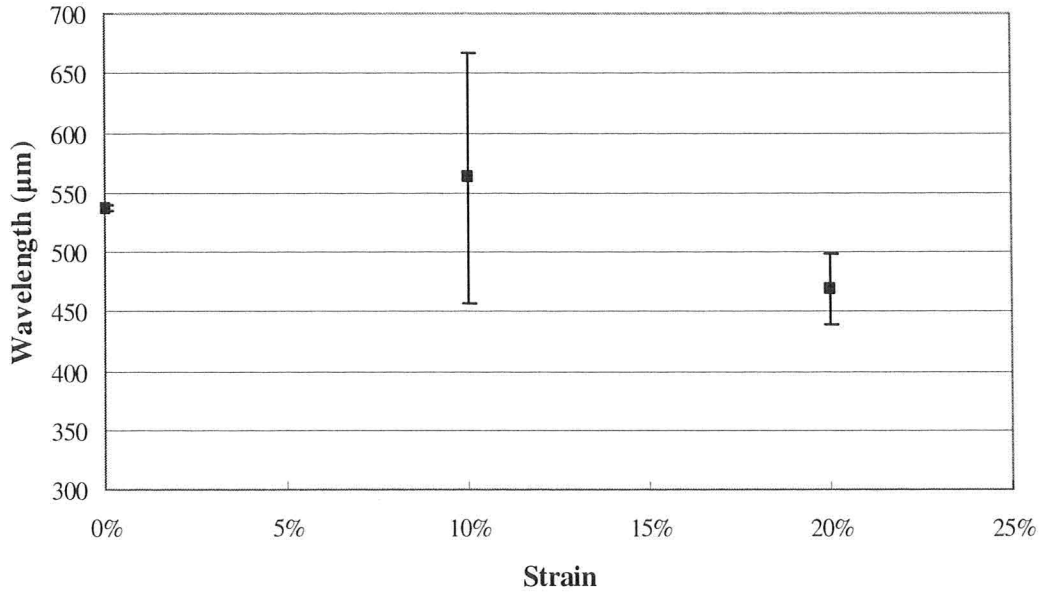


**Figure 4-20.** Wavelength changes for unstrained, 10% and 20% strained plastic laminates. Error bars represent standard deviation over four measurements on four samples.

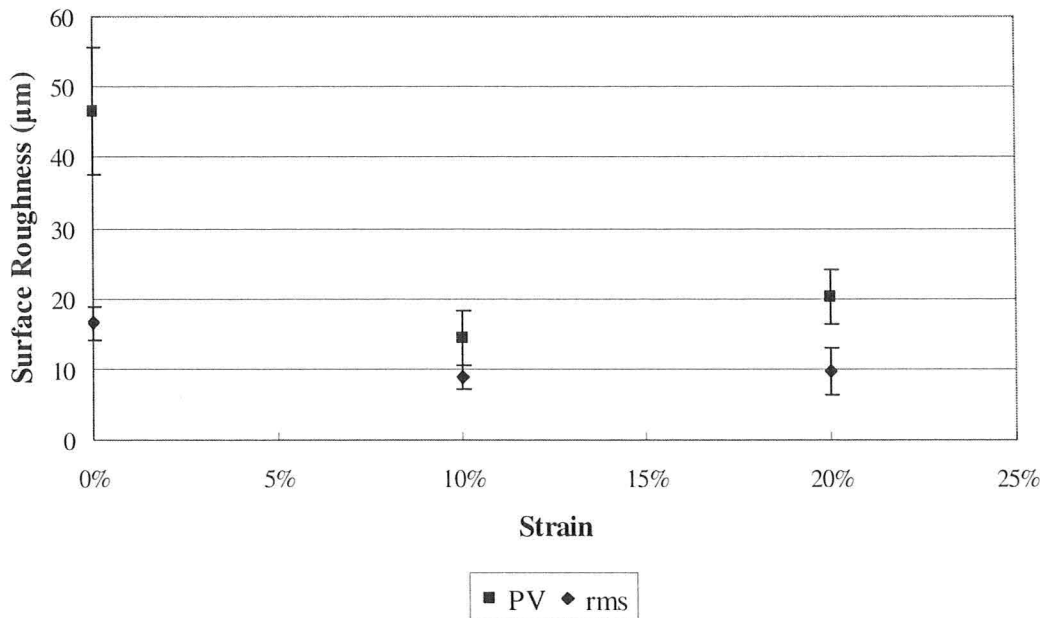


**Figure 4-21.** Surface roughness changes for unstrained, 10% and 20% strained plastic laminates. Error bars represent standard deviation over four measurements.

#### 4.2.6. Vacuum-fixed vs. loose Samples

Due to the complex response of the plastic laminates compared to metal laminates for heat induced wrinkling, several side experiments were conducted to better assess the underlying physical parameters causing the differences. As part of the experiments, it was decided to try another way of heating and study it under two different cases where the laminate was held rigidly in place by vacuum (similar to all other samples earlier tested in the same device) or loose sitting on a surface. A Heat Gun (Milwaukee MHT3300) was utilized in order to heat the samples. The hot air gun creates a broad cone-shaped dispersal of heated air with a radial gradient of temperature. The approximate heating rate was  $60^{\circ}\text{C/s}$  and the samples reached around  $200^{\circ}\text{C}$  for less than a second. The experiment produced a different pattern in each case, whether vacuum was applied or not, as shown in Figure 4-22.

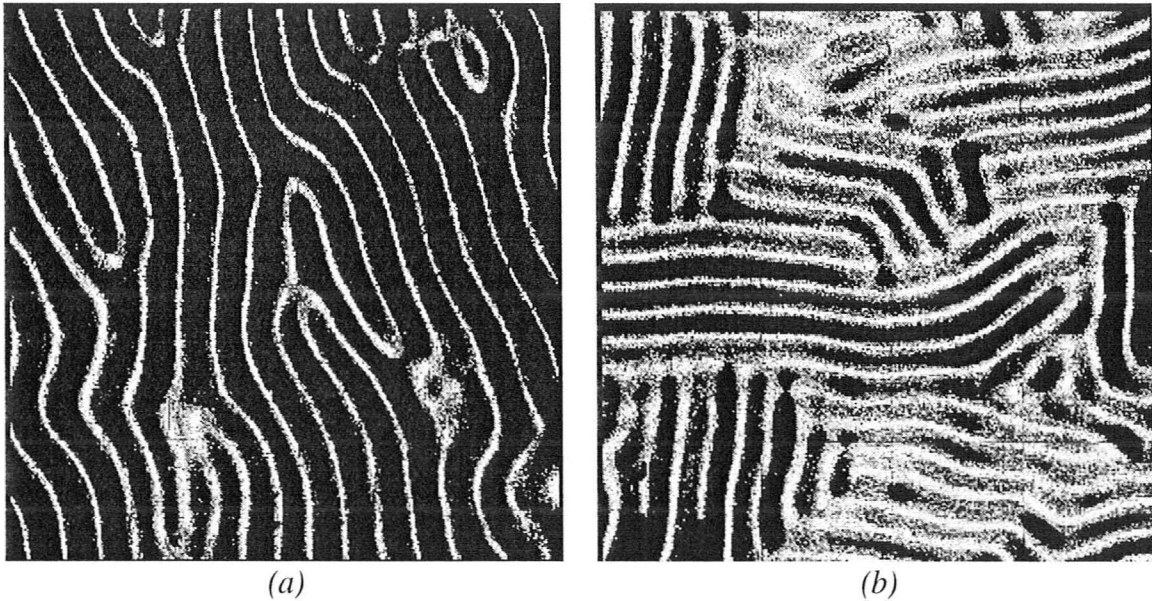


**Figure 4-22.** Solid plot of *a*) loose sample *b*) vacuum-fixed sample. Longitudinal direction is horizontal in both cases.

The pattern on the loose sample looks more like the unstrained vacuum-fixed samples heated in the Hot Stage (Figure 4-21). Heating was different between the two methods of mounting the laminate due to the nonuniformity of air flow. Further studies are needed. Despite the differences in the pattern itself, surface metrology showed that the developed wavelengths for the two mounting conditions were statistically similar, indicating the equilibrium condition had been reached in both cases. The difference in the pattern itself was more notably reported by PV and rms values, which were higher in the loose sample.

**Table 4-6.** Surface metrology values for the loose and vacuum-fixed plastic laminates in  $\mu\text{m}$ .

| Sample       | Wavelength   | PV          | rms        |
|--------------|--------------|-------------|------------|
| Loose        | 629 $\pm$ 34 | 69 $\pm$ 11 | 23 $\pm$ 5 |
|              |              |             |            |
| Vacuum-fixed | 560 $\pm$ 65 | 29 $\pm$ 5  | 9 $\pm$ 2  |

### 4.3. *Wrinkle Appearance Threshold*

Based on the image analysis and also white-light interferometer measurements for different samples it was apparent early in this work that wrinkles started by forming small bumps and blisters and then as the temperature increased they gradually connected and formed stripes/herringbones and finally formed into complex zigzag (labyrinth) patterns when the ratio of compressive stress over stiffness of the film reached a maximum. For different samples due to different reasons (i.e. either not being high enough temperature for the film to be soft enough or not experiencing a sufficiently fast enough heating rate) the necessary compressive stress was not reached, therefore, wrinkles did not develop into the final complex labyrinthine pattern, being stopped at early stages of development. Figure 4-23 shows 2D top view of these stages in wrinkles formation obtained by the

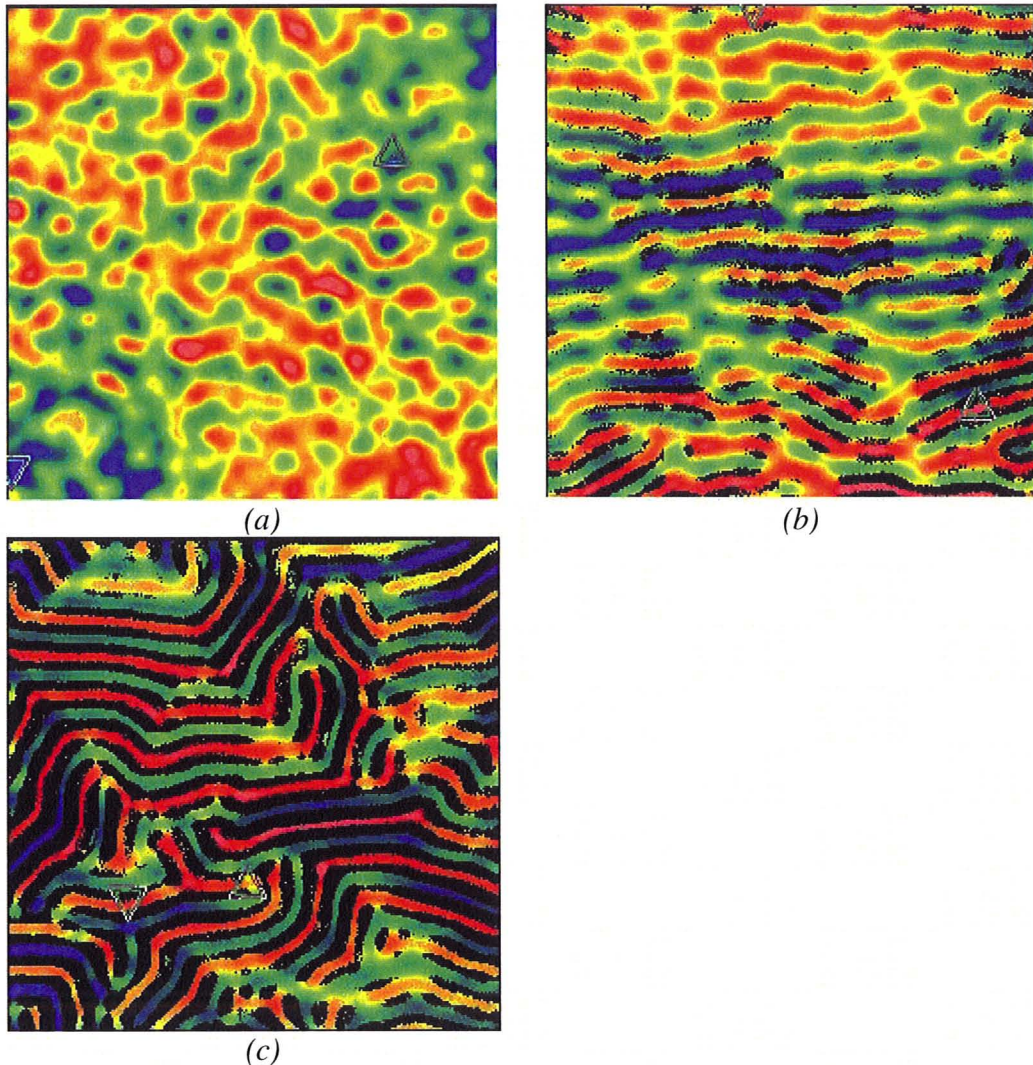


**Figure 4-23.** 2D top view images obtained from white-light interferometer for three different steel laminates, *a*) sample heated to 150°C at almost 1°C/min, only small blisters formed on the surface, no wrinkles were formed, *b*) sample heated to 150°C at around 40°C/min, blisters connected to one another and formed stripes/herringbones, *c*) sample heated to 150°C at around 146°C/min, not only did the wrinkles form, but also developed into complex labyrinth pattern.

white-light interferometer for three different steel laminates heated to 150°C at three different rates.

To quantify the threshold surface roughness for when wrinkles formed a definitive shape in the film where a wavelength was recognizable, the data from all trials mentioned

above were analyzed. Using the PV value for this correlation it was found that as the blisters exceeds a threshold value of 7  $\mu\text{m}$  wrinkles with a defined wavelength were distinguishable in 9000J. Figure 4-24 shows a graph of the analysis. The dashed line on the graph showing the threshold state.

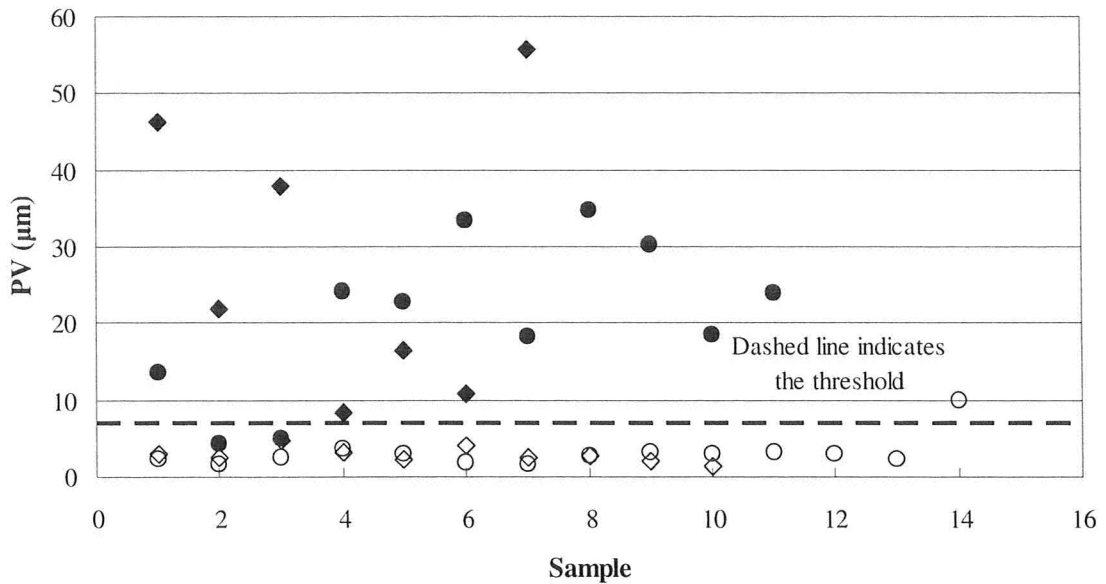


**Figure 4-24.** Graph showing PV values for samples that did and did not experience wrinkling. Hollow and solid markers represent “no wrinkles” and “wrinkled” samples, respectively. Diamonds represent plastic laminates, circles indicate steel laminates. Dashed line shows the threshold of PV values at 7 $\mu\text{m}$  above which wrinkles formed.

---

---

## ***CHAPTER V:***

### ***Discussion***

---

---

#### **5.1. Examination of wrinkling in a film structure**

Adhesive failure at the pressure sensitive adhesive layer can be produced by quenching a heated sample with liquid nitrogen, which allows examination of the cross section of the wrinkles in the film/primary substrate. The detached film structure from a metal secondary substrate was gold sputtered (thickness of 90 nm) to provide mechanical rigidity so the wrinkle pattern would be preserved during mounting in a cold-cure epoxy resin. The fully cured mounting was subsequently cut and then observed under an optical microscope. Figure 5-1 shows the cross-section of a wrinkled film. This image reflects what was schematically shown in Figure 2-9. It shows buckling localized on the film side of the primary substrate, indicating the primary substrate complied under compressive forces induced by thermal stresses. In the picture three different layers are identified which are the PET film, PP/PE primary substrate and the bottom layer is the pressure sensitive adhesive (PSA) that is used to bond the film to either of the secondary substrates (the gold layer was too thin to be observed). It should be mentioned that in our studies, the effects of PSA have not been taken into account on the basis that at high temperatures the adhesive does not play a definitive role in the system based on lap shear tests conducted by E. Takacs.

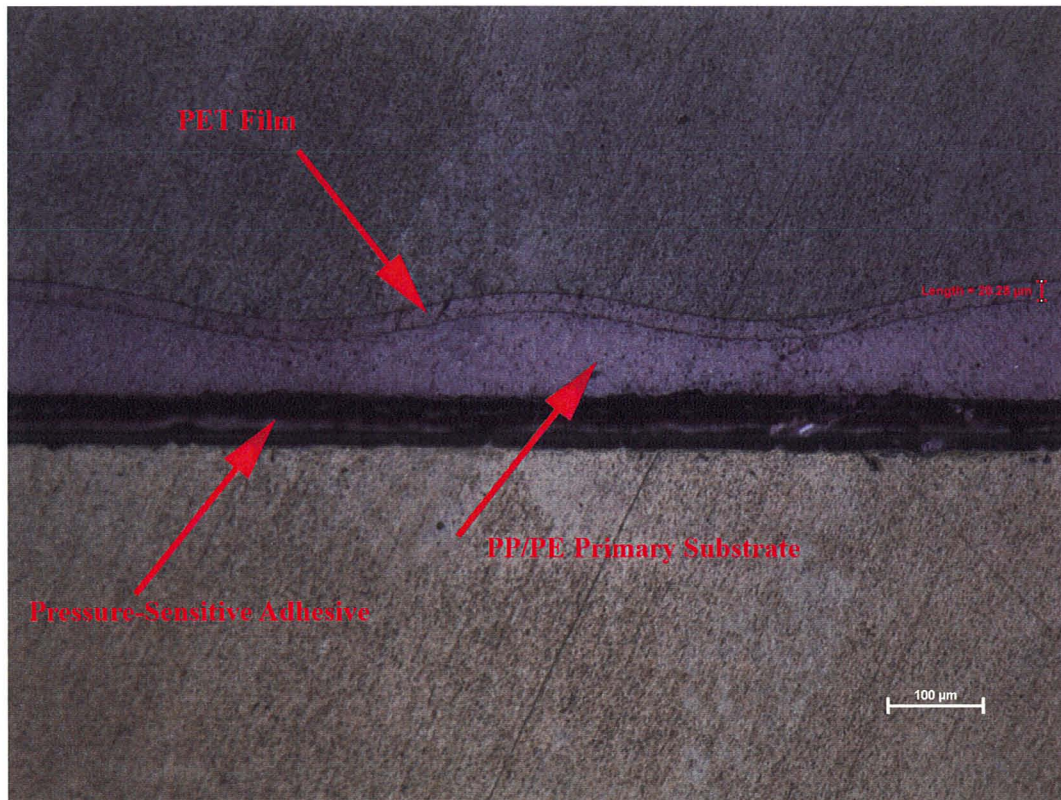


**Figure 5-1.** Cross-section view of the detached film sandwich from a steel laminate via quenching in liquid nitrogen.

## 5.2. *Description of wrinkling initiation and growth*

In the literature review we defined two different stress thresholds, glassy- and rubbery-state critical stresses required to cause wrinkles, with the glassy-state critical stress being larger than the other one. At room temperature the residual stresses within the film are at least less than the glassy state critical stress, therefore it is expected that the film will be stable in geometry at the glassy state and no wrinkles will form. By

increasing the temperature two different phenomena happen. First, the amount of stress in the film increases due to volumetric expansion. Second, as the temperature rises, the mechanical properties (stiffness) of polymers decrease. The first one of these phenomena has been studied by many researchers, though differently from our case (being normally induced by solvent swelling or physical compression rather than thermal stresses), while the latter has been neglected by most as isothermal conditions are better suited to modeling. Only Basu *et al.* (Basu, Bergstreser, Francis, Scriven, & McCormick, 2005) considered decreasing mechanical properties in their model for a system of polyvinyl acetate (PVA) film on polyethyl acrylate (PEA) primary substrate, and their model being significant to this work is introduced in this chapter for special consideration rather than having been introduced in Chapter 2 in the category with the other physical models.

In our case, thermal stresses and mechanical properties must both be considered to explain the wrinkling behaviour as both display significant temperature dependency for our polymer-polymer film structure. The implication is that by increasing the temperature not only do we increase the initial compressive stress in the film due to thermal expansion, but also we decrease the film's ability to resist that stress by decreasing in stiffness. This decrease is due to an increase in chain mobility and melting of crystals (if a semicrystalline material) as the temperature increases which both cause a drop in the elastic modulus. At some point the critical stress required for the film to wrinkle drops due to a sufficient decrease in the stiffness of the material. At this point accumulated compressive stresses in the film are large enough to cause wrinkles to form. Figure 5-2 is a schematic visual description of what happens to the elastic modulus, critical and initial

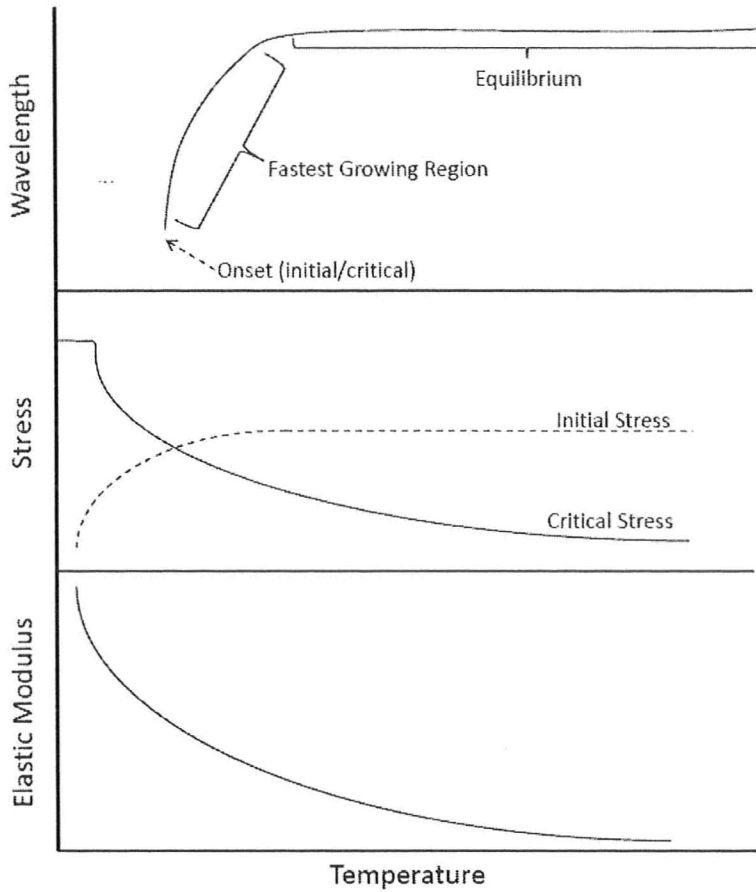


**Figure 5-2.** Conceptual description of changes occurring due to increasing temperature to Elastic modulus of the film, stresses and wavelength growth.

stresses of a film and once formed the wavelength of wrinkles, as temperature increases for the sandwich structure.

As it was shown in Section 4.3, the instabilities start in the form of small bumps on the surface of the film. At that stage the stress is small enough to be relieved by forming only these blisters. This point has not been discussed before in the literature, possibly from a lack of consideration or inadequate resolution of surface features in those other studies, or from the use of a PSA for the adhesive layer in our work. However, as the thermal compressive stresses increase with temperature, blisters become insufficient

to relieve the interfacial energy, and so they grow larger and become connected to one another, forming a recognizable wrinkle (i.e. threshold roughness was a PV value of 7  $\mu\text{m}$  for our film composition). These wrinkles as it can be seen in Figure 4-23 first formed as parallel stripes/herringbones in the longitudinal direction, suggesting anisotropic biaxial stresses in the early stages of their formation. As the process continued, compressive stresses increased but also become more isotropic, and consequently the wrinkles formed into a chaotic zigzag (labyrinth) pattern.

Seen in Figures 4-2 and 4-15, once the wrinkles were formed they grew fast to relieve the accumulated compressive stress but then after some time they slowed down and reached an equilibrium. Basu *et al.* (Basu et al., 2005) mentioned that although increasing temperature creates more in-plane compressive stress, it does not change the critical stress. Therefore, increasing the temperature after some point would not change the wavelength of the wrinkles in the film. For our case, after the appearance of the wrinkles at approximately 130°C they grew fast until the film reached 140°C but then from that point up to 150°C heating did not change the wavelength of the wrinkles. The value of 130°C will be an important temperature in the models below, presenting a threshold which relates to the system exceeding a critical stress limit. The trend of a fast growing wrinkle which then reached a plateau wavelength was also stated by (R. Huang, 2005). One reason for that might be due to the fact that according to Huang (R. Huang, 2005) the wavelength is kinetically determined in its early stages of formation and is independent of the viscoelasticity of the substrate, being only dependent upon the compressive stresses in the film. Only after passing some point where the amplitude/film

thickness ratio increased, the wavelength is energetically selected such that it is completely dependent upon the thickness and viscoelasticity of the primary substrate. At that threshold the primary substrate is considered as being deformed in a completely viscous manner.

### **5.3. Comparison of wrinkling models**

In this section different models were compared based on their ability to predict/estimate the physical properties of the film structure as well as the level of compressive stress in our system, in order to explain the underlying deformation across the different layers of our film structure as wrinkling occurred. Most models are based on an assumption that wrinkling is a thermodynamic phenomenon; however, as seen in the last chapter wrinkling appears to be a kinetic process over the tested range of heating rates. The kinetic nature is related to the fact that the properties of the materials will change drastically under transient heating. The models presented, unless otherwise stated, only considered constant physical properties in their calculations and in most cases their experiments to justify said models were only performed at constant temperature conditions. To make comparisons to our system, this requires certain assumptions which will allow the use of constant physical properties in the calculations.

It was recognized from the experimental trials that 130°C was a critical temperature at which wrinkles started to develop from small blisters for 9000J. A second characteristic temperature for our system was the final temperature of 150°C and accordingly we defined two different temperature regions: the *onset region* from 30-130°C to calculate/estimate the physical system values (such as critical stress, elastic

modulus and so on) before appearance of the wrinkles; and then the *growth region* from 130-150°C for the calculation/estimation of those same physical values as well as wrinkle wavelength after their occurrence. Table 5-1 summarizes the physical properties for our material system estimated for the two regions. Since experimentally only the DMA data for the intact film structure was available and not the individual components, some estimates were required to proceed with our calculations. This section outlines how those estimations were made

**Table 5-1.** Estimated material properties and calculated wavelengths for onset and growth region

| Properties          | Onset Region      |                   | Growth Region     |                   |
|---------------------|-------------------|-------------------|-------------------|-------------------|
|                     | PET               | Primary Substrate | PET               | Primary Substrate |
| $E (Pa)$            | $455 \times 10^6$ | $91 \times 10^6$  | $9 \times 10^6$   | $280 \times 10^3$ |
| Secondary Substrate | Plastic           | Steel             | Plastic           | Steel             |
| Wavelength          | 268 $\mu\text{m}$ | 200 $\mu\text{m}$ | 550 $\mu\text{m}$ | 450 $\mu\text{m}$ |

For estimating the moduli in the onset region, since the exact values for PET film and PP/PE primary substrate was unknown in the commercial product of 9000J, we had to estimate the most reasonable values. Based on detected melting transitions at 110°C and 160°C (assigned to PE and PP, respectively) having similar areas under their peaks in the DSC thermogram of the film, the modulus of the PP/PE copolymer substrate was felt to be reasonably approximated as having equal portions of both as separate phases. In the literature, the elastic modulus of PET is almost 5 times higher than the average modulus value for a PP/PE copolymer blend at room temperature (1.5 GPa versus 300 MPa, (Basu et al., 2005) and (Dhoble, Kulshreshtha, Ramaswami, & Zumbrennen, 2005)). Having the elastic modulus of the entire film sandwich at room temperature (160 MPa by DMA) and using the moduli and thickness ratios, we estimated a modulus of 455 MPa for the PET

film and 91 MPa for the primary substrate. For the growth region, the measured values for elastic modulus of the entire film sandwich through DMA showed a value of 2 MPa at 150°C. Considering one phase in the copolymer will have passed its melting point by this temperature and being close to the softening point of the other, we assumed that the modulus of PP/PE would be negligibly small. Therefore, we could assume that the major part of that 2 MPa modulus is associated with PET. Modulus of PET according to Basu *et al.* (Basu *et al.*, 2005) is about 500 MPa after the glass transition temperature ( $T_g$ ) of 80°C. Since there was no data in the literature regarding any estimation of moduli values at high temperatures, we had to come up with an estimated value that also made sense in our system. Since 150°C is close to PET softening point of 170°C, we assumed a drastic drop in modulus at  $T_g$  and estimated a modulus of 9 MPa. Using the thickness ratio of PET layer to the primary PP/PE substrate (0.2/0.85), and knowing the total modulus of the system (2 MPa), we calculated the copolymer modulus to be around 280 kPa which is reasonable and made sense to the calculations in this chapter. These moduli values were all summarized in Table 5-1 above.

It is recognized these assumed values incorporate large error which is estimated to be ~25%; however, directly measuring these values (if the film structure could be separated) would likely bring about comparable levels of error. The only two methods for mechanical measurements of such thin films are nanoindentation and induced wrinkling; the former being highly affected by the indenter tip and depth of indentation while the latter must assume one of the models we explore below is an exact physical description of the wrinkling phenomenon of that structure.

Another assumption made in this thesis was in regards to the wavelength. For the initial wavelength, the first defined, measurable wavelength that was observed in the process was used (Figures 4-2 and 4-15). This is also referred to as critical wavelength in calculations later on. As for the equilibrium values for wavelength an averaged value of 450  $\mu\text{m}$  for steel laminates and 550  $\mu\text{m}$  for plastic laminates was taken for all of the calculations. The initial wavelengths as noted in Table 5-1 were taken to be the first defined wavelength experimentally observed, which were 200  $\mu\text{m}$  and 268  $\mu\text{m}$  for the secondary steel and plastic substrates, respectively. These values will be used in equations from now on.

Having stated the assumptions deemed important to our system and the means by which important variables used were estimated, the models can be now discussed. The first sets of models were stated in Chapter 2 and are differentiated based on their assumption of the principle mode of deformation for the film and primary substrate, i.e. elastic, viscous or viscoelastic. These models do not consider the relevance of the secondary substrate or the effects of temperature upon the wrinkling pattern. One additional note to be made here was that in Chapter 2 some authors had introduced analytical expressions for the fastest growing wavelength, however, as they never fully defined this term and we are unclear of its relevance, its calculation was not included in this chapter.

### 5.3.1. Elastic Models

Based on Eqn. (2-1) with the assumption of elastic wrinkling, and the values listed in Table 5-1, the predicted wavelength at the equilibrium condition (i.e. 150°C) was 152  $\mu\text{m}$  and 283  $\mu\text{m}$  for the onset and growth regions, respectively. These values are 24% and 36% lower than the experimental determined wavelengths for those regions. The critical stresses estimated by this model using Eqn. (2-2) were 270 MPa for the onset region which was 17% lower than the values calculated by Basu's model described later in this Chapter. For the growth region a value of 549 kPa was obtained which was 45% lower the value calculated by Basu's model. Since the model is for an elastic film/elastic primary substrate, we can assume that the value for the onset region to be quasi accurate but not for above that temperature as the primary substrate is not in the elastic region based on the storage modulus values in relation to loss modulus values obtained from DMA at 130-150°C for the film.

### 5.3.2. Viscous Models

Equation (2-7) proposed by Im *et al.* (Im & HUANG, 2005) was intended to calculate the critical wavelength for a system comprised of an elastic film on a viscous primary substrate. We will have two approaches here, 1) taking the initial wavelength observed in the experiments to calculate the initial stress, or 2) taking the initial compressive stress within the film calculated by Basu's model and trying to see how the model estimated the wavelength and compare it to our value. Since there are two different wavelengths based on the different secondary substrates, the approach of option 1 was most interesting, calculated for the onset temperature region. Based on the initial

wavelengths stated in Table 5-1, the first approach yielded -18 MPa and -10 MPa as for the compressive stresses existing in the film for steel and plastic laminates, respectively. These values are respectively 8 and almost 4 times higher than the corresponding values in Table 5-2. The values in Table 5-2 are based on the model proposed by Basu *et al.* (Basu et al., 2005) and will be described later in this Chapter. The second approach cannot be used for the PP substrate if the values in Table 5-2 are used since the positive sign of the initial stress calculated using Eqn. (5-5) (a negative sign will remain in the radical sign), but for the steel laminate it predicted the critical initial wavelength to be about 487  $\mu\text{m}$ . This value is only 8% higher than the experimentally obtained value of 450  $\mu\text{m}$ . However, the model calculates the initial wavelength for a viscous primary substrate while the experimental wavelength was the equilibrium wavelength. The equilibrium wavelength based on Eqn (2-17), yielded a value of 97  $\mu\text{m}$  which was more than 4 times lower than the experimental value.

### 5.3.3. Viscoelastic Models

Using Eqn. (2-9) and (2-10) for glassy and rubbery state critical stresses, respectively, we got 145 MPa and 829 kPa regardless of the secondary substrate. These values are analogous to  $\sigma_c$  and  $\sigma_{eq}$  in Table 5-2 as they used the corresponding moduli in each region (i.e. below  $T_g$  for glassy and above  $T_g$  for the rubbery state.). The glassy state value is 58% lower and the rubbery state value is 22% lower than the values calculated by Basu *et al.* (Basu et al., 2005). It is of great essence to mention that the glassy-state critical stress was calculated based on the modulus of the film and the primary substrate in the onset region and the rubbery-state critical stress was calculated

based on those moduli in the growth region. Accordingly, using Eqn. (2-11) and (2-12), the wavelengths calculated for glassy and rubbery state were 109  $\mu\text{m}$  and 202  $\mu\text{m}$ , respectively, with no distinction between the two different secondary substrates. Both these values are around 50% lower than experimentally observed ones.

#### 5.3.4. Basu’s Model – Consideration of the secondary substrate

The models described till now have only considered the film structure itself and neglect the secondary substrate as having any effect on the wrinkles. The results Chapter has already made the point that differences in wrinkling behaviour were found for the two secondary substrates, i.e. carbon steel versus plastic (PP), tested in the study. The only model known to take into consideration the effects of the secondary substrate on wrinkling behaviour was proposed by Basu *et al.* (Basu et al., 2005). The authors studied the case of a glassy rigid film layer of PVA attached to a compliant rubbery primary substrate of PEA. PET was used as the secondary “rigid” substrate in their system. Basu heated the sample to 130°C and observed wrinkles as soon as the temperature passed 75°C which was the Tg for PVA.

Basu *et al.* (Basu et al., 2005) used the following equations suggested by Allen (Allen, 1969) in their studies to calculate the critical compressive elastic stress required to produce wrinkles in the film:

$$\sigma_f = \frac{E_f}{12} \left( \frac{h_f}{h_s} \theta \right)^2 + E_s \left( \frac{h_s}{h_f} \right) g(\theta) \quad \text{Eqn. 5-1}$$

where  $\theta = 2\pi h_f / \lambda$  and the function  $g(\theta)$  is given by:

$$g(\theta) = \frac{2(3 - \nu_s) \sinh \theta \cosh \theta + (1 + \nu_s)\theta}{\theta(1 + \nu_s)(3 - \nu_s)^2 \sinh^2 \theta - (1 + \nu_s)^3 \theta^2} \tag{Eqn. 5-2}$$

**Table 5-2:** Calculated values based on equations in Appendix B and 5-1 and 5-2 for temperature onset and growth regions for steel and plastic secondary substrates.

|   | Steel Laminate | Plastic Laminate |
|---|----------------|------------------|
| $\sigma_f$ (MPa)  | -3.1           | 2.4              |
| $\sigma_s$ (MPa)  | -1             | -0.01            |
| $\sigma_{ss}$ (MPa)   | 0.08           | -0.07            |
| $\theta_c$  | 2.67           | 1.99             |
| $\theta_{eq}$   | 1.19           | 0.97             |
| $g(\theta_c)$   | 0.216          | 0.312            |
| $g(\theta_{eq})$  | 0.841          | 1.24             |
| $\sigma_c$ (MPa)  | 328            | 481              |
| $\sigma_{eq}$ (MPa)   | 1.06           | 1.51             |
| * Indices <i>f</i> , <i>s</i> and <i>ss</i> represent film, primary substrate and secondary substrate, respectively, and <i>c</i> and <i>eq</i> stand for critical and equilibrium. |                |                  |

For the steel secondary substrate, referring to Table 5-2, we realize that the estimated compressive stress within the film in the onset region was -3.1 MPa while the critical stress to cause wrinkles with the wavelength of 200 μm (initiation wavelength, Figure 4-2) in the film at temperatures below 130°C is 328 MPa. Therefore, the stress within the film in that region was not sufficient to cause wrinkles. However, at this temperature the moduli of the film and the primary substrate dropped significantly (by two orders of magnitude for the film and three orders of magnitude for the primary substrate, measured by DMA) causing the critical compressive stress required to cause wrinkles to drop by about two orders of magnitude to 1.06 MPa. At this point the accumulated compressive stress in the film (-3.1 MPa) was large enough to create wrinkles. Although these values for critical stresses and the compressive stress in the film

are based on the calculated data from Basu's model, this phenomenon was also stated by Huang (R. Huang, 2005) and seems well justified by the visual observations in this study. The effect of the secondary rigid substrate was taken into account only for determination of the dominant layer. The layer which holds the highest axial stiffness controls the dimensions of the multilayer system (Basu et al., 2005). For example, in case of steel laminates we can realize that the axial stiffness-weighted thermal expansivity of the whole system was the same as that of steel (refer to Appendix B). The same fact holds true for axial stiffness-weighted strain, as well. For plastic laminates, however, the situation was different. The values of strain and stress for the film suggested that there was no compression in that layer (positive sign as opposed to negative in the case of steel substrate). Nevertheless, the model suggests compression in the primary as well as secondary substrates. The main reason for that was the higher thermal expansivities of these substrates compared to that of the PET layer. Although none of the layers could be considered stiff compared to one another, the plastic substrate still had a higher nondimensional axial stiffness by one order of magnitude compared to the other two layers. This difference is about 4 orders of magnitude in the case of the steel secondary substrate. Heating the plastic secondary substrate alone (not laminated) did not produce any wrinkles; therefore it could be assumed that the wrinkles were not solely caused by the secondary substrate. It should also be noted that detaching the film sandwich, after being wrinkled, from the plastic secondary substrate revealed that the wrinkle pattern was also visible on the surface interface of the secondary substrate. Considering at 150°C the adhesive layer possessed little tack strength (based on lap shear tests) to play a role, it was

reasonably assumed that the plastic secondary substrate had softened sufficiently to comply under the compressive stresses of the primary substrate. Yet, one important fact that should not be overlooked is that for the experiments with the plastic laminates, the substrate was vacuum-fixed in the hot stage which definitely restricted its thermal expansion resulting in a lower actual  $\alpha$  (thermal expansion coefficient). For that case, however, it was not possible to estimate  $\alpha$  value and therefore no calculation was based on that thermal expansion coefficient value. This could justify why wrinkles happened in that system. The other scenario, however, is what was observed for the plastic laminates heated by the heat gun. In those experiments even the samples that were not vacuum-fixed developed wrinkles. This outcome leaves the question whether another phenomenon was involved in the case of wrinkling in secondary plastic substrates. The importance of heating rates or even direction of heating (for the case of heat gun, the rate was almost 20 times faster and the heat direction was from the film side as opposed to the other experiments where they were heated from the substrate side) are not considered factors in these models, even Basu's.

Based on Eqn. (B-6), a negative sign in strain indicates that expansion of that layer had been larger than the average expansion of the whole system, therefore causing compressive stress in that layer. On the other hand, a positive strain indicates that the expansion of that layer had been smaller than that of the whole system, suggesting that the layer is under tension. Having had a positive strain for the film proposes that this layer was under tension and with the knowledge that compressive stress causes wrinkles, it is believed that this layer could have not initiated the wrinkles. Now knowing that the

primary and secondary substrates have expanded more than the whole system, in order for it to buckle, there should have been a peripheral restriction. One hypothesis here could be that the PET layer which had the lowest uniaxial strain among other layers ( $5 \times 10^{-3}$  as opposed to  $8 \times 10^{-3}$  for the other two layers, not normalized by the stiffness factor,  $S_i$ ) could have restricted the expansion of the secondary substrate causing it to buckle. Further in-depth studies are required to pinpoint the exact phenomenon behind wrinkle development in the plastic secondary substrate system.

To sum up, although some predicted values by the models above were close to our experimental results, most of models seemed incapable of reasonably predicting the properties and behaviour of such systems as ours. The model for the elastic substrate calculated the glassy critical stress pretty close to the values obtained through Basu's model (17% lower) but failed to do so for the rubbery critical (45% lower). Considering at 130°C the primary substrate is not in the elastic regime (based on the storage modulus values obtained from DMA), it makes sense for the model to fail to predict that value. The model for initial wavelength on a viscous substrate (Eqn. 2-7) also predicted a value quite close to our wavelength for the steel laminates (487  $\mu\text{m}$  which is 8% higher than the average of 450  $\mu\text{m}$ ). Other than that no other method could predict close values. The main shortcoming to these models are, first, they consider wrinkling mostly as a thermodynamically driven phenomenon and when they do consider kinetics, they do not consider heating rate as part of the kinetics of the process, which in our system was a major factor. The second problem is that they have a limiting case for the thicknesses of the film and the primary substrate ( $h_s/h_f > 40$  or  $h_s/h_f > 10$ ) which can be a reason why we

did not get the desirable outcome for our system ( $h_s/h_f \approx 4$ ). The third hypothesis behind the failure of these models is that they assume elastic deformation of the film, but in our systems due to the fact that wrinkles did not relax even in slow cooling rates, suggests that we are dealing with at least some degree of plastic deformation. Another reason for the discrepancy within the models and our system can be the fact that they do not consider the effects of the secondary substrate into account. It has already been proven that the secondary substrate plays a major role in our system. Of all those methods, only the model by Basu *et al.* could describe the behaviour of our system properly based on the levels of stress at different stages in the process.

#### **5.4. Effects of Heating/Cooling Rate**

From the experimental data it was obvious that heating rate played a significant role in the wrinkling process; a variable never studied before as a factor in wrinkling. The effects of heating rate are associated with thermal shock phenomena. Thermal shock occurs when different parts of an object expand differently due to a gradient in temperature. This expansion obviously can be worded as strain or stress which is the cause of wrinkling in multilayer systems. This phenomenon is what causes glass to break when heated or cooled down abruptly. One way to reduce the stress caused by thermal shock is to change the temperature slowly, allowing the layers to expand/contract more uniformly. It is exactly what we observed, when the heating rate was fast, samples wrinkled instantaneously because of the large amount of compressive stress imposed on the film. On the other hand, in a slow heating process the layers had enough time to compensate for the change in the length by expanding in a closer manner. This fact holds

true for both secondary substrates. In the case of secondary plastic substrate, however, we realized that the heating rate that caused wrinkles in steel laminates did not produce any wrinkles in plastic laminates. This can be associated with two different issues. First, it can be a matter heat transfer. Since the secondary plastic substrate has a very low thermal conductivity, it does not transfer the heat to the top layers as fast as it receives it (being almost 130 times slower based on the thermal resistivities of steel and plastic substrate), therefore, giving them more time to comply with the length change. Second reason can be attributed to the fact that all the layers in the plastic laminate have almost the same thermal expansion coefficients. Thermal shock has been known to cause failure in the material due to the large difference in thermal expansion coefficients between the mated surfaces. It would then seem that, to overcome this, the expansion coefficients of the two materials should be chosen so that there is minimal difference. The closeness of thermal expansion coefficients seems to be the case with our plastic laminates. The layers' almost similar thermal expansion coefficients make them expand together with the same rate which causes very low compressive stress in the layers. Therefore, in order for the film to wrinkle, the amount of stress imposed on it should increase which can be performed by increasing the heating rate. By heating faster not only do we impose more stress in the layers, but also we compensate for the first issue which was slow heat transfer due to low thermal conductivity of the secondary plastic substrate, as well. This hypothesis was proved by experiments with higher heating rates. Based on the same hypothesis, it was expected that slow cooling rates would cause the wrinkles to diminish; however, we did not observe any difference in the wavelengths of the samples, neither for steel laminates

nor plastic ones. In all the models that were mentioned in the Literature Review chapter, they all assumed an elastic deformation of the film. This observation of ours can mean that we are experiencing a degree of plastic deformation for the PET film since it cannot retain its original state. Slow cooling rates, however, had some effects on the surface roughness quantifying factors of PV and rms for the plastic laminates. This can be attributed to the fact that, again, under slow cooling conditions all layers have enough time to relax as the compressive thermal stresses were allowed to relieve.

### **5.5. Pre-straining**

Edge effects were always observed in unstrained samples in the form of stripes perpendicular to the edges localized around the perimeter of the specimen. There is always a higher concentration of stress near the edges compared to the center of the material and straining the sample makes this stress preferentially more concentrated in only one direction (i.e. perpendicular to the strain direction), thereby reducing the effect of the other axis. This phenomenon suggested that the compressive stresses at the edges were more dominant in one direction than the other (perpendicular to the orientation of the wrinkles). But straining the sample causes those stripes from the edge perpendicular to the direction of elongation (i.e. longitudinal direction) to extend further into the specimen. Pre-straining the samples in the longitudinal direction also increased the mechanical properties of the system in that direction making it more resilient against the longitudinal compressive stresses that existed in the film.

For the case of steel laminates the change in the pattern of the wrinkles (from biaxial labyrinth to uniaxial stripes) was not achieved for strain level of 10%. For 20%

strain, it was quite clear that the pattern of the wrinkles changed from chaotic labyrinth into longitudinally oriented stripes/herringbones suggesting first, that the film became stronger enough in the longitudinal direction which was not affected (i.e. wrinkled) as a result of stresses in that direction, and second, due to large amount of the transversal compressive stress built up in that direction, this stress became dominant and caused wrinkles to form longitudinally. For the case of the plastic laminates this threshold was lower than 10% strain, because even applying 10% strain caused the orientation of the wrinkles to change. This suggested that the secondary plastic substrate contributed to the increase in the transversal stresses more than its steel counterpart.

---

---

## ***CHAPTER VI:***

### ***Conclusion***

---

---

In the beginning of this study, it was believed that the wrinkling behaviour observed while heating a film laminate was a product of the cooling process. However, through experiments on 9000J blackout films, supplied by 3M Canada, not only was it proved that it was the heating process that caused the wrinkles, but also its reproducibility was confirmed after seeing the same effect on multiple samples. It was understood that the rationale behind the wrinkling process was the compressive stress existent in the film that, in this case, had been caused by non-uniform thermal expansion of the constituting layers of the entire film sandwich. As suggested by Basu *et al.* (Basu et al., 2005) and also Huang (R. Huang, 2005) there is a critical stress to be overcome in order for the wrinkles to grow. In this study this critical stress was overcome by heating the sample to 130°C where the first wrinkles appeared. At this temperature, not only did the initial stress in the film increase, but also the critical stress dropped due to softening of the layers, which both in turn made wrinkling possible. Heating was continued to 150°C and the wrinkles reached an equilibrium value. This critical stress was not overcome for the lower temperature of 110°C.

Studies showed that heating rate and the final temperature are the most important factors affecting the appearance of the wrinkles. For the samples that were heated to the lower temperature of 110°C (lower limit for thermoforming), regardless of the heating

rate (fast or slow) or the secondary substrate, wrinkles were not observed. For the higher temperature of 150°C, well-defined wrinkles developed in the fast heating cycles for both secondary substrates. However, for the slow heating rates, the PV threshold of 7  $\mu\text{m}$  was not exceeded and no wrinkles were formed in either case of the substrates, although the surface roughness factors increased compared to the control sample for both secondary substrates. On the other hand, cooling rates seemed not to have any effects on the wavelength of the wrinkles and only in the case of secondary plastic substrate, a slow cooling rate resulted in lower values for surface roughness factors of the fast-heated samples (for 150°C).

Although samples with different secondary substrates followed the same trend, they showed different values for wavelength (about 100  $\mu\text{m}$  difference) and also different patterns for wrinkles. These two were the result of the contribution of the secondary plastic substrate in relieving the compressive stress in the film. One very important observation here was that plastic laminates required higher heating rates in order to wrinkle (almost twice as much), which was attributed to the dampening effect from the low thermal conductivity of the secondary plastic substrate compared to metal. In general due to almost similar thermal expansion coefficients for the layers in plastic laminates, and also slower heat transfer through the layers, wrinkling was not observed as distinctly or as readily as in the steel laminates.

Based on these observations, it is believed that wrinkling can be avoided or at least minimized, provided that the right conditions are met. If the materials are selected in a way that they have relatively similar stiffness as well as similar coefficients of thermal

expansion and are used in processes with relatively low heating rates, wrinkles can be avoided. For this case, the closer the values of stiffness and thermal expansion coefficients are, the faster the heating rate can be applied. For example, for our plastic laminates heating rates of up to 80°C/min can still yield samples with a relatively acceptable surface roughness. Otherwise, we always see wrinkles for a system comprised of very different materials as for stiffness and thermal expansion coefficients. Obviously, the bigger this difference is, the slower the heating rate should be in order to avoid the wrinkles.

## ***References:***

Allen, H. G. (1969). *Analysis and design of structural sandwich panels* (1st ed.). Oxford, New York .: Pergamon Press.

Andreussi, F., & Gurtin, M. E. (1977). *On the wrinkling of a free surface* AIP.  
doi:10.1063/1.324298

Basu, S. K., Bergstreser, A. M., Francis, L. F., Scriven, L. E., & McCormick, A. V. (2005). Wrinkling of a two-layer polymeric coating. *Journal of Applied Physics*, 98(6), 063507. doi:10.1063/1.2043255

Bowden, N., Brittain, S., Evans, A. G., Hutchinson, J. W., & Whitesides, G. M. (1998). Spontaneous formation of ordered structures in thin films of metals supported on an elastomeric polymer. *Nature*, 393(6681), 146-149. Retrieved from <http://dx.doi.org/10.1038/30193>

Bowden, N., Huck, W. T. S., Paul, K. E., & Whitesides, G. M. (1999). *The controlled formation of ordered, sinusoidal structures by plasma oxidation of an elastomeric polymer* AIP. doi:10.1063/1.125076

Chan, E., & Crosby, A. (2006). *Fabricating microlens arrays by surface wrinkling* - WILEY-VCH Verlag. doi:- 10.1002/adma.200601595

- Chan, E., Smith, E., Hayward, R., & Crosby, A. (2008). *Surface wrinkles for smart adhesion* WILEY-VCH Verlag. doi:10.1002/adma.200701530
- Cheng, W., Finnie, I. (2007). Introduction to residual stresses. In *Residual stress measurement and the slitting method* (1st ed., pp. 1-8). New York: Springer.
- Chng, A. C., Curtin, W. A., Tay, A. A. O., & Lim, K. M. (2008). Effect of residual stress on fracture in confined thin films: A discrete dislocation study. *Modelling and Simulation in Materials Science and Engineering*, 16(1), 015002. Retrieved from <http://stacks.iop.org/0965-0393/16/i=1/a=015002>
- Choi, H., Kim, J., Lee, H., Song, S., Lee, H., Han, J., & Moon, M. (2010). *Wrinkle-based measurement of elastic modulus of nano-scale thin pt film deposited on polymeric substrate: Verification and uncertainty analysis* Springer Boston.  
doi:10.1007/s11340-009-9243-8
- Choi, J., Kim, H., & Yoon, S. (1992). Effects of the reaction parameters on the deposition characteristics in ZrO<sub>2</sub> CVD. *Journal of Materials Science: Materials in Electronics*, 3(2), 87-92. doi:10.1007/BF00695722
- Chua, D. B. H., Ng, H. T., & Li, S. F. Y. (2000). Spontaneous formation of complex and ordered structures on oxygen-plasma-treated elastomeric polydimethylsiloxane. *Applied Physics Letters*, 76(6), 721-723. doi:10.1063/1.125873

- Clyne, T., & Gill, S. (1996). Residual stresses in thermal spray coatings and their effect on interfacial adhesion: A review of recent work. *Journal of Thermal Spray Technology*, 5(4), 401-418. doi:10.1007/BF02645271
- Dhoble, A., Kulshreshtha, B., Ramaswami, S., & Zumbunnen, D. A. (2005). Mechanical properties of PP-LDPE blends with novel morphologies produced with a continuous chaotic advection blender. *Polymer*, 46(7), 2244-2256. doi:DOI: 10.1016/j.polymer.2005.01.057
- Efimenko, K., Rackaitis, M., Manias, E., Vaziri, A., Mahadevan, L., & Genzer, J. (2005). Nested self-similar wrinkling patterns in skins. *Nat Mater*, 4(4), 293-297. Retrieved from <http://dx.doi.org/10.1038/nmat1342>
- Espinosa, H. D., Prorok, B. C., & Fischer, M. (2003). A methodology for determining mechanical properties of freestanding thin films and MEMS materials. *Journal of the Mechanics and Physics of Solids*, 51(1), 47-67. doi:DOI: 10.1016/S0022-5096(02)00062-5
- Fernández, R., Bruno, G., & González-Doncel, G. (2004). Correlation between residual stresses and the strength differential effect in PM 6061Al–15 vol% SiCw composites: Experiments, models and predictions. *Acta Materialia*, 52(19), 5471-5483. doi:DOI: 10.1016/j.actamat.2004.08.005

- Flavenot, J. F. (1996). Handbook of measurement of residual stresses. In J. Lu (Ed.), *Handbook of measurement of residual stresses* (, pp. 35-48). Lilburn, GA: Fairmont Press, Distributed by Prentice Hall PTR.
- Gheeraert, E., Deneuille, A., Bonnot, A. M., & Abello, L. (1992). Defects and stress analysis of the raman spectrum of diamond films. *Diamond and Related Materials*, 1(5-6), 525-528. doi:DOI: 10.1016/0925-9635(92)90157-J
- Gioia, G., & Ortiz, M. (1997). Delamination of compressed thin films. In John W. Hutchinson and Theodore Y. Wu (Ed.), *Advances in applied mechanics* (, pp. 119-192) Elsevier. doi:DOI: 10.1016/S0065-2156(08)70386-7
- Groenewold, J. (2001). Wrinkling of plates coupled with soft elastic media. *Physica A: Statistical Mechanics and its Applications*, 298(1-2), 32-45. doi:DOI: 10.1016/S0378-4371(01)00209-6
- Grove, G. L., Grove, M. J., & Leyden, J. J. (1989). Optical profilometry: An objective method for quantification of facial wrinkles. *Journal of the American Academy of Dermatology*, Vol. 21(Issue 3), 631-637.
- Hobart, K., Kub, F., Fatemi, M., Twigg, M., Thompson, P., Kuan, T., & Inoki, C. (2000). Compliant substrates: A comparative study of the relaxation mechanisms of strained films bonded to high and low viscosity oxides. *Journal of Electronic Materials*, 29(7), 897-900. Retrieved from <http://dx.doi.org/10.1007/s11664-000-0177-2>

Huang, Z., Hong, W., & Suo, Z. (2004). Evolution of wrinkles in hard films on soft substrates. *Phys.Rev.E*, 70(3), 030601. Retrieved from 10.1103/PhysRevE.70.030601

Huang, R. (2005). Kinetic wrinkling of an elastic film on a viscoelastic substrate. *Journal of the Mechanics and Physics of Solids*, 53(1), 63-89. doi:DOI: 10.1016/j.jmps.2004.06.007

Huang, R., & Suo, Z. (2002a). Instability of a compressed elastic film on a viscous layer. *International Journal of Solids and Structures*, 39(7), 1791-1802. doi:DOI: 10.1016/S0020-7683(02)00011-2

Huang, R., & Suo, Z. (2002b). *Wrinkling of a compressed elastic film on a viscous layer* AIP. doi:10.1063/1.1427407

Huang, R., & Im, S. H. (2006). Dynamics of wrinkle growth and coarsening in stressed thin films. *Phys.Rev.E*, 74(2), 026214. Retrieved from 10.1103/PhysRevE.74.026214

Huang, Z. Y., Hong, W., & Suo, Z. (2005). Nonlinear analyses of wrinkles in a film bonded to a compliant substrate. *Journal of the Mechanics and Physics of Solids*, 53(9), 2101-2118. doi:DOI: 10.1016/j.jmps.2005.03.007

Huck, W. T. S., Bowden, N., Onck, P., Pardo, T., Hutchinson, J. W., & Whitesides, G.

M. (2000). Ordering of spontaneously formed buckles on planar surfaces.

*Langmuir*, 16(7), 3497-3501. doi:10.1021/la991302l

Hutchinson, J. W., Thouless, M. D., & Liniger, E. G. (1992). Growth and configurational

stability of circular, buckling-driven film delaminations. *Acta Metallurgica Et*

*Materialia*, 40(2), 295-308. doi:DOI: 10.1016/0956-7151(92)90304-W

Im, H. S., & HUANG, R. (2005). Evolution of wrinkles in elastic-viscoelastic bilayer thin

films. *American Society of Mechanical Engineers*, 72(6), 955-961.

Jang, J. (2009). Estimation of residual stress by instrumented indentation: A review.

*Journal of Ceramic Processing Research*, 10(3), 391-400.

Jones, J., Lacour, S. P., Wagner, S., & Suo, Z. (2003). A method for making elastic metal

interconnects. *Mat. Res. Soc. Symp. Proc.*, 769, H6.12.

Keyu, L. (1997). Application of interferometric strain rosette to residual stress

measurements. *Optics and Lasers in Engineering*, 27(1), 125-136.

doi:10.1016/S0143-8166(95)00014-3

Kim, D., & Rogers, J. A. (2008). Stretchable electronics: Materials strategies and devices.

*Advanced Materials*, 20(24), 4887-4892. doi:10.1002/adma.200801788

Lacour, S., Wagner, S., Huang, Z., & Suo, Z. (2003). Stretchable gold conductors on elastomeric substrates. *Applied Physics Letters*, 82(15), 2404-2406. Retrieved from <http://dx.doi.org/10.1063/1.1565683>

Lu, Y. F., Choi, W. K., Aoyagi, Y., Kinomura, A., & Fujii, K. (1996). Controllable laser - induced periodic structures at silicon–dioxide/silicon interface by excimer laser irradiation. *Journal of Applied Physics*, 80(12), 7052-7056.

Makino, A., & Nelson, D. V. (1997). *Determination of sub-surface distributions of residual stresses by a holographic-hole drilling technique* ASME.  
doi:10.1115/1.2805981

Malhotra, S. G., Yalisove, S. M., & Bilello, J. C. (1997). Analysis of thin film stress measurement techniques. *Thin Solid Films*, 301(1-2), 45-54. doi:10.1016/S0040-6090(96)09569-7

Mei, H., Huang, R., Chung, J. Y., Stafford, C. M., & Yu, H. H. (2007). Buckling modes of elastic thin films on elastic substrates. *Applied Physics Letters*, 90(15), 151902. Retrieved from 10.1063/1.2720759;  
<http://adsabs.harvard.edu/abs/2007ApPhL..90o1902M>

Mei, Y., Kiravittaya, S., Harazim, S., & Schmidt, O. G. (2010). Principles and applications of micro and nanoscale wrinkles. *Materials Science and Engineering: R: Reports, In Press, Corrected Proof* doi:DOI: 10.1016/j.mser.2010.06.009

- Murdoch, A. I. (1978). On wrinkling induced by surface stress at the boundary of an infinite circular cylinder. *International Journal of Engineering Science*, 16(2), 131-137. doi:DOI: 10.1016/0020-7225(78)90086-1
- Nelson, D. V., Makino, A., & Fuchs, E. A. (1997). The holographic-hole drilling method for residual stress determination. *Optics and Lasers in Engineering*, 27(1), 3-23. doi:10.1016/S0143-8166(97)89899-5
- Nolte, A. J., Cohen, R. E., & Rubner, M. F. (2006). A two-plate buckling technique for thin film modulus measurements: applications to polyelectrolyte multilayers. *Macromolecules*, 39(14), 4841-4847. doi:10.1021/ma0606298
- Nolte, A. J., Rubner, M. F., & Cohen, R. E. (2005). Determining the young's modulus of polyelectrolyte multilayer films via stress-induced mechanical buckling instabilities. *Macromolecules*, 38(13), 5367-5370. doi:10.1021/ma0507950
- Noyan, I. C., Huang, T. C., & York, B. R. (1995). *Residual stress/strain analysis in thin films by X-ray diffraction* Taylor & Francis. Retrieved from <http://www.informaworld.com/10.1080/10408439508243733>
- Oliver, W. C., & Pharr, G. M. (1992). An improved technique for determining hardness and elastic modulus using load and displacement sensing indentation experiments. *Journal of Materials Research*, 7(6), 1564-1583.

- Orowan, E. (1970). Surface energy and surface tension in solids and liquids. *Proceedings of the Royal Society of London. Series A, Mathematical and Physical Sciences*, 316(1527), 473-491. Retrieved from <http://www.jstor.org/stable/77634>
- Perry, A. J., Sue, J. A., & Martin, P. J. (1996). Practical measurement of the residual stress in coatings. *Surface and Coatings Technology*, 81(1), 17-28. Retrieved from [http://resolver.scholarsportal.info/resolve/02578972/v81i0001/17\\_pmotrsic](http://resolver.scholarsportal.info/resolve/02578972/v81i0001/17_pmotrsic)
- Poole, L. (2007). Decorative film laminates. *International Coatings for Plastics Symposium*, Retrieved from <http://www.pcimag.com>
- Reynolds, O. (1886). On the theory of lubrication and its application to mr. beauchamp tower's experiments, including an experimental determination of the viscosity of olive oil. *Philosophical Transactions of the Royal Society of London*, 177, 157-234. Retrieved from <http://www.jstor.org/stable/109480>
- Sasaki, K., Kishida, M., & Itoh, T. (1997). The accuracy of residual stress measurement by the hole-drilling method. *Experimental Mechanics*, 37(3), 250-257. Retrieved from <http://dx.doi.org/10.1007/BF02317415>
- Serrano, J. R., & Cahill, D. G. (2002). Micron-scale buckling of SiO<sub>2</sub> on si. *Journal of Applied Physics*, 92(12), 7606-7610.

- Sharpe, W. N., Jr., Yuan, B., & Edwards, R. L. (1997). A new technique for measuring the mechanical properties of thin films. *Microelectromechanical Systems, Journal of*, 6(3), 193-199.
- Shugurov, A. R., & Panin, A. V. (2010). Mechanisms of periodic deformation of the film-substrate system under compressive stress. *Physical Mesomechanics*, 13(1-2), 79-87. doi:DOI: 10.1016/j.physme.2010.03.010
- Stafford, C. M., Vogt, B. D., Harrison, C., Julthongpipit, D., & Huang, R. (2006). Elastic moduli of ultrathin amorphous polymer films. *Macromolecules*, 39(15), 5095-5099. doi:10.1021/ma060790i
- Tahk, D., Lee, H. H., & Khang, D. (2009). Elastic moduli of organic electronic materials by the buckling method. *Macromolecules*, 42(18), 7079-7083. doi:10.1021/ma900137k
- Tolpygo, V. K., & Clarke, D. R. (1998). Wrinkling of  $\alpha$ -alumina films grown by thermal oxidation—I. quantitative studies on single crystals of Fe–Cr–Al alloy. *Acta Materialia*, 46(14), 5153-5166. doi:DOI: 10.1016/S1359-6454(98)00133-5
- Torres, J. M., Stafford, C. M., & Vogt, B. D. (2009). Elastic modulus of amorphous polymer thin films: Relationship to the glass transition temperature. *ACS Nano*, 3(9), 2677-2685. Retrieved from 10.1021/nn9006847; <http://pubs.acs.org/doi/abs/10.1021/nn9006847>

- Wang, S. H., Quan, C., Tay, C. J., & Shang, H. M. (2000). Surface roughness measurement in the submicrometer range using laser scattering. *Optical Engineering*, 39(6), 1597-1601. doi:10.1117/1.602535
- Wang, Y. Y., & Chiang, F. P. (1997). Experimental study of three-dimensional residual stresses in rails by moiré interferometry and dissecting methods. *Optics and Lasers in Engineering*, 27(1), 89-100. doi:10.1016/S0143-8166(97)89900-9
- Watanabe, M., Shirai, H., & Hirai, T. (2002). *Wrinkled polypyrrole electrode for electroactive polymer actuators* AIP. doi:10.1063/1.1505674
- Windecker, R., & Tiziani, H. J. (1999). *Optical roughness measurements using extended white-light interferometry* SPIE. doi:10.1117/1.602154
- Withers, P. J., & Bhadeshia, H. K. D. H. (2001a). *Residual stress. part 1 - measurement techniques*. Leeds, ROYAUME-UNI: Maney.
- Withers, P. J., & Bhadeshia, H. K. D. H. (2001b). Residual stress. part 2 - nature and origins. *Materials Science and Technology*, 17, 366-375(10). Retrieved from <http://www.ingentaconnect.com/content/maney/mst/2001/00000017/00000004/art0002>; doi:10.1179/026708301101510087
- Xiang, Y., Chen, X., & Vlassak, J. J. (2002). The mechanical properties of electroplated cu thin films measured by means of the bulge test technique. *Mat. Res. Soc. Symp. Proc.*, 695, L4.9.1.

- Xu, B., Zhao, B., & Yue, Z. (2006). Investigation of residual stress by the indentation method with the flat cylindrical indenter. *Journal of Materials Engineering and Performance*, 15(3), 299-305. Retrieved from <http://dx.doi.org/10.1361/105994906X108701>
- Yang, F. (2004). *Size-dependent effective modulus of elastic composite materials: Spherical nanocavities at dilute concentrations* AIP. doi:10.1063/1.1664030
- Yang, F. (2006). *Effect of interfacial stresses on the elastic behavior of nanocomposite materials* AIP. doi:10.1063/1.2179140
- Yao, M., & Xu, B. (2007). Evaluating wrinkles on laminated plastic sheets using 3D laser scanning. *Measurement Science and Technology*, 18, 3724-3730(7). Retrieved from <http://www.ingentaconnect.com/content/iop/mst/2007/00000018/00000012/art00007>; doi:10.1088/0957-0233/18/12/007
- Yin, H., Huang, R., Hobart, K. D., Suo, Z., Kuan, T. S., Inoki, C. K., Shieh, S. R., Duffy, T. S., Kub, F. J., & Sturm, J. C. (2002). Strain relaxation of SiGe islands on compliant oxide. *J. Appl. Phys.*, 91, 9716.
- Yoo, P. J., & Lee, H. H. (2003). Evolution of a stress-driven pattern in thin bilayer films: Spinodal wrinkling. *Phys.Rev.Lett.*, 91(15), 154502. Retrieved from 10.1103/PhysRevLett.91.154502

## APPENDIX A: DMA Plot

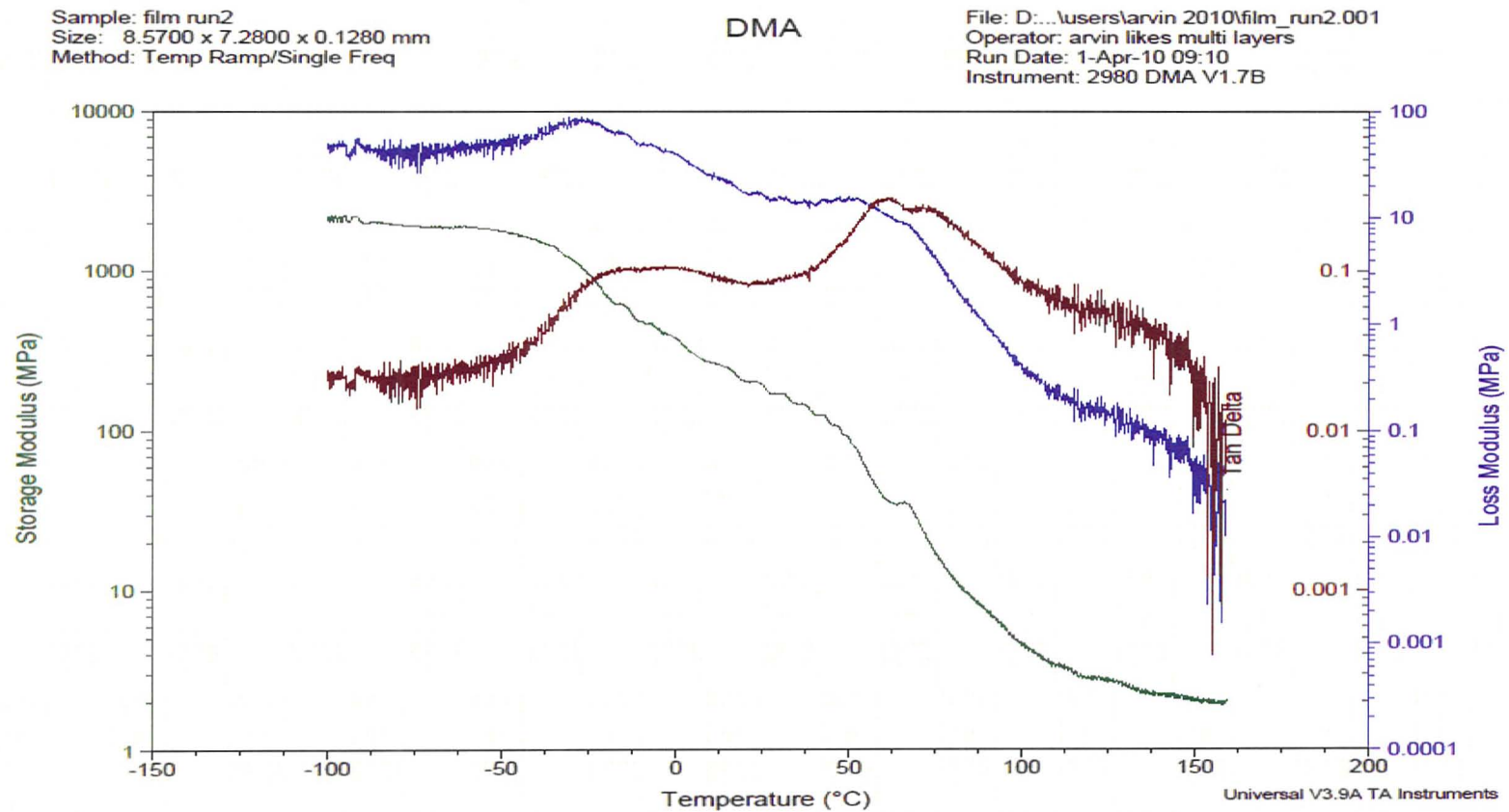


Figure A-1. DMA plot for 9000J film

## **APPENDIX B:**

### ***Basu's Model***

Basu *et al.* (Basu et al., 2005) in their studies came up with a series of equations to measure the stress and strain of the layers taking the effects of temperature and secondary substrate into account. For the uniaxial strain caused by deformation between the initial state and the stress-free state of the  $i$ th layer they suggested the following equation:

$$\varepsilon_{i,sfs} = \alpha_i \Delta T \quad \text{B-1}$$

where  $\alpha$  is the thermal expansion coefficient. Then they defined  $S_i$  as the nondimensional axial stiffness as:

$$S_i = \frac{h_i E_i}{\sum_j h_j E_j} \quad \text{B-2}$$

Based on this value, they came up with an axial stiffness-weighted average thermal expansivity as:

$$\bar{\alpha} = \sum_i \alpha_i S_i = \frac{\sum_i \alpha_i h_i E_i}{\sum_j h_j E_j} \quad \text{B-3}$$

They also pointed out that using the same equation it is possible to determine other stiffness-weighted average values such as stiffness-weighted average stress-free strain just by substituting  $\alpha_i$  with  $\varepsilon_{i,sfs}$  as follows:

$$\bar{\varepsilon}_{sfs} = \sum_i \varepsilon_{i,sfs} S_i = \frac{\sum_i \varepsilon_{i,sfs} h_i E_i}{\sum_j h_j E_j} \quad \text{B-4}$$

Using Eqn. B-3 they calculated the amount of stress caused by a change in temperature by the following equation:

$$\sigma_i = \frac{E_i}{(1-\nu_i)} (\bar{\alpha} - \alpha_i) \Delta T \quad \text{B-5}$$

The amount of elastic strain of the  $i$ th layer, however, can be calculated using Eqn. B-1 and B-4:

$$\varepsilon_i = \bar{\varepsilon}_{sfs} - \varepsilon_{i,sfs} \quad \text{B-6}$$

or simply by:

$$\varepsilon_i = \frac{\sigma_i}{E_i / (1-\nu_i)} \quad \text{B-7}$$

Basu *et al.* (Basu *et al.*, 2005) used the following equations suggested by Allen (Allen, 1969) in their studies to calculate the critical compressive elastic stress required to produce wrinkles in the top layer.

$$\sigma_f = \frac{E_f}{12} \left( \frac{h_f}{h_s} \theta \right)^2 + E_s \left( \frac{h_s}{h_f} \right) g(\theta) \quad \text{B-8}$$

where  $\theta = 2\pi h_f / \lambda$  and the function  $g(\theta)$  is given by:

$$g(\theta) = \frac{2}{\theta} \frac{(3-\nu_s) \sinh \theta \cosh \theta + (1+\nu_s) \theta}{(1+\nu_s)(3-\nu_s)^2 \sinh^2 \theta - (1+\nu_s)^3 \theta^2} \quad \text{B-9}$$

In the above equations if the value of  $\lambda$  is set to its initial value, which was obtained from the experiments, it yields the critical amount of stress on the film at that point in time. However, minimizing the derivative of this function ( $d\sigma_f / d\theta = 0$ ) yields the equilibrium wavelength at which, obviously, the compressive stress in the film is

minimum. That critical stress was taken as the critical stress passed 130°C. This derivative yields the following equation:

$$\left(\frac{6g'(\theta)}{\theta}\right)^{1/3} = -\frac{h_f}{h_s} \left(\frac{E_f}{E_s}\right)^{1/3} \quad \text{B-10}$$

Using the abovementioned equations, the amounts of initial compressive stress, and critical stresses at two regions were calculated. All these values are summarized in Table A5-1 below for the steel as well as plastic laminates.

**Table B-1:** Estimated and calculated values based on equations B-1 to B-10 for temperature brackets of 30°C to 130°C and 130°C to 150°C for steel and plastic secondary substrates.

|  | Steel Laminate         | Plastic Laminate       |
|--|------------------------|------------------------|
| $\alpha_f$ ( $^{\circ}\text{C}$ )            | $5 \times 10^{-5}$     | $5 \times 10^{-5}$     |
| $\alpha_s$ ( $^{\circ}\text{C}$ )            | $8 \times 10^{-5}$     | $8 \times 10^{-5}$     |
| $\alpha_{ss}$ ( $^{\circ}\text{C}$ )         | $1.15 \times 10^{-5}$  | $8 \times 10^{-5}$     |
| $\bar{\alpha}_{<130}$ ( $^{\circ}\text{C}$ ) | $1.15 \times 10^{-5}$  | $7.90 \times 10^{-5}$  |
| $\bar{\alpha}_{>130}$ ( $^{\circ}\text{C}$ ) | $1.15 \times 10^{-5}$  | $7.95 \times 10^{-5}$  |
| $\Delta T_{<130}$ ( $^{\circ}\text{C}$ )     | 100                    | 100                    |
| $\Delta T_{>130}$ ( $^{\circ}\text{C}$ )     | 20                     | 20                     |
| $E_{f<130}$ (MPa)                            | 455                    | 455                    |
| $E_{s<130}$ (MPa)                            | 91                     | 91                     |
| $E_{ss<130}$ (MPa)                           | $200 \times 10^3$      | 485                    |
| $E_{f>130}$ (MPa)                            | 9                      | 9                      |
| $E_{s>130}$ (MPa)                            | 0.28                   | 0.28                   |
| $E_{ss>130}$ (MPa)                           | $192 \times 10^{3**}$  | 19                     |
| $h_f$ (m)                                    | $2 \times 10^{-5}$     | $2 \times 10^{-5}$     |
| $h_s$ (m)                                    | $8.50 \times 10^{-5}$  | $8.50 \times 10^{-5}$  |
| $h_{ss}$ (m)                                 | $1.5 \times 10^{-3}$   | $5.50 \times 10^{-4}$  |
| $\nu_f$                                      | 0.44                   | 0.44                   |
| $\nu_s$                                      | 0.37                   | 0.37                   |
| $\nu_{ss}$                                   | 0.29                   | 0.36                   |
| $S_f$  | $3.03 \times 10^{-5}$  | $3.21 \times 10^{-2}$  |
| $S_s$  | $2.85 \times 10^{-5}$  | $2.73 \times 10^{-2}$  |
| $S_{ss}$                                     | 1.00                   | 0.941                  |
| $\epsilon_f$                                 | $-3.85 \times 10^{-3}$ | $2.9 \times 10^{-3}$   |
| $\epsilon_s$                                 | $-6.85 \times 10^{-3}$ | $-9.63 \times 10^{-5}$ |

|   |                       |                        |
|---|-----------------------|------------------------|
| $\epsilon_{ss}$   | $2.93 \times 10^{-7}$ | $-9.63 \times 10^{-5}$ |
| $\sigma_f (MPa)$  | -3                    | 2.36                   |
| $\sigma_s (MPa)$  | -0.99                 | -0.014                 |
| $\sigma_{ss} (MPa)$   | 0.08                  | -0.07                  |
| $\lambda_c (\mu m)$   | 200                   | 268                    |
| $\lambda_{eq} (\mu m)$  | 450                   | 550                    |
| Compressive Elastic Stress Calculations (Eqn. 5-8)  |                       |                        |
| $\theta_c$  | 2.67                  | 1.99                   |
| $\theta_{eq}$   | 1.19                  | 0.97                   |
| $g(\theta_c)$   | 0.216                 | 0.312                  |
| $g(\theta_{eq})$  | 0.841                 | 1.24                   |
| $\sigma_c (MPa)$  | 328                   | 481                    |
| $\sigma_{eq} (MPa)$   | 1.06                  | 1.51                   |
| * Indices $f$ , $s$ and $ss$ represent film, primary substrate and secondary substrate, respectively, and $c$ and $eq$ stand for critical and equilibrium. “<130” and “>130” stand for below and above 130°C. |                       |                        |
| ** Based on ASME B31.1-1995   |                       |                        |